Wave Energy Converters

A methodology for assessing power performance, applied to a quasi-rigid submerged pressure differential device

J.M. van der Jagt

Technische Universiteit Delft

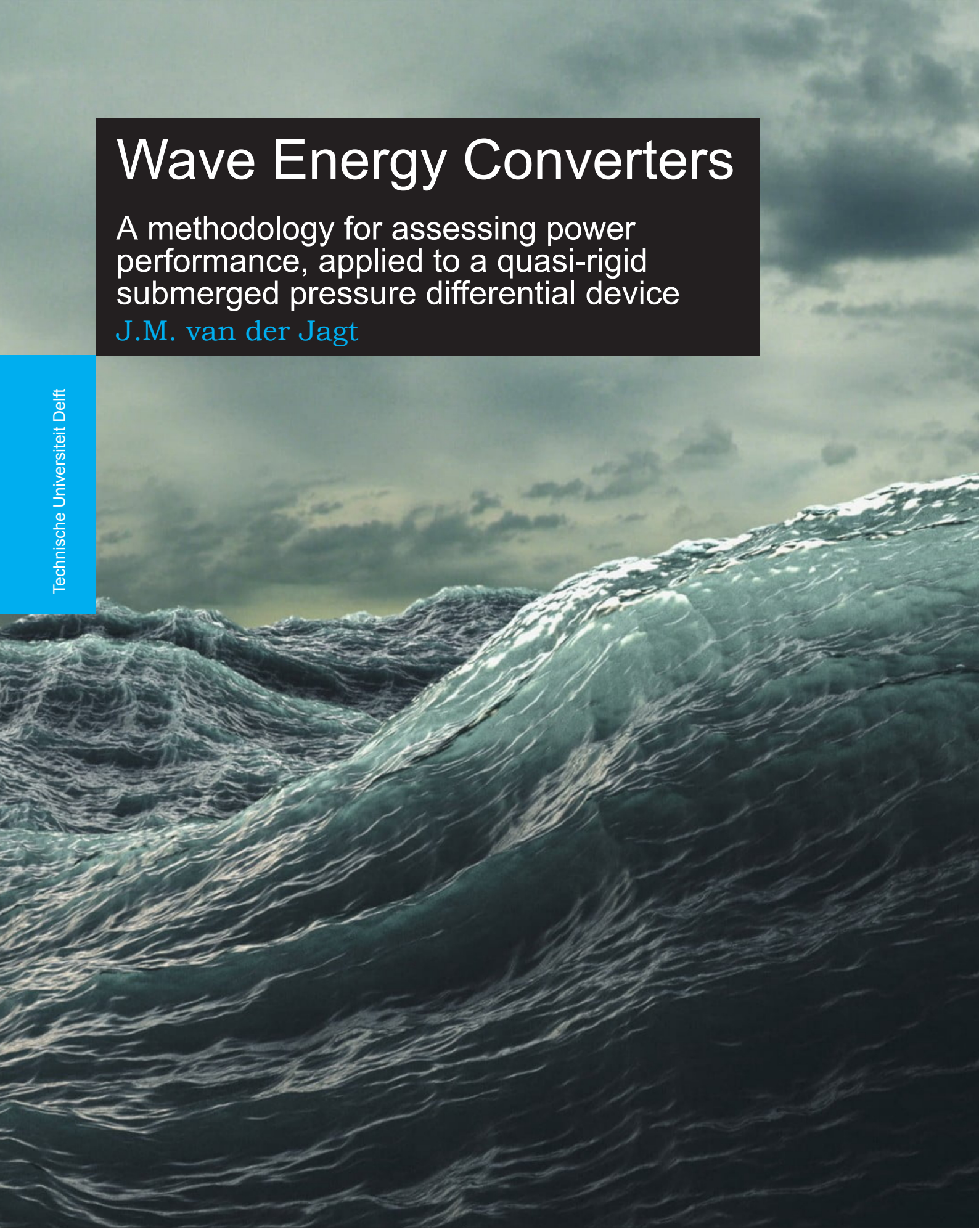

TU Delft Delft University of Technology

VUYK DESIGN TO FUNCTION.

Challenge the future

Wave Energy Converters

A methodology for assessing power performance, applied to a quasi-rigid submerged pressure differential device

by

J.M. van der Jagt

to obtain the degree of Master of Science
at the Delft University of Technology,
to be defended publicly on Friday December 21, 2018 at 09:30 AM.

Student number:	4012593	
Project start:	January 15, 2018	
Thesis committee:	Prof. Dr. ir. H. Polinder,	TU Delft
	Dr. ir. S. A. Miedema,	TU Delft
	Dr. ir. P. Naaijen,	TU Delft
	Ir. G.W. Jacobse,	Vuyk Rotterdam

TU Delft

VUYK DESIGN TO FUNCTION.

Abstract

Many designs have been developed in the recent years in order to demonstrate the feasibility of wave energy conversion (WEC) for electric power generation. Several designs for WEC have demonstrated proof of concept and began development for commercial scale. The majority of these developments failed to survive when large scale production started, failures that can partially be traced back to concept performance.

Due to improved facilitative test-berth sites in recent years the number of WEC-devices coupled to the grid has increased and the installed capacity grew to 8MW in 2017.

In the first part of this thesis an assessment is made of the different methods used to develop systems for wave energy conversion and a means of ranking the performances of competitive systems is given.

The majority of recent WEC developments is focused on"point absorber" concept types. There are three different types of point absorbers: floating, submerged and volume changing systems.

One promising point absorber concept is being developed by Teamwork, a Dutch company. This system is a submerged pressure differential device (SPD) called 'The Symphony Wave Energy Converter'. Despite the SPD concept showing advantages when compared to other point absorbers, it is not included in relevant comparison studies found in literature.

The second part of this thesis aims to make a comparison between the performance of an SPD concept, a quasi-rigid body or volume changing system, and the floating and submerged point absorbers.

For technical comparison, a simplified model of the SPD has been developed. The model enables a numerical calculation of the most important characteristics of the system. Hydrodynamic characteristics for rigid bodies are calculated using linear radiation diffraction models in AQWA. Hydrodynamic characteristics for the quasi-rigid bodies required to partly rebuild and extend the AQWA functionality. The extended method described in this thesis assesses the power performance of the SPD as a result of a time-domain simulation and defines the maximum power limits for the concept.

Next to the technical performance of the system, the economical performance has been analysed. It is clear, however, that more research is required in order to assess the economical performance of WEC-systems in general, and the economical performance of the SPD system in particular.

Contents

Cover source: https://zalarieunique.ru - image nr.5435605

Nomenclature

Abbreviations

BEM	Boundary Element Method
DOF	Degree of Freedom
EOM	Equation of motion
$ForceRAO$	Force excitation coefficient for unit wave amplitude
OWC	Oscillating water column
PA	Point absorbers
PST	Panel Selection Tool
PTO	Power Take-Off
RAO	Response Amplitude operator
SPD	Submerged Pressure Differential
WEC	Wave Energy Converter

Physics Constants

ρ_w	Density of water	$1025\,kg/m^3$
g	Acceleration of gravity	$9.81\,m/s^2$

Other Symbols

$\dot{z}$	Velocity in z direction
$\dot{z}_0$	Velocity amplitude in z direction
ϵ_F	Wave force amplitude
η	Surface elevation
λ	Wave length
ω	Angular wave frequency
ω_0	Natural frequency
ϕ_0	Velocity potential for the undisturbed wave
$\phi_{1\ldots6}$	Velocity potential for every degree of freedom
ϕ_7	Velocity potential for the diffracted wave
A	Amplitude
a_{mass}	Added Mass
b_{pto}	Power take-off damping coefficient
b_{rad}	Radiation damping coefficient
c	Restoring coefficient
F_e, i	Excitation force in i direction
F_0	Wave force amplitude
F_{exc}	Wave excitation force
F_{hs}	hydrostatic force
F_m	Mooring force
F_{pto}	Power take-off force
F_{rad}	Wave radiation force
F_v	Viscous forces
g	Gravitational acceleration
H	Wave height, regular waves

h	Depth
H_s	Significant wave height
J	Wave power resource
k_{pre}	Stiffness of pre-tensioned element
m	Mass
T	Wave period
t	Time
T_e	Wave energy period
T_p	Wave peak period
V	Volume

1. Introduction

The need for an alternative renewable energy source has shifted parts of the market's attention to wave energy conversion. Wave energy is a largely untapped resource of renewable energy. Since the oil crisis in the 1970's many solutions for Wave Energy Conversion (WEC) have been suggested and have demonstrated proof of concept. However, to date no WEC-concept survived the growth to commercial stage. Mainly because the cost for producing the power exceeds the returns from selling the power. Reduction of costs are expected after a successful concept enters large scale production. Various methods were developed to determine the viability of a new concept for wave energy conversion. In this research these methods for determining viability of WEC-concepts are assessed and improvements are suggested. This thesis started in collaboration with the TU delft and with Vuyk Engineering Rotterdam who where involved over the complete duration of the process.

When focusing on the absorption phase in wave energy conversion, three main categories of obtaining energy can be defined. The majority of WEC's are oscillating body devices. Within this category, point absorbers show to be promising for being axisymetric, and easily maintainable. Moreover, due to resonance, by adjusting the system's natural imbalance to the incident wave frequency, they are able to address a larger wave field than their width. This allows for increased power production while reducing the body size, and reducing the energy costs.

Floating and submerged rigid body point absorbers have been evaluated by a number of studies. A recently promising third type of point absorber can be defined as a quasi-rigid point absorber that relies on the submerged pressure differential (SPD) principle. Studies that evaluate and compare power limits and estimate the power to be gained from a concept in certain conditions have illustrated the performance of floating and submerged point absorbers. SPD devices have not yet been included in these studies, presumably because their methods cannot directly be applied to non-rigid bodies and the concept only recently became a much more viable option, with the design of a WEC-device called 'The Symphony'. Using the diffraction method for the SPD device, the comparison studies can be complemented and the performance of quasi-rigid bodies in WEC's can be evaluated as well. This thesis describes the required adaptations of the methods and illustrates the performance of the SPD based WEC's compared to floating and submerged point absorbers.

1.1. Motivation of Vuyk Engineering Rotterdam

Vuyk Engineering Rotterdam initially formulated the research topic of this thesis and has been involved throughout the entire research. The company objective is defined as follows:

Assess methods for determining viability of wave energy conversion concepts

With the expertise in offshore operations, Vuyk Engineering Rotterdam has contributed to demo's for WEC-concepts in the past. In order to make future contributions effective, the company aims to find a way to evaluate the viability of existing WEC concepts. This allows to further develop advisory and assistance services concerning mooring and installation of WEC-systems.

1.2. Prior research

Prior to the research, a literature study is performed to assess the current state of wave energy conversion and the methods that already exist to determine the the viability of wave energy.
The findings from this literature study will be described in chapters 2 to 4. From this literature, some conclusions are drawn:

1. In order to assess viability of wave energy conversion both costs as well as the energy production of a device must be evaluated.
2. There are several methods and calculation-tools available that, when combined, would allow to make an educated guess for both cost and energy production. A part of these tools are specially developed for Wave Energy Conversion (WEC), others are commonly used in naval engineering or for economic assessments.
3. There are renowned studies that made comparisons on energy production between WEC-concepts. These studies applied some of the available methods and calculation-tools that allow to make an educated guess for the energy production.
4. A WEC that utilises resonance, enhances power production or allows to reduce the device size. Resonance refers to a WEC that utilises its natural imbalance (resonance frequency) adjusted to the wave for optimal absorption and enhanced power production.
5. WEC-concepts that are horizontally symmetrical are able to perform in any direction regardless of the wave direction.
6. Finally, the comparison studies found, fall short in addressing one specific type of concept. This concept is the so called: Submerged Pressure Differential converter (SPD).

1.3. Problem definition

The conclusions from the literature study lead to the following problem definition:

> *Influential comparison studies contribute to the convergence of developed concept types to a single optimal approach, but do not account for one particular promising concept, the SPD.*

1.4. Objective

The research objective is:

> *To assess existing comparison studies for the viability of WEC-systems and to complement these studies by adapting them for application on an SPD concept.*

1.5. Approach

In order to apply the methods presented in comparison studies to the SPD, an adoptation of the method is required. The validity of the adaptation is verified by comparing the outcomes to existing data from the other two types of point absorbers.

This thesis adopts and applies the follwing two methods:

1. *A. Babarit (2012)* [4]
   Numerical benchmarking study of a selection of wave energy converters
2. *N.Y. Sergiienko (2017)* [47]
   Performance comparison of the floating and fully submerged quasi-point absorber wave energy converters

The two methods are separately described in two phases of the research. The required adaptation of the first method, the verification of this adaptation and the results are described in chapter 5. The same topics are covered for method 2 in 6. Each phase consists of a number of steps in order to answer the research question.

Phase I
This phase applies method 1 presented by Babarit [4] to obtain *performance indicators* through the following steps.

Step 1: Model description of the time-domain simulation model
Step 2: Verification[1] test, comparing results with analytical methods for an unloaded case.
Step 3: Power matrix calculation for the reference model
Step 4: Verification[1] test of power matrix with a case from the reference study
Step 5: Power matrix calculation for the research model
Step 6: Calculation of performance indicators at several example locations
Step 7: Comparing performance indicators with reference cases

Phase II
This phase applies method 2 presented by Sergiienko (2017) [47] in order to analyse limitations for theoretical maximum efficiency.

Step 1: Model description of the numerical frequency-domain calculations
Step 2: Verification test of the theoretical maximum efficiency for a reference case
Step 3: Performing calculations for theoretical maximum efficiency for the research model
Step 4: Compare frequency-domain limits for theoretical maximum power with exemplary power production obtained in time-domain simulations and describe the results.

1.6. Thesis report structure

This thesis first describes findings from literature in chapter 2 to 4. The study with the described objective and approach is described in 5 and 6.
Basic principles of wave energy conversion are described in chapter 2. Chapter 3 presents the methods found for determining viability. Chapter 4 describes basic theory for point absorbers, with respect to floating an submerged buoys. That chapter continues with a short introduction of a submerged pressure differential device that can also be characterised as a point absorber. Chapter 5 comprises the research method for power performance estimation of WEC devices via time-domain simulations of a dynamical representation of the WEC system (Method 1). The calculation method of theoretical limits for maximum absorbed power by a WEC-body (Method 2) are described in Chapter 6. The conclusions and recommendations are described in Chapter 7.

[1]Verification: Performing an analytical method reliably and precisely for its intended use

2. Wave Energy Conversion principles

This chapter elaborates on the question: What principles are used by wave energy converters currently in development in order to absorb wave energy for the production of electric energy?

Waves energy conversion (WEC) is the creation of usable energy from the oscillating water mass below a surface wave in sea water. Waves are mainly formed by continuous and steady interaction with wind for a long duration or by interaction with tumultuous winds in storm conditions during a short period of time. In the context of WEC, waves are the elevation of the water surface within a period of 0.5 to 30 seconds, [43]. Estimates of the global oceanic wave power resource based on quantitative analysis suggest that the annual coastal wave power exceeds 2 TW, [38]. For Europe it is suggested that a total of 100 GW installed capacity of ocean energy (including tidal and wave technology), by 2050 is a realistic target [48]. Due to improved facilitating test-berth sites the global deployment of WEC-devices coupled to the grid has doubled in 2017 and the installed capacity grew to 8MW in 2017, [41]. By Magagna et al. (2016) [36] was presented that the pipeline of announced European projects that secured funding, in potential could reach 65 MW of wave energy capacity by 2020. More information concerning the availability of wave energy is found in Appendix A.

2.1. Process from waves to electrical power

To convert the energy in waves to electricity in the grid, the total WEC installation generally consist of four phases of conversion. In direct drive devices, however, the transmission phase can be neglected, as the generator is directly connected to the absorbing body. In Figure 2.1 the four stages are displayed, starting from waves (left) towards grid (right). The arrows depict the mechanical and electrical parameters that define these interactions.

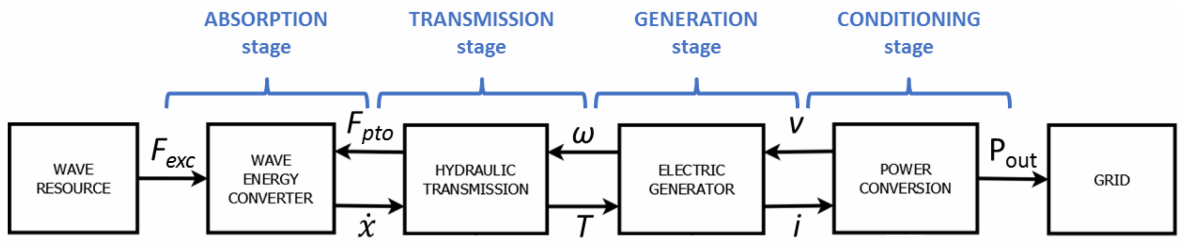

Figure 2.1: Stages of conversion, including interacting parameters and coefficients

- Absorption stage: Conversion of energy from waves to mechanical energy (Kinetic and potential energy) of the WEC body. This body is often defined as the hydrodynamic subsystem. Wave force (F_{exc}) acting on this body causes the body motions. The velocity ($\dot{x}$) of the body is used for power production while an adverse directed force reduces the motion.
- Transmission stage: Conversion of the motion energy in the body to energy in the transmission system. The design of this stage is strongly connected to the characteristics of the generator. Hydraulic cylinders generating pressurised hydraulic fluid are commonly used. Other types of systems could contain pressurised gas, fluid(sea-water) or a direct shaft.

- Generation stage: Generating electric current from the transmission energy. Together with the transmission stage, this is called the PTO system. Often used hydraulic systems generally contain a hydraulic motor, used to generate electricity. Other systems can make use of air turbines, low head water pressure turbines, linear generators or a direct drive mechanical PTO. [44]
- Conditioning stage: Conversion (and transmission) of the generated electric charges to the right type of current and voltage to deliver to the power grid.

2.2. Absorption principles

Wave energy converters can be classified in several ways: by operating water depth, the size directional to the waves or the working principle of the absorption stage. The most popular classification criteria the latter. There are three main distinctions to be made in WEC concepts: (See Figure 2.2)

(a) Oscillating water column devices (OWC)
(b) Overtopping devices
(c) Oscillating body devices

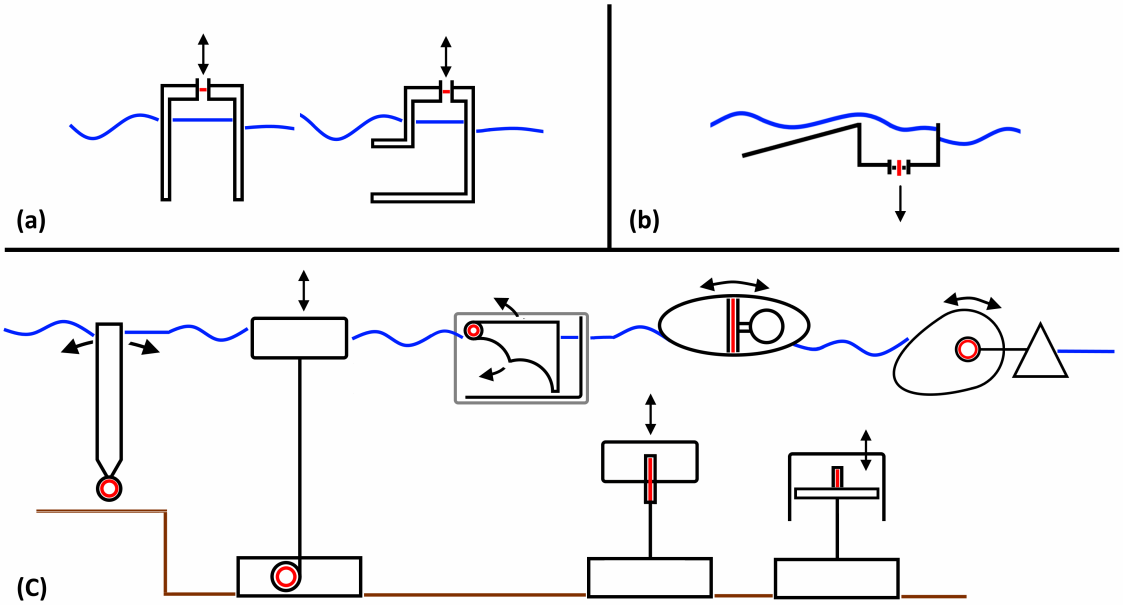

Figure 2.2: Schematic representation of the three categories of converter principles: (a) Oscillating water columns, (b) Overtopping converters (c) Oscillating bodies (excitation due to wave forces)

This classification and many examples of designs tested in the past are described by, [21], [16] and per country of origin in [41]. A general discription is given in the following subchapters, more device examples are placed in Appendix F.

2.2.1. Oscillating water column devices

Oscillating water column devices (OWC's) consists of a half-submerged shaft in which water can enter and exit enforced by the local wave pressure. Inside the device, above the oscillating water surface, a volume of air is forced trough a turbine in either inward or outward direction. These concepts contain turbines that are able to maintain their rotational direction even though the air flow is bi-directional. The efficiency of a one-directional turbine is generally higher than two-directional turbines. However, a separate inflow and outflow would require

two turbines which would be much less costs efficient. Concepts of this type exist with multiple chambers in an array.

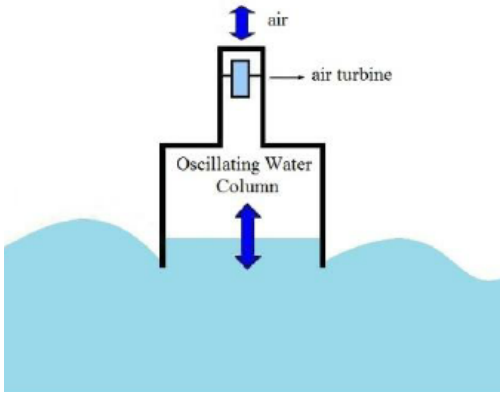

(a)

(b)

Figure 2.3: Example of an oscillating water column device: (a) schematic representation (source: [35]) and (b) WEC by Havkraft

2.2.2. Overtopping devices

Overtopping systems force water to pass over the structure into a reservoir, that is elevated above the sea water level. The water in the reservoir is released back to sea through turbines that produce power.

A typical example of such a converter is the Wave Dragon, see fig. 2.4(b). The rated capacity of this device is 1.5 – 12 MW depending on the wave climate at the deployment site. [15]

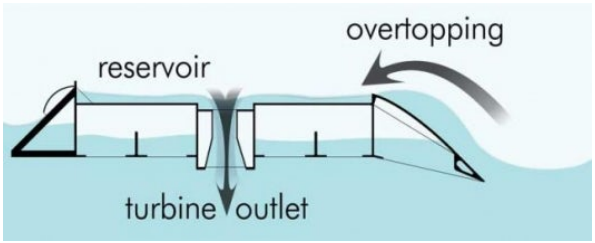

(a)

(b)

Figure 2.4: Example of an overtopping device: (a) schematic representation (source: [49]) and (b) WEC by WaveDragon

2.2.3. Oscillating body devices

The majority of concepts in development are rigid-bodies that oscillate, due to excitation by wave induced forces. The motion of the body relative to a reference object is utilised for the extraction of power. Power is produced by applying resistance through damping on the relative velocity with the reference object. The reference object is often the connection to a fixed structure (the seabed or a platform). Sometimes the oscillating body is connected to another object in the water with a difference in phase (submerged or floating reference objects).

Many combinations of shapes and modes of motion (translations or rotations) have been demonstrated. Another important distinction is found in floating versus submerged devices.

- Fixed oscillating wave surge converter

- Floating oscillating wave surge converter
- Point absorbers (combinations of surge, heave, pitch)
- Pitching devices
- Hinged floating bodies

Two examples of oscillating bodies are the Oyster (a fixed OWSC by aquamarine, see fig. 2.5(b)), and a point absorber by Seabased, fig. 2.6(b). A technical assessment of fixed OWSC design was performed by Folley et al. (2007) [26].
Oscillating bodies that interact with waves in a similar way in any direction are called point absorbers. In Chapter 4 the different types of point absorbers are described and their characteristics are listed.

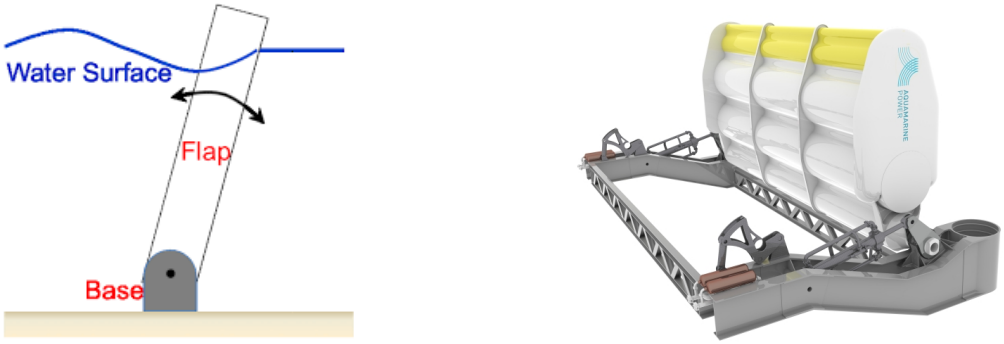

(a) (b)

Figure 2.5: Example of an Oscillating wave flap: (a) schematic representation (source: [34]) and (b) WEC by Seabased Industry AB (SIAB)

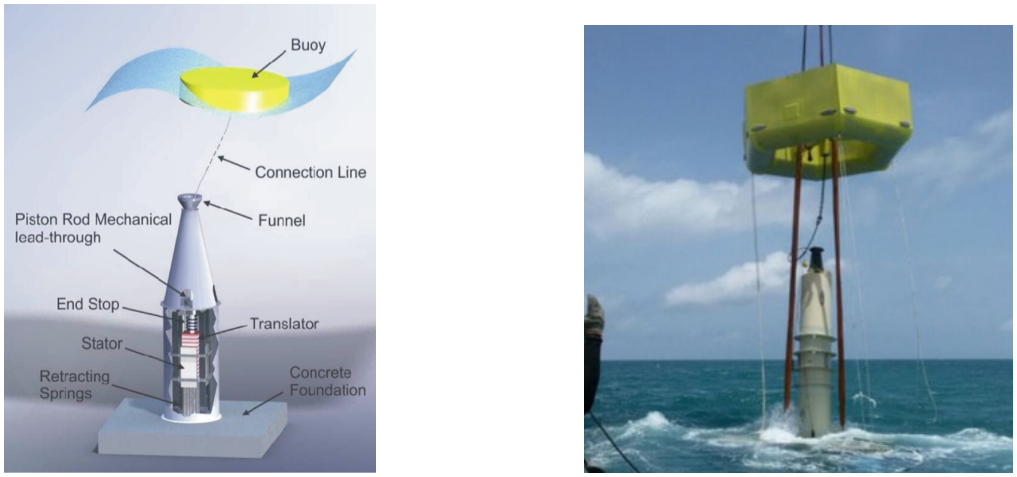

(a) (b)

Figure 2.6: Example of a point absorber developed by Uppsala University (UU) [9]: (a) Schematic representation , (b) WEC by Seabased Industry AB (SIAB)

2.3. Conclusion

The majority of WEC developing organisations are working on oscillating body devices. The category oscillating body devices contains various subcategories with distinctive conceptual differences. Based on research in 2015 [1], the heaving point absorbers and fixed oscillating wave surge converters are most extensively tested. The following chapter explains why this study will focus on Point absorbers.

3. Methods for determining viability

This chapter gives answers to the question: what key performance indicators would best indicate the viability of Wave Energy Converters?

3.1. Commercial viability

Many concepts have been tested and developed. Some successful companies are gradually growing towards the production of commercial concepts, but many companies have failed when mass production started. Failure of a concept is generally attributed to:

1. not being able to meet the economic requirements of commercial application
2. not being able to endure the conditions of the ocean environment

The WEC-industry is expected to experience rapid price decrease once production volumes increase, similar to the transformation of the wind industry, Reaching competitive price levels when experiences are improved and a first 10 MW power plant is installed. Unlike the wind industry however, opinions about best practices are widely spread and indecisive on what type of WEC-system should be up to this task. This would imply, not to ask ”if” WEC will have a break trough, rather the question should be asked ”how soon” and by ”what concept” a level of maturity is accomplished. This implication is emphasised when considering the following set of outlines:

1. the trend of continuous improvement of marine technology,
2. the oceanic waves potentially provide a significant amount of energy,
3. the global trend of increasing consumption of electric energy,
4. a significant market potential, as the percentage of the global population that lives in reach of this resource is significant (with a conservative estimate of at least 1% of the population, going up to 10% or even more, when including lower levels of wave energy).

This unveils a need for convergence towards one WEC-concept and the urge for a method to distinguish concepts that are promising. The main goal of this thesis is to assess the methods to rate commercial success of wave energy converters.

From this perspective it is evident to look at the performance by combining; (A) one technology driven characteristic: the amount of produced energy by a device, with (B) one economic characteristic: the costs over lifetime of that device. Combining these two characteristics into one ratio results in a term, well known in the energy (investment) industry as, levelized cost of energy (LCOE).

3.2. Economical assessment

3.2.1. Levelized Cost of Energy

Levelized Cost of Energy (LCOE) is the ratio of the total costs of the project during the designed life time over the produced energy during the designed life time. Assessment of the LCOE

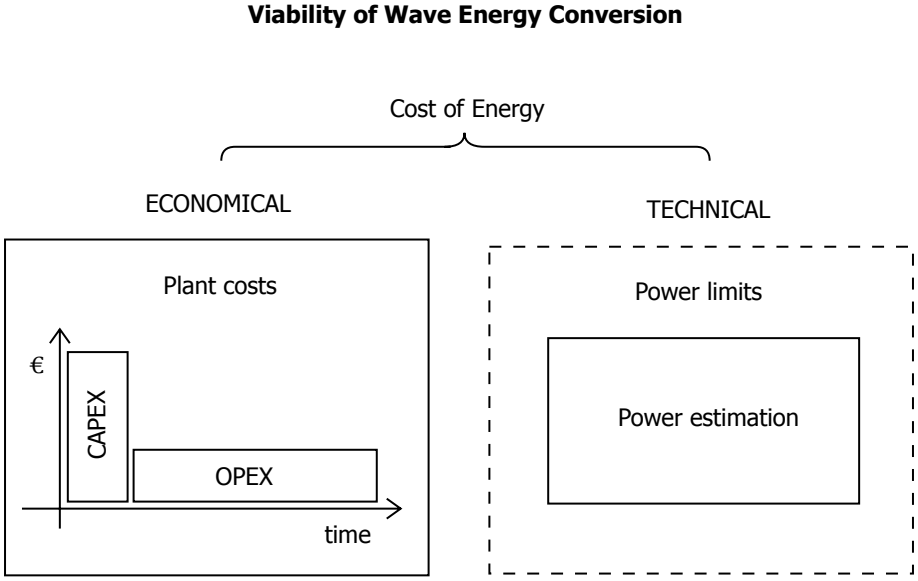

Figure 3.1: Determining viability of wave energy production [43]

indicates what price should minimally be paid for the produced power to cover the project. This makes LCOE an important indicator for both investors as developers. When investment in wind energy concepts are discussed, the LCOE is often mentioned as an aspect to take into consideration [43]. Figure 3.1 illustrates that alongside the economical aspect, the technical performance of a concept is also a vital indicator. Chapter 5 and 6 give a detailled explanation of this determiner.

To give an example that indicates the revenue that can be created by a WEC-device, a basic set of calculations could be applied. In the example in Table 3.1 a fixed Cost of Energy is assumed for delivering electric power to the grid: $0.15€/kWh$. It is however important to note that simplified calculations generally over-estimate the power production, and the outcomes should be assumed indicative.

Table 3.1: Example of basic revenue calculation for a single WEC-device

Input	Parameter	Equation	Value	Unit
J	Resource		30	kW
cw	Effective width		10	m
f	Efficiency of conversion		20	%
C	Consumption p. capita		7000	kWh
$€_{revenue}$	Lifetime cost WEC device		80	$k€$
Calculation				
P_{avg}	Power averaged p.yr	$J \cdot cw \cdot f$	60	kW
E_{yr}	Energy per year	$J \cdot cw \cdot f \cdot (hrs/yr)$	526	MWh
Results				
	Capita provided	E_{yr}/C	75	$\#capita$
$€_{elec}$	Energy price,	$€_{elec}/E_{yr}$	0.15	$€/kWh$

The costs for obtaining LCOE are split capital expenditure (CAPEX) and Operational expenditure (OPEX). Capital expenditure is spent before the start of the project, operational expenditure are costs during the project's operation.

For WEC systems the CAPEX are comprised of expenses for:

- the device
- the mooring and foundation
- the installation
- connection to the grid and development

See Figure 3.2.
In general, the OPEX is assumed to be a smaller (at least by a factor two) than the CAPEX (See Figure 3.3). Large scale production of WEC device is assumed to lead to cost reduction, lowering the CAPEX per device. Increased amounts of devices in a power plant reduces the operational cost per device.

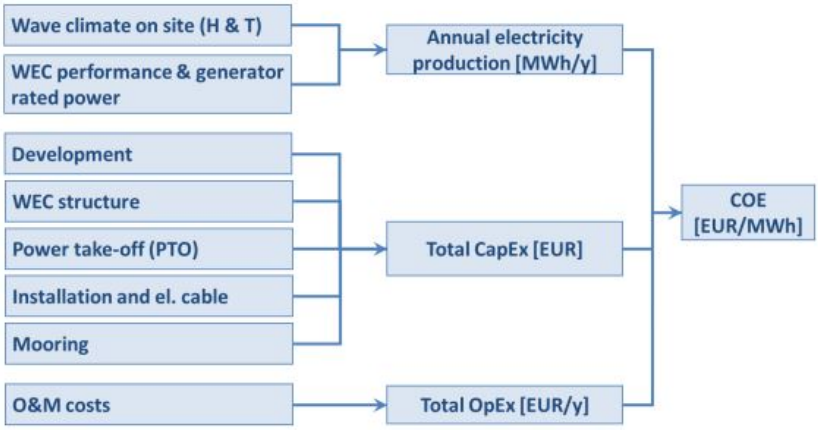

Figure 3.2: Input for LCOE calculations

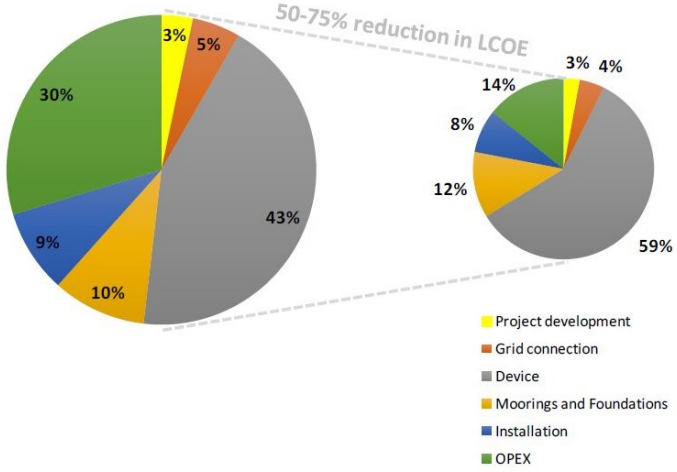

Figure 3.3: chart of cost breakdown before and after development improvements.

Figure 3.4, as example, illustrates the influence of environmental and situational conditions on the cost of energy. By placement of the WEC close or further offshore several parameters influence the cost of energy, resulting in an optimum construction range.

Levelized Cost Of Energy is defined as the present value of all costs over the project lifetime divided by the estimation of the net present value of all energy production over the lifetime. The costs include expenditures such as: planning, permitting, building, connection to power grid, lease, depreciation, service and maintenance, management, costs of scrapping. In calculations the energy production is often obtained on a yearly averaged basis, Averaged Energy

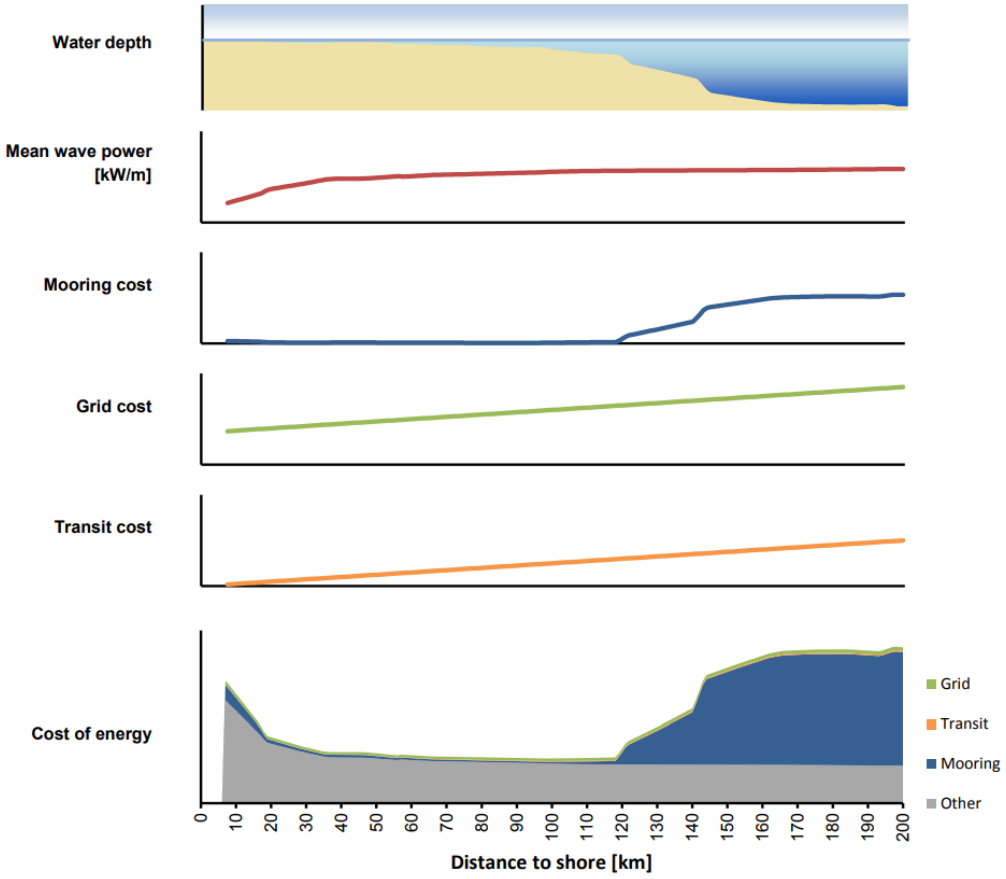

Figure 3.4: Example; Assessment of the influence of coastal variation and distance on cost

Production (AEP). The LCOE is calculated by Equation (3.1).

$$LCOE = \frac{CapEx + \sum_{y=0}^{Y} PV(OpEx_y)}{\sum_{y=0}^{Y} PV(AEP_y)} \tag{3.1a}$$

Where:

$$PV(X) = \frac{X_y}{(1+r)^y} \tag{3.1b}$$

In which:

PV - Present Value
CapEx - Capital expenditure [Eur]
OpEx - Operational expenditure [Eur]
AEP - Annual Electricity production [MWh/y]
r - Discount rate
Y - Lifetime of the system
y - Year from start of project

For simplicity the CapEx is assumed to occur in year zero.

3.2.2. LCOE in literature

The research project Opera WP7, resulted in a cost of energy model. Besides the LCOE assessment it also included Life-cycle assessment and socio-economic cost of energy calculations, and is therefor referred to as the Global Economic Model.

In a publication by Chozas [10], an overview is created for three development stages of wave energy, compared to tidal energy and OTEC technology. See Table 3.2. The maximum operational cost (OPEX) estimations presented here, show to be only 80% of the OPEX presented in [43, p. 130]. So this study is assumed to be more on the (over)optimistic side compared to a more conservative result by Costello & Pecher.

Table 3.2: Performance range estimations for wave, tidal and OTEC in three stages of development, based on research by F. Chozas.

Deployment Stage	Variable	Wave		Tidal		OTEC	
		Min	Max[1]	Min	Max	Min	Max
First array / First Project[2]	Project Capacity (MW)	1	3 [3]	0.3	10	0.1	5
	CAPEX ($/kW)	4000	18100	5100	14600	25000	45000
	OPEX ($/kW per year)	140	1500	160	1160	800	1440
Second array/ Second Project	Project Capacity (MW)	1	10	0.5	28	10	20
	CAPEX ($/kW)	3600	15300	4300	8700	15000	30000
	OPEX ($/kW per year)	100	500	150	530	480	950
	Availability (%)	85%	98%	85%	98%	95%	95%
	Capacity Factor (%)	30%	35%	35%	42%	97%	97%
	LCOE ($/MWh)	210	670	210	470	350	650
First Commercial-scale Project	Project Capacity (MW)	2	75	3	90	100	100
	CAPEX ($/kW)	2700	9100	3300	5600	7000	13000
	OPEX ($/kW per year)	70	380	90	400	340	620
	Availability (%)	95%	98%	92%	98%	95%	95%
	Capacity Factor (%)	35%	40%	35%	40%	97%	97%
	LCOE ($/MWh)	120	470	130	280	150	280

The study showed an estimation of the LCOE breakdown in percentages for wave energy in general with distinction of first array projects to full scale commercial projects. See Table 3.2. This table shows that the expenses for first arrays devices itself are generally comprising 43% of the total project and the operational costs are estimated to consume one-third of the project budget. When the concept is developed in full commercial scale, the operational costs are estimated to take up 40% while the device costs only one-third of the total project expenses. The other expenses only reduce a few percentage in this estimation, except for the mooring and foundation part which increases, this might be caused by design for larger forces and longer project design life for the commercial scale project.

About the expectations for LCOE on short a term, the publication concluded: ”At commercial scale, developers expect a rapid decrease in LCOE through learning, innovation and scale leading to around 100-300 $\$/MWh$.”

The handbook of ocean wave energy, [43, p. 130] describes a method of calculating the LCOE for a wave production field in comparison with Wind energy field. Interestingly, a strong separation is made between device cost and general cost. Parts of the cost breakdown have been assumed independent of the device, so expenses have been estimated for these items.

For the final calculation, the LCOE calculation, costs that are assumed to be independent from the device are: Development and consent, Installation and commissioning and the OpEx. Another efficient assumption is made, since the size of the field is assumed fixed,

Table 3.3: Calculation method used by Costello & Pecher: Device independent balance compared to wind energy in costs per unit: 90 MW farm of 25 x3.6MW WT and WEC and of 120 x 0.75MW WEC - [43]

Category and sub-category	3.6 MW wind (k€)	3.6 MW WEC (k€)	0.75 MW WEC (k€)
Tower/Mooring	972	X	X
Foundations	2592	X	X
Cables			
Inter array	227	227	47
Export	664	664	138
Offshore substation			
electrical	810	810	270
Other	227	227	47
Onshore electrical			
Electrical	324	324	68
Other	113	113	24
Total	5929	2365 + X	594 + X

a the base capacity factor could be assumed partially independent of the device. This results in a mean annual energy production, which is used to calculate the 'base' LCOE, without the LCOE for the device. One comment on this text is that it is not consistent with the use of the "X". First the X is demeaning the device cost and in the same figure it should contain the LCOE of the device (Device cost divided by mean annual energy production).

Figure 3.5: Calculation method used by Costello & Pecher: Device independent Total cost breakdown overview compared to wind energy, costs per unit: 90 MW farm of 25 x3.6MW WT and WEC and of 120 x 0.75MW WEC

Costs	3.6 MW Wind (k€)	3.6 MW WEC (k€)	0.75 MW WEC (k€)
Development and consent	649	588	271
Turbine/WEC	5281	X	X
Balance of plant	5929	2365 + X	594 + X
Installation and commissioning	4163	2219	1077
Total CapEx	**16022**	**5822 + X**	**1941 + X**
Annual OpEx	721	721	361
Discounted OpEx (20 years)	**6138**	**6138**	**3069**
Total (CapEx & OpEx) costs	22160	11960 + X	5010 + X
Revenue			
Approx. capacity factor (%)	30	30	20
Mean annual energy production (MWh)	9467	9467	1315
Levelized cost of energy	(€/kWh)	(€/kWh)	(€/kWh)
Base LCoE (without OpEx)	0.085	**0.031 + X**	**0.074 + X**
Total LCoE	**0.117**	**0.063 + X**	**0.191 + X**

In a study about cost-breakdown and LCOE calculation published in [14], a separate calculation is performed per device type (categorisation by wave-body interaction type). As it includes a low, average and max expenditure case this study gives insight in the range where devices are practical and where developers could find cost items that need improvement. For half of the device types the connection costs and installation costs show to be critical cost items. Costs for the structure, PTO and O&M are the least critical items concluding this research.

3.2.3. LCOE tools

Research performed by Chozas (2015) [10] resulted in a comprehensive calculation tool openly available. A positive aspect of this tool is that, although this tool was designed for more extensive analysis at an advanced development stage, this tool can already be used in an early stage due to predefined input values.

Publication [13] stated in 2014, that the LCOE levels are 1.7 - 5 Eur/kWh. It concluded that the LCOE should decrease significantly in order to compete with other renewable sources such as offshore wind. It also states that for the studied scenarios the bottom mounted devices are significantly outperformed by the floating devices. (Detail: Surprisingly the average resource values for EMEC test site are 30% higher than used in [4].)

A more recent publication [46] from 2018, presents an estimation of the wave energy LCOE. But this information is based on a report from the world energy council from 2013 which used values in US dollars. It presents the LCOE for high costs at: € 897/MWh, for medium costs at: € 420/MWh and for low costs at: € 241/MWh.

3.2.4. LCOE forecast

Carbon Trust conducted research at realistic expectations for LCOE in the future, and concluded that €19 cents/kWh by 2050 would be achievable. This is still much higher than offshore wind. [17].

SI Ocean published an LCOE outlook on renewable energy for the period 2017 to 2050, and concluded that a LCOE could be achieved, that is similar to the current LCOE of offshore wind [48], see Figure 3.6.

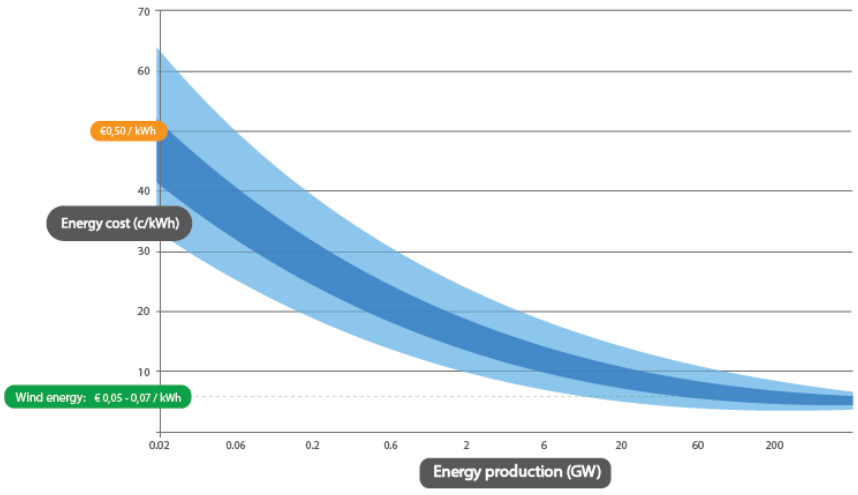

Figure 3.6: LCOE prediction after the first project of 10 MW is installed.

3.3. Technical assessment

Alongside the complexity of economic estimation, the main technical difficulty in obtaining comparable LCOE values, is found in the accuracy of predicting wave power production.

Computational modelling is used for establishing this early-stage prediction of the production of wave power. Recent reviews on the current-state of theoretical and numerical modelling of WEC's are given by: Folley (2016) [25], Falcão (2010) [21], Cruz (2007) [12] and Falnes (2007) [23].

From the literature, two paths have been assessed, for defining this early-stage potential power production: a so called *bottom-up* approach and a *top-down* approach. The top-down approach defines boundaries for achievable energy extraction for a body forced by waves, equivalent to the Betz-limit that exists for wind energy turbines. The bottom-up approach assembles all the dynamical and electrical aspects to create a calculation model to create estimates of power production for specified environmental circumstances.

Examples for the top-down and bottom-up methods are found in literature. A few studies attempted to perform power calculations for several different WEC-concepts in order to make a comparison between their power production. From these comparison studies have many insights could be gained and they influenced several ventures for WEC projects.

The bottom-up method estimates power performance of concepts in certain conditions. This is applied in Method 1 by Babarit[4]. The top down method described by Sergiienko [47] (Method 2) addresses the theoretical power that can be absorbed by a buoy while leaving out power losses, as they are often dependent on improvements by technological advancements.

3.3.1. The need for maximum power absorption limits

The energy available in waves, often used as reference for efficiency, is the first step of defining the theoretical power. When the absorber shape and depth is not changed there is a limit that can be described for the system including both: waves and absorber. These limits where first described by Budal and Falnes (1980) [8]. These are fundamental equations of maximum power absorption for axisymmetric bodies that are floating or submerged. For development of WEC's these limits are an important guide for designing for efficiency based on local environmental wave conditions. Another part of the importance is linked to concept comparison. Concepts are not easily compared on their competences for the future in an objective manner as their level of technology may be in different stages of development.

On the one hand, this top-down method explains the differences in power extraction between different concepts. On the other hand it also presents the margin of improvement that technological enhancements on a concept still can achieve by an improved power take-off device or control strategy.

3.3.2. Dynamic modelling with time-domain simulations

With the bottom up-approach, power performance is calculated based on as much detailed conceptual characteristics as is available. This approach is often referred to as Wave-to-Wire modelling, because the estimation for power performance is quantified by numerical simulations of a dynamic representation of a concept under a computational representation of local wave conditions. When every detail is known this approach accurately predicts the power performance. However, in early stage not all details are set, therefore introducing errors due to rough estimates or oversimplification.

Babarit et al. (2012) [4], presents a comparison of 8 different types of WEC-devices. For these 8 devices, the yearly averaged power levels at 5 locations are calculated. A computational physical model is created, representing the dynamic behaviour for every WEC-device. The dynamic models are used in time-domain simulations. The result is the total produced energy during the simulation from which the averaged produced power of the device is derived (AEP). The paper selected 8 different designs that had different dimensions, causing difficulty for

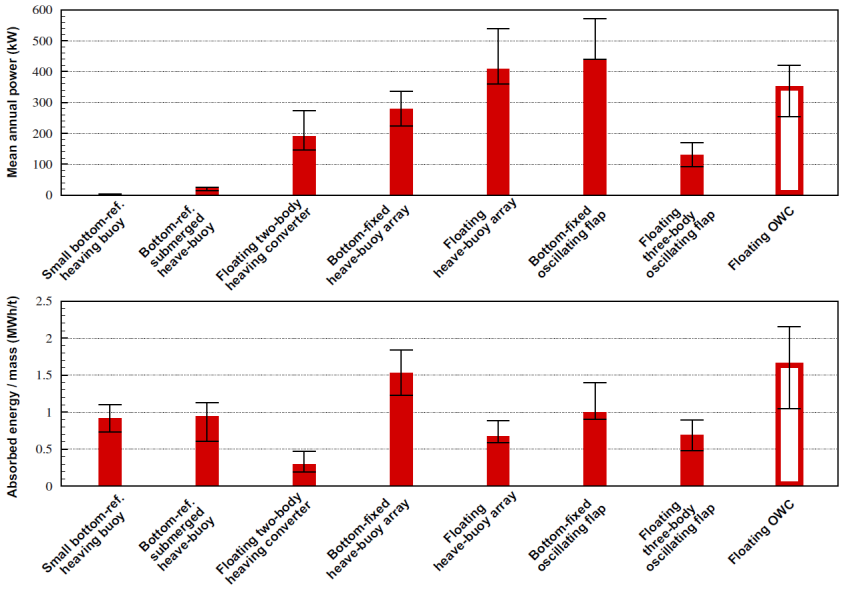

Figure 3.7: Results by Babarit et al. (2012) [4]

making a fair comparison of their performance. In order to compare their result the paper tried several ratios, one of them is the ratio for produced energy (E_y) over mass (m).

$$\frac{E_y}{m} \quad [W/kgorm^2/s^2] \tag{3.2}$$

Since the mass of an object is often assumed proportional to its cost price, could be seen as the closest alternative to LCOE. Note however that the two are inversely related, such that, at an increase of the produced energy, the LCOE becomes smaller as it is obtained from costs over energy production, while the ratio for produced energy over mass becomes larger. The results are shown in Figure 3.7.

3.4. Conclusion

Useful methods for performance estimation of WEC-devices are comprehensively described by the studies of Babarit et al. (2012) [4] and Sergiienko et al. (2017) [47]. Dynamic modelling of a different WEC-devices in time-domain simulations (wave-to-wire modelling) allows to compare power performance under similar wave conditions. However, this comparison is prone to bias by different levels of optimisation that are applied to the tested designs. This mainly refers to the optimisation of the control strategy used for the power-take-off system. Until the implementation costs of these different strategies can be taken into account, the comparison is only indicative. Theoretical power limits help to assess the absorption efficiency and allow for a more singular comparison between devices. The economics of WEC's show that the current cost of energy production with WEC's is much higher than in offshore wind power production. Although, studies for the future outlook of WEC show the prognosis for a change towards competitive cost of energy levels under certain circumstances.

4. Point Absorbers

This chapter discusses the different types of point absorbers as a category of WEC-devices.

4.1. Introduction to Point Absorbers

Point absorbers are a type of oscillating body devices that consist of a small buoy in comparison with one wavelength, and interacts with the wave field similarly in all directions. Two types of point absorbers can be defined by the position of the buoy. It is either floating or submerged. In general point absorbers are a source-mode radiator. This means that the motion of the body in still water creates a radial outwards travelling wave, see Figure 4.1(a).

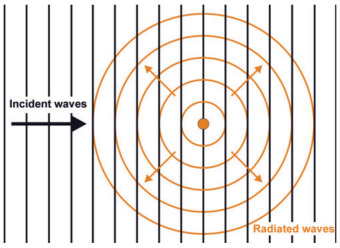

(a) Point Absorber radiation pattern

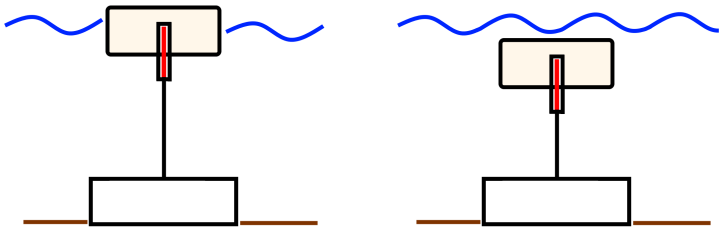

(b) floating point absorber (c) submerged point absorber

Figure 4.1: Schematic illustrations of (a) radiation pattern[28], a floating point absorber (b) and a submerged point absorber (c)

Harleman and Shapiro (1960) [27] first studied submerged moored spheres oscillatory waves. The interaction of waves on fixed bodies was extensively described by Newman and Taylor (1963) [39]. this formed the basis of the patential theory. The interaction with small buoys is studied in detail by Budal and Falnes in (1974) [6] and (1975) [7] (And his corrections to that work: Budal (1975) [5])

Mavrakos et al [37] investigated the power absorption performance of a tightly moored symmetric WEC.

The following sections discuss both the technological and economic aspects of point absorbers based on two specific studies.

4.2. Technical assessment

In order assess the two methods for performance comparison of WEC's (described in 1), first the dynamics of these systems has to be discussed in more detail.

4.2.1. Dynamics of point absorbers

A good wave absorber has to be a good wave maker [22]

When a buoy in water is brought into motion, part of the energy that was present in the incoming wave is translated into kinetic and potential energy in the buoy. In order to absorb energy from a wave the buoy has to move in a manner that otherwise, in calm water, would have created a wave. In the ideal situation, the produced wave patterns cancel out the transmitted wave behind the buoy. In this idealised situation, optimal buoy motions in surge, heave and pitch allow absorption of all incoming energy from the waves. This means that behind the buoy no wave energy is transmitted. This theoretical ideal situation is depicted in Figure 4.2. The power is extracted from the motion of the floating or submerged buoy. The

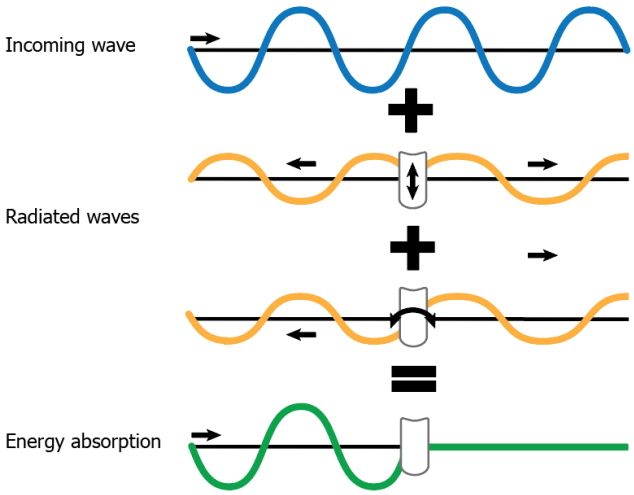

Figure 4.2: The summation of wave heights produced in front and rear direction shows how in theory all incoming wave energy can be absorbed. [28]

system that extracts the power is the Power Take-Off system (PTO). This system is therefore connects the buoy to a reference point. For convenience this reference point is assumed to be the bottom. In a linear simplification for the PTO the forces are defined by linear constants for stiffness and damping. Figure 4.3, shows a floating buoy with a spring and damper PTO system. The Power Take-off system (PTO) converts the mechanical power from the body into electrical power. For dynamic modelling of the system the PTO-system is often simplified to a linear system with a spring and damping coefficient. When all forces on a moored buoy moving in water are considered, as shown in Equation (4.1), then the Equation of Motion (EOM) can be defined.

$$m\ddot{z} = F_{hs} + F_{exc} + F_{rad} + F_{PTO} + F_m + F_v \tag{4.1}$$

m - Mass matrix of the object [kg]
$\ddot{z}$ - Acceleration vector of WEC $[m/s^2]$
F_{hs} - Hydrostatic restoring force [N]
F_{exc} - Wave excitation force [N]
F_{rad} - Radiation force [N]

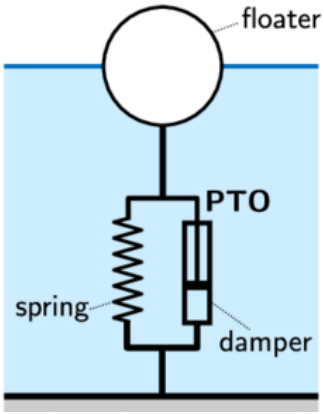

Figure 4.3: Example: schematic model of a floating buoy WEC with submerged PTO

F_{PTO} - Power Take-Off force [N]
F_m - Mooring force [N]
F_v - Viscous forces [N]

The first important difference between a floating and a submerged buoy is in the hydrostatic restoring force. The hydrostatic restoring force for a floating buoy (F_{hs}) is equal to the weight of its displaced water.

$$F_{hs} = \rho g A_{wp} z \tag{4.2}$$

Where A_{wp} is the water plane area of the buoy. And z is the vertical displacement from the buoy's balanced position. This restoring force is the result from the force balance between the weight of the buoy and the weight of the displaced water (∇). This balance is: $\rho g \nabla = gm$.

For a buoy that is fully submerged, there is no restoring force because the displaced water (∇) is constant for variations of the vertical position (z) (within the submerged range). In Equation (4.3), the EOM are presented for heave motion. In this equation the incoming wave is simplified to a sinusoidal function. The excitation force is assumed to be a linear oscillation (a regular wave) of the form: $F_{exc} = F_0 \cos(\omega t)$. Here F_0 is the amplitude of the oscillation and ω is the radial wave frequency, and t is time. For a more realistic representation (irregular waves) the incoming waves often are assumed to consists of a finite summation of different sinusoidal functions. (The theoretical background of waves and motions is included in Appendix A).

$$(m + a)\ddot{z} + (b_{rad} + b_{PTO})\dot{z} + (k_{hs} + k_m)\ddot{z} + F_v = F_0 \cos(\omega t) \tag{4.3}$$

In which:

a_{mass} - Added mass $[kg]$
z - Displacement of the buoy $[m/s^2]$
$\dot{z}$ - Velocity of the buoy $[m/s^2]$
b_{rad} - Radiation damping coefficient $[Ns/m]$
b_{PTO} - Power Take-Off damping coefficient $[Ns/m]$
k_{hs} - Hydrostatic stiffness $[N/m]$
k_m - Mooring stiffness $[N/m]$

The Radiation damping coefficient (b_{rad}), Added mass (a_{mass}) and Excitation loads (F_{exc}) are hydrodynamic coefficients. They represent the interaction of the body with water. Calculation methods to obtain the hydrodynamic coefficients assume the forces on a floating body in waves to be composed from two separate (experimental) situations, that can be described by three components in the equation. The first situation observes the forces on a body due to

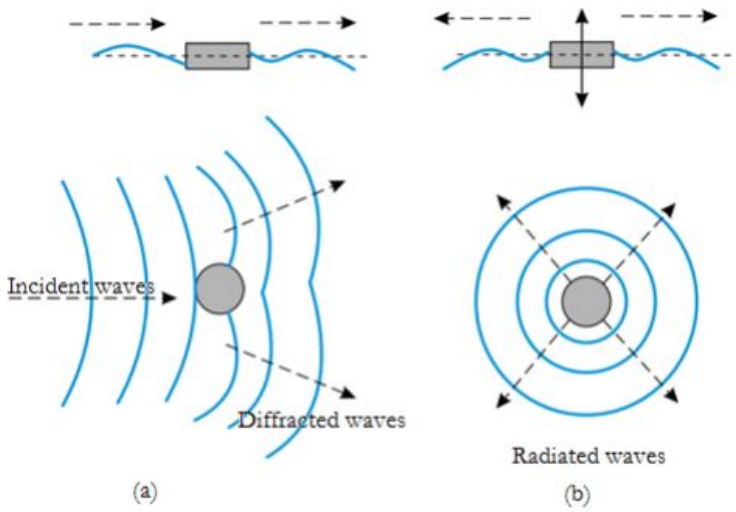

Figure 4.4: Diffraction and radiation for a point absorber

motion in still water, this is where b_{rad} and a_{mass} are obtained. The second situation observes the forces of a fixed body subjected to waves, resulting in the (F_{exc}). The first situation is generally described in the equations by two components, a static part, the hydrostatic restoring force (F_{hs}) and a dynamic part, the radiation force F_{rad}. In turn, also the dynamic part consists of two components: the damping (b_{rad}) and the added mass (m_a)). Figure 4.4 displays the diffraction effect of a fixed body on the incoming waves (a), and the radiation effect of body motion in calm water (b).

As a reaction to the wave excitation forces, the motion of the body may be assumed to be also a sinusoidal function, but now with a certain delay to the force (phase difference) so that: $z = z_0 \sin(\omega t - \phi)$. The equation of motion in Equation (4.3) can now be rearranged. As a result the solution for heave displacement is obtained, Equation (4.4). For convenience the viscous force F_v is neglected here.

$$\hat{z}_0 = \frac{1}{\omega} \frac{F_0}{\left\{ b_{rad}^2 + \left(\omega(m + a_{mass}) - \frac{c}{\omega} \right)^2 \right\}^{\frac{1}{2}}} \tag{4.4}$$

F_0 - Excitation force $[N]$
m - Mass $[kg]$
z - Vertical displacement of the buoy $[m]$
a_{mass} - Added mass $[kg]$
$\dot{z}$ - Vertical velocity of the buoy $[m/s]$
ω - Radial frequency $[rad/s]$
c - Hydrostatic stiffness coefficient $[N/m]$

With use of the displacement equation, the absorbed power can be derived. The power is obtained by multiplying the damping force $[N]$ and velocity $[m/s]$, $P_{PTO} = F_{PTO} z$. The damping force is already presented in the equation of motion $F_{PTO} = b_{PTO} z$. Therefore, the power is defined as $P_{PTO} = b_{PTO} \dot{z}$. Further derivation of the power equations is found in D. The largest heave amplitudes of the buoy z_0 are found at the resonance frequency, when the buoy is excited by the wave force with a frequency close to the natural frequency of the buoy.

To obtain a system that acts in resonance at certain wave frequency, the right balance is required between mass, stiffness and damping of the system. Figure 4.5 shows the heave

amplitudes for an arbitrary floating body. It demonstrated that the object in waves with very large wave periods, moves along with the wave amplitude. And the system is said to be dominated by spring terms. For very short wave periods the motion is dominated by the mass terms of the object as it will oscillate with a much smaller amplitude than the wave amplitude. Close to the resonance period the body will move with larger amplitudes than the wave amplitude as nearly all of the wave excitation force over time contributes to the amplification of the bodies oscillatory motion.

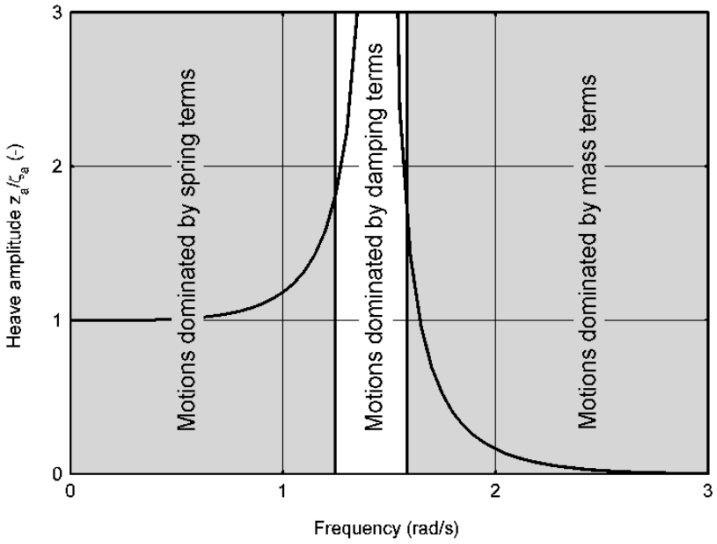

Figure 4.5: The amplification of a floating body. [32]

A floating or a submerged buoy point absorber in general has a fixed mass and a fixed water displacement ∇. As waves generally are described by a period, it is convenient to use period instead of frequency ($T = 1/f$). For a floating buoy this resonance period is:

$$T_{fl,heave} = 2\pi \sqrt{\frac{m + a_{mass}}{\rho g A_{wp}}} \tag{4.5}$$

$T_{fl,heave}$ - Resonance period of a floating buoy in heave $[s]$
A_{wp} - Water plane area of the buoy $[m/s^2]$

As submerged buoys have no natural restoring force there is only resonance by introducing a mooring stiffness. For a submerged buoy this resonance period is therefor:

$$T_{sub,heave} = 2\pi \sqrt{\frac{m + a_{mass}}{k_m}} \tag{4.6}$$

$T_{sub,heave}$ - Resonance period of a submerged buoy in heave $[s]$
k_m - Mooring stiffness of the buoy $[N/m]$

The theoretical maximum power ($P_{max,heave}$) that can be absorbed by the heave motion of this body in regular waves is described by Equation (4.7). This result is described in Falnes (2002) [22]. It is a theoretical maximum since lossess are always present in reality. This equation of maximum power is obtained assuming resonance conditions, and requires that the power take-off damping (b_{pto}) is equal to the hydrostatic damping (b_{rad}).

$$P_{max,heave} = \frac{1}{8} \frac{F_0^2}{b_{rad}} \tag{4.7}$$

$P_{max,heave}$ - Maximum absorbed power of a buoy in heave $[s]$
F_0 - Amplitude of the wave excitation force $[N]$

For a irregular waves, defined by a spectrum, the theoretical maximum power ($P_{max,heave}$) is described by Equation (4.8).

$$P_{max,heave} = \frac{1}{4}\frac{(\frac{F_0}{\eta_a})^2}{4b_{rad}}\frac{H_s^2}{16} \tag{4.8}$$

H_s - Significant wave height $[m]$
f_0 - Response Amplitude Operator of the wave excitation force (Force RAO) for a unit wave amplitude ($\eta_a = 1$) $[N/m]$

These equations show that the maximum power that can be absorbed by a heaving buoy is positively influenced by the wave excitation force squared. While the radiation damping negatively influences the maximum absorbed power.

4.2.2. Estimations of power performance by dynamic modelling

Determining the Annual Energy Production (AEP), as described in 3.2.1, is required for the assessment of the levelized cost of energy for a wave energy converter. A quantitative method for estimating the AEP applicable to multiple locations can be obtained when the device characteristics for power production are calculated for a range of sea states using a dynamic model of the WEC-system. These characteristics can then be used in connection with local wave data to obtain local performance estimates. Babarit et al. (2012) [4] shows for various WEC-device types, how a dynamic model is created that resembles the most important characteristics of the device. The schematic drawings of the systems dynamic representation for floating and submerged point absorbers are presented in Figure 4.6 and Figure 4.6. The systems dynamic representation consists of several combined functionalists such as, a hydrodynamic object, a power take off system and motion constraints that define the degree of freedom of all connection points.

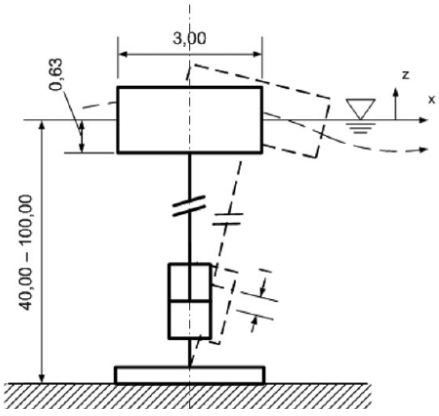

Figure 4.6: Schematic of a floating PA

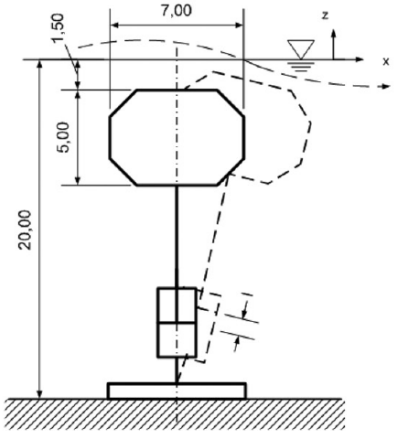

Figure 4.7: Schematic of a submerged PA

Power production characteristics of a concept can be captured in a power matrix. This power matrix consists of averaged power production values for a range of wave heights (on the vertical axis) and a range of wave periods (on the horizontal axis). The local wave data is captured in a wave scatter-diagram, and contains values for occurrence of a sea-state (the combination of wave-height and wave period). The scatter-diagram has similar axis as the power matrix with the values in hours or percentage of time in a year. The creation of a Power

Matrix is described in: [33]. In Figure 4.8(a) and Figure 4.8(a) the power matrix for floating and submerged point absorbers are included, that are obtained by Babarit et al. (2012) [4].

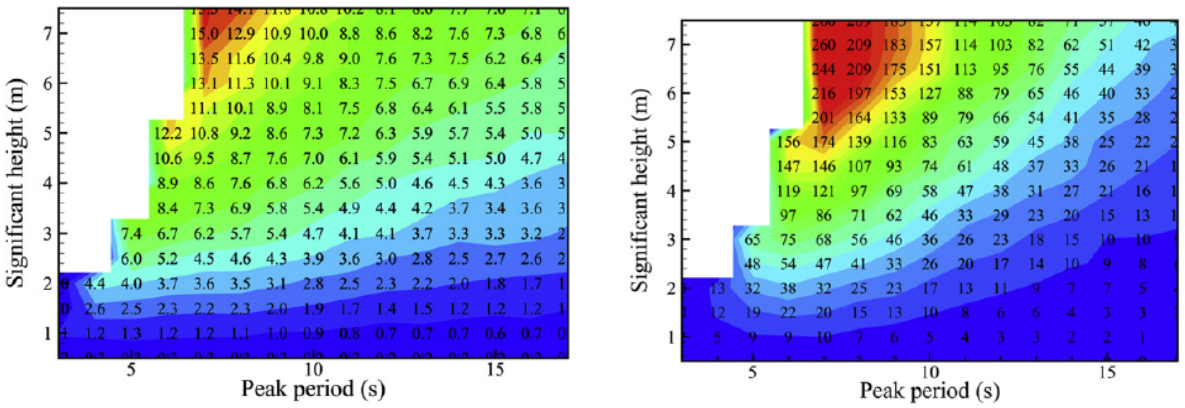

(a) floating point absorber (b) submerged point absorber

Figure 4.8: Schematic illustrations of a floating point absorber (left) and a submerged point absorber (right)

4.2.3. Maximum power absorption limits

Similar to the Betz limits for wind power generation [52], limits for point absorbers are established. The theory for limitations in power absorption have been established by both Budal & Falnes and Evans. Evans published his work first in 1976 (Evans (1976) [18]) and reviewed the topic in 1981 (Evans (1981) [20]).

The limits present the maximum power that can be obtained from the waves by the method shape and motion of hydrodynamic subsystem of this device. These limits show the margin of improvement that technological enhancements still can achieve.

Two limits for power production can be defined: P_a and P_b. The first boundary (P_a) corresponds to the maximum energy that can be removed from an incident wave by the objects ability to radiate waves in order to compensate incoming waves. This compensation leads to absorption. P_b is defined as the power production growth by increasing device width.

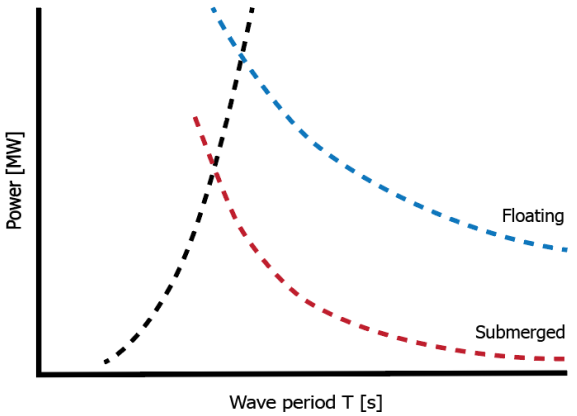

Figure 4.9: Budal diagrams, showing the upper bounds for power absorption of floating and submerged point absorbers of similar shape and size. Sergiienko et al. (2017) [47]

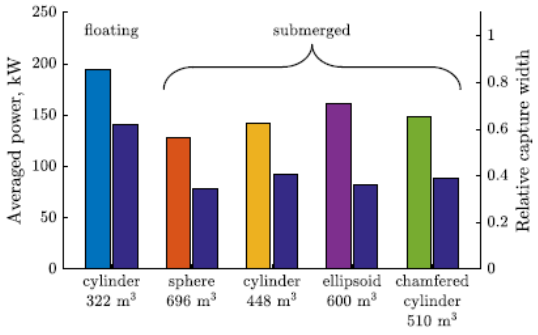

Figure 4.10: Levels of the averaged absorbed power(colour bars on the left) and relative capture width (dark blue bars on the right) of the floating and submerged converters at the irregular wave time-series of $H_s = 2.83m$ and $T_p = 10s$. Sergiienko et al. (2017) [47]

Figure 4.11 and Figure 4.12 show results from Sergiienko et al. (2017) [47]. They show the relation between different dimensions and between different array configurations. The

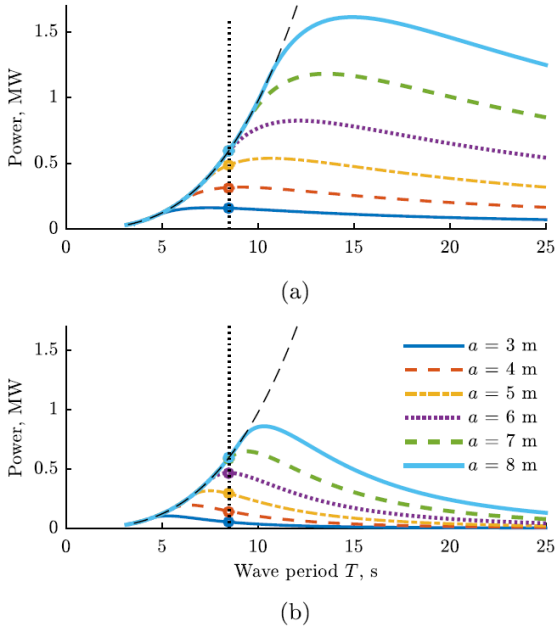

Figure 4.11: The Sergiienko et al. (2017) [47]

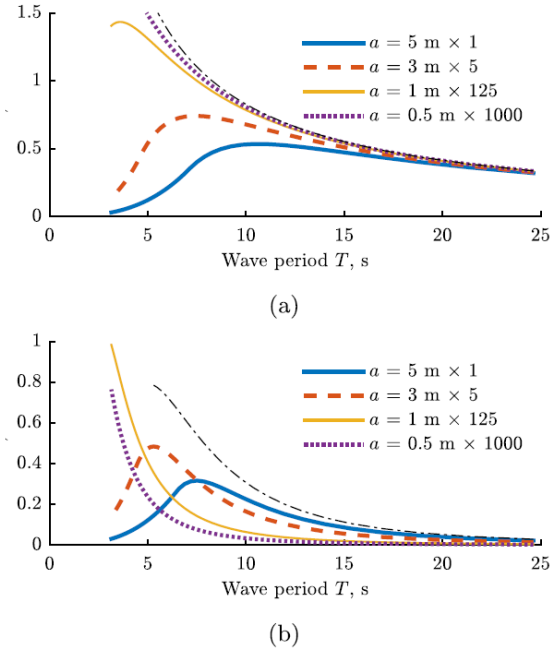

Figure 4.12: The Sergiienko et al. (2017) [47]

first figure shows that an increase in buoy diameter increases the absorbed power, both for floating and submerged buoys (top and bottom image). An increase of dimensions in all direction would however increase the volume to the power third. When the likely assumption is made that costs increase for an increased WEC volume, it suggests there would be an optimum for the amount and volume of WEC devices in an array. An assessment for such an optimum is presented by the second figure (Figure 4.12), where the total volume of WEC's is kept constant, while the amount of WEC's varies. The performance of one floating buoy with a diameter of five meter is surpassed by a group of 5 buoys with a diameter of three meter. For floating buoys this seems to continue for even smaller buoys. For a submerged buoy, this is different, a smaller buoy diameter means a reduction of power at long wave periods, while the increased performance peak is shifting towards the shorter waves. These relations are relevant to assess the opportunities for up-scaling a WEC-device.

The power absorption depends on the wave excitation force, and a floating buoy is more optimal subjected to wave forces than a similar submerged buoy Sergiienko et al. (2017) [47]. A derivation to this conclusion is described in Appendix D. When the power in waves is described as $J = (\rho g^2 D(kh)/(8\omega k))|A|^2$, (Appendix C) the maximum absorption width (ratio between P and J) is:

$$d_{max} = \frac{P_{max}}{J} = \frac{1}{k} = \frac{\lambda}{2\pi} \tag{4.9}$$

d_{max} - Present Value $[m]$
P_{max} - Maximum absorbed power $[W]$
J - Resource Wave Power $[W]$
k - Wave number $[m^-1]$
λ - Wave length $[m]$

Here $D(kh)$ is the function for the depth, and $D(kh)$ equals 1 for deep water. This result was found independently by Budal and Falnes [8] and Evans [19].

Figure 4.9 illustrates the different for power absorption limits of floating and submerged point absorbers. As floating devices benefit from the high intensity wave fields at the ocean surface they are able to absorb more energy than submerged buoys.

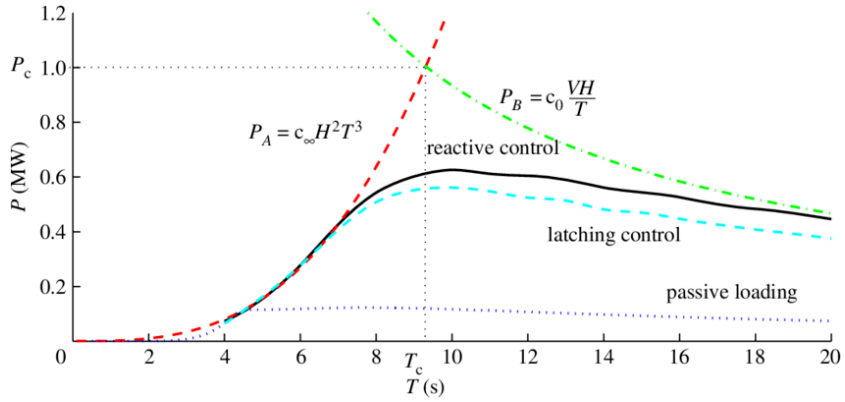

Figure 4.13: Budal diagram for a floating buoy. The indicating the difference in power output for three types of control strategy: passive control, latching control and reactive control. The upper bounds are indicated with P_a and P_b. Source, Falnes and Hals (2012) [24]

Figure 4.13 shows the comparison of numerical results to the upper bounds for a heaving floating sphere in waves. The results are obtained from numerical simulations that applied different complexity levels of control strategies: passive control, latching control and reactive control. For the passive control strategy the PTO characteristics are not changed during operation. For the latching control, the PTO forces the body at certain intervals.

4.3. Submerged pressure differential wave energy converter

This section describes the characteristics of the Submerged Pressure Differential (SPD) device that is used as a test case in this research. This device presents a small submerged buoy, that just like other submerged buoys is in potential more sheltered in storm condition than a floating buoy. However, the working principle is significantly different from the average submerged point absorber. The differences are found in both the wave interaction, as well as in the power-take-off system, as will be assessed and explained in this thesis.

4.3.1. Device description

Company

The geometry and working principle the volume changing WEC has been inspired by the Symphony Wave Energy Converter that is being currently developed by Teamwork in the Netherlands.
The inventor of the Symphony, (F. Gardner) previously worked on a similar concept, the Archimedes wave swing [11]. This device contained a linear generator as power-take off system. A demo version of this device had been tested successfully in real sea, before a failure of the test-frame sunk the demo. Licenses of the concept have been sold to a Scottish company and the contract prohibited Gardner to work on the concept for a duration of 12 years. After the licensed duration ended Gardner started created the Symphony. The Symphony is based on the same working principle (submerged pressure differential) but with a different power take off system, that should improve the performance. Teamwork has created a simulation model for the Symphony. This model is confidential. It is understood that this model is a 1 dimensional simulation, only including the heave motion.

The Precursor of the Symphony, the Archimedes Wave Swing (AWS) was studied by Van der Pluijm in 2002 [51], by Costa & Garner in 2003, by Valerio & costa in 2007 and by Kurniawan in 2014.

Technology

The Symphony wave energy converter consists of two half-enclosed rigid hulls are connected by a rubber membrane. The upper half, the top shell, moves over the lower half, the base, that has a smaller diameter. That together they enclose an air volume immersed at several meters (5 a 10 meters) below the sea surface, see Figure 4.14(b). The two shells can move relative to each other in vertical direction. The vertical motion of the top is induced by the difference in pressure outside and inside the top shell. This vertical motion drives the water turbine located in the bottom buoy. See Figure 4.14.

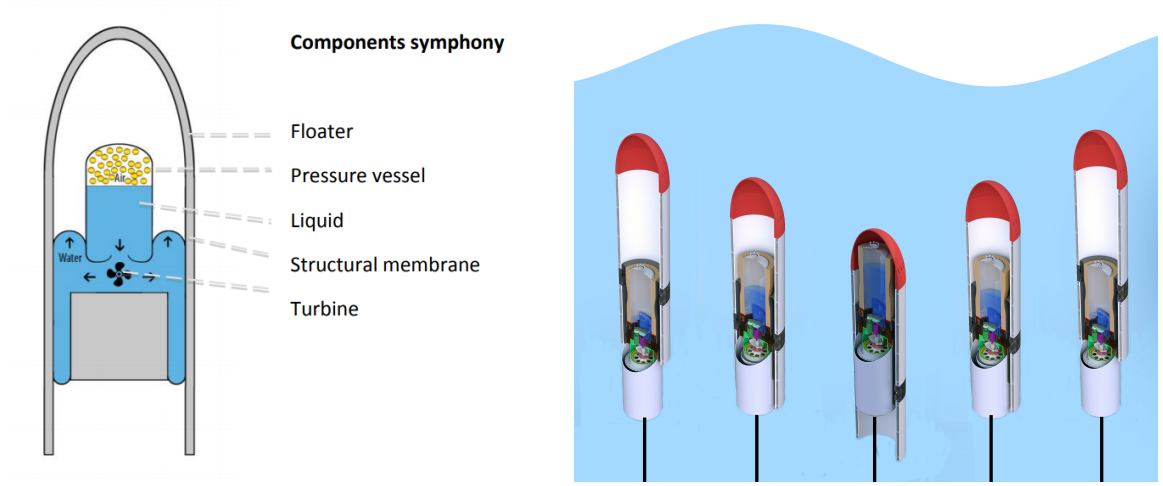

(a) (b)

Figure 4.14: Illustration of components inside the Symphony

The top shell has a cylindrical shape with a closed top and open end at the bottom. The top shell is connected to the bottom shell by a torus shaped flexible membrane. The topside of this membrane seals off the air volume in the top shell from the seawater outside while the volume inside the membrane is filled with water and forms a closed volume with the turbine and gas spring. The volume inside the membrane changes with the vertical position of the top shell and that way it pumps water trough the turbine to the gas spring and vice-verse. A simplified sketch of the system is found in Figure 4.14(b).

Tests are performed by Teamwork with a first prototype of their turbine and generator in 2018. The tests resulted in a first assessment of the turbine efficiency performance, results are shown in Figure 4.16.

Total internal system efficiency

Te\Hs	0,75	1,25	1,75	2,25	2,75	3,25	3,75	4,25
4,5	50%	58%						
5,5	52%	64%	69%	76%				
6,5	60%	71%	79%	81%	84%	86%		
7,5	65%	74%	80%	83%	85%	88%	91%	90%
8,5	69%	79%	82%	86%	87%	89%	90%	91%
9,5		77%	85%	87%	89%	89%	90%	90%
10,5		82%	86%	87%	88%	88%	89%	91%
11,5		81%	86%	87%	89%	89%	90%	91%
12,5				88%	88%	89%	90%	90%
13,5					88%	88%	89%	91%
14,5								89%
15,5								
16,5								

Figure 4.15: Total efficiency of the turbine and generator combined. Source: Wikkerink et al. (2018) [53]

The result shows that the turbine efficiency, depending on the sea conditions, is somewhere between 50 and 91 %.

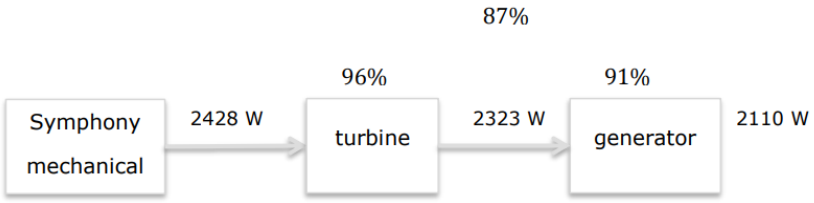

Figure 4.16: Example of the efficiency calculations including the turbine and the generator as separate stages. Source: Wikkerink et al. (2018) [53]

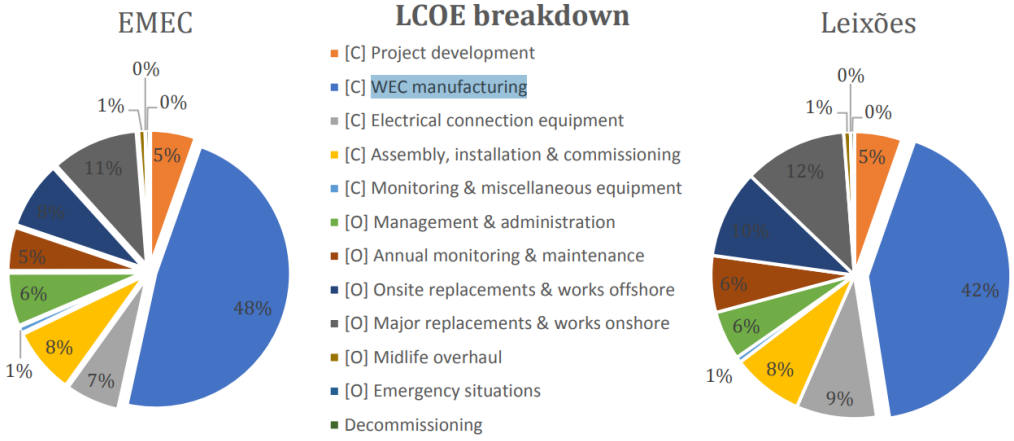

FIGURE 3:14 LCOE BREAKDOWN FOR REFERENCE CASE

Figure 4.17: Capital costs Symphony concept

Economics

The LCOE values have been presented by the company (Teamwork), for two different locations, at one location the LCOE was estimated at 1.05€/kWh and at the second location 0.94€/kWh. The expenses shares from this assessment (performed by the developer Teamwork) is shown in Figure 4.17.

4.4. Conclusion

The the majority of wave energy concepts (WEC's) are oscillating body devices. Within this category, point absorbers show most promise for being axisymetric, and easily maintainable.

Point absorbers have following benefits:

1. Does not require a rotation compensation system, the absorber is axisymetric.
2. Research showed that a specific array of multiple small sized point absorbers performed better than a small array of large point absorbers when both arrays where of equal volume. Which suggests that smaller devices perform better than devices with a larger surface area. As the objects are smaller, they are easier to transport and replace.
3. Is able to interact as a fictitious larger object in water than the true width of the buoy, due to resonance by optimal control of the dynamic parameters. As a result, the material cost per absorbed energy could reduce the cost of wave energy conversion systems.

Although floating point absorber generally have a higher power production due to their surface location, they are damage prone when targeted by extreme wheather conditions. Submerged buoys enjoy a protection from these conditions, but show limited performance. The third type of point absorber (SPD) has shown potential by combining a the high power performance with the submerged sheltered positioning.

For two types of point absorbers, the floating and submerged buoy, literature provides methods to estimate power performance. Two methods are highlighted. Method 1 [4] describes a time-domain simulation incorporating different conditions in which the device can be assessed. Method 2 [47] illustrates how to determine maximum power limits for WEC's.

These methods have however not bee applied to the SPD device presumably due to it's volume-changing nature. A comparison between all three point absorbers would define the extend to which the SPD shows promise.

5. Time domain analysis of the dynamic system of a quasi-rigid point absorber

This chapter describes the adaptation tho Method 1. The phases for simulating the dynamics of the selected test model are described in datail in order to obtain estimations for the average produced power performance.

5.1. Approach

As described, this thesis adopts two paths,to assess the power production performance of a concept:

1. Method 1: Dynamics simulations for estimated average power, as applied by Babarit et al. (2012) [4].
2. Method 2: Calculation of Budal theoretical limits for maximum power as described by Sergiienko Sergiienko et al. (2017) [47]

Method 1, described in this chapter, simulates a dynamic representation of a WEC system in order to estimate the average produced power performance. This result is specific for the simulated device type, body shape and PTO control strategy (linear and non-linear power take-off damping coefficients and stiffness coefficients, latching control or declutching control). Losses in the concepts power generator and transmission systems (friction, limited stroke lengths) can be added to the model for more realistic power performance results. Once more characteristics of the design are known, the losses of each transition phase can be calculated which would increase the accuracy of the performance assessment.

In contrast, Method 2, that will be the subject in Chapter 6, uses calculation of the Budal limits that result in maximum theoretical power values as a function of the wave period, and are independent of PTO control strategy. These limits are different for different dimensions and submersion of the object. The Budal limits exclude the influence of any conversion principles used to transmit the absorbed power after the absorption stage.

Both methods have so far only been applied to rigid bodies, based on the reference studies [4] [47]. For this research the two methods are extended, as none of the studies that applied these methods applied it to quasi-rigid (volume changing) bodies of which the SPD is an example. Amongst the most important adaptations that have been made, was the calculation of hydrodynamic coefficients. Both methods require hydrodynamic coefficients of the objects interaction with water waves. For rigid-bodies software tools exist to obtain reliable coefficients that represent the interaction with waves. For a quasi-rigid body however the common methods and tools do not

Figure 5.1 depicts the different point absorbers that are compared by the two methods. A floating buoy, a submerged buoy and the Submerged Pressure Differential device.

A flow-chart of the steps and tools used to compute the performance of the three types of point absorbers, is shown in Figure 5.2.

Step 1: Design of a test-concept - 3D model (Rhino) and mesh of the model (Ansys APDL)
Step 2: Determining the velocity potentials for all panels, (using AQWA).
Step 3: Calculating the hydrodynamic coefficients, (using the Panel Selection Tool).
Step 4: Performing time-domain simulations
Step 5: Creating a power matrix
Step 6: Calculating the power performance indicators

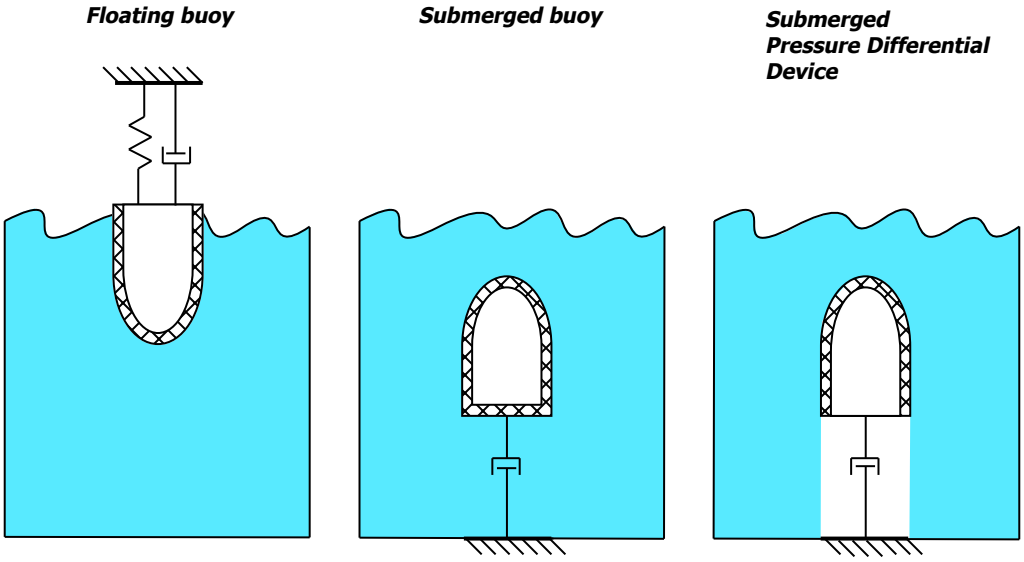

Figure 5.1: Schematic representation of the modelling approach used for hydrodynamic forces on three point absorber bodies with different working principle.

Average power values are obtained by creating a time-domain model for each of the concepts that include all basic physical characteristics. The model shape is created in a 3D software package, Rhino, is meshed with a 3D meshing software-package, Ansys APDL. The time domain models are performed in WECSim. Data of average power performances, obtained from multiple runs in WECSim, are used to create a power matrix (similar to the Babarit method) and a power curve for a unit wave height (similar to the Sergiienko method).
The implementation of the complete computational method required verification of the applied methods at every step. For verification, the methods were applied to a reference WEC and the results compared to the literature results. Following verification, the computational method is applied to the test-concept (SPD), allowing for comparison the SPD's performance in relation to the other point absorbers.

The following sub-chapters describe for each step first the method and tools to execute this step. Secondly, when applicaple, the verification of the method by applying it to a reference model and comparing these results to data from the prior studies. Thirdly, the method of each step is applied to the SPD concept and results of this calculation are shown.

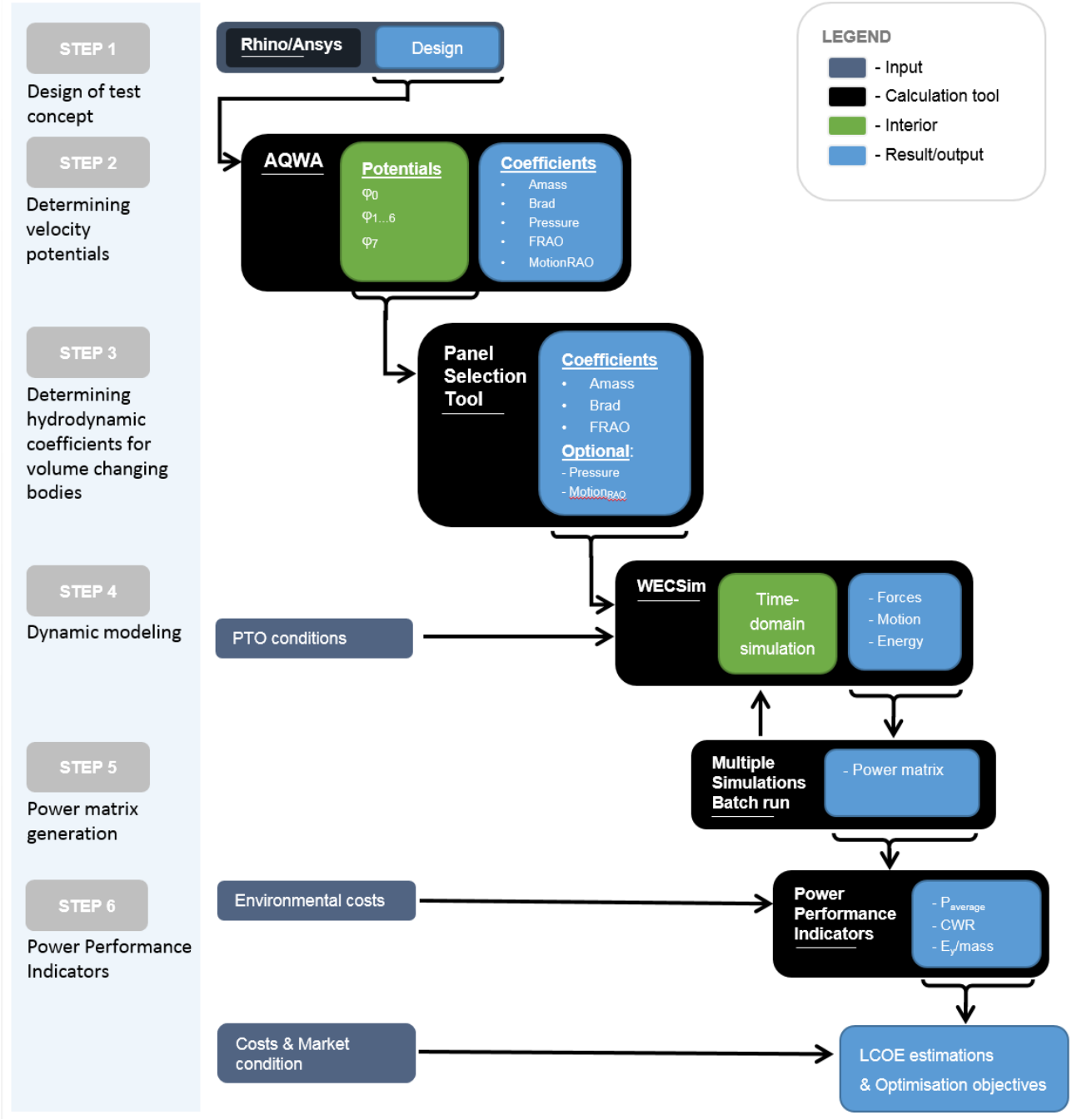

Figure 5.2: Flowchart for Method 1: The application of the panel selection functionality with input from AQWA and output to WECSim in order to calculate power yield and mooring forces

5.2. Design of a test-concept (Step 1)

Designing the hull of the absorbers, the softwarepackage *Rhino* is used. The model is meshed, using Ansys APDL. A mesh size is applied with sides of circa 3 cm wide. For C1 and C2 this resulted in around 3000 to 4000 panels.

5.2.1. Designs

In order to perform the verification steps in the following phases towards a numerical model, a reference model has been generated. This reference model (C1) is based on the Bottom referenced Submerged Heaving Buoy - Bref-SHB, from Babarit et al. (2012) [4]. The model used in that paper is based in-turn on the *Ceto 5* WEC developed by *Carnegie*. The second model (C2) is a first step toward modelling the symphony. It is a model with the same width as reference model C1.
To test the functionality of the applied methods, described in the up-coming phases, two different reference-designs have been created, both with characteristic diameter of 7 meter.

C1. Chamfered cylinder (Figure 5.3(a) and Figure 5.3(b))
Used for verification as floating and submerged buoy.

C2. Bullet shaped cylinder (Figure 5.3(c) and Figure 5.3(d))
Used for analysis as both rigid and quasi-rigid submerged buoy.

C3. Selected model for the SPD (Figure 5.4)
The selected design for this research to extend the existing comparison studies with.

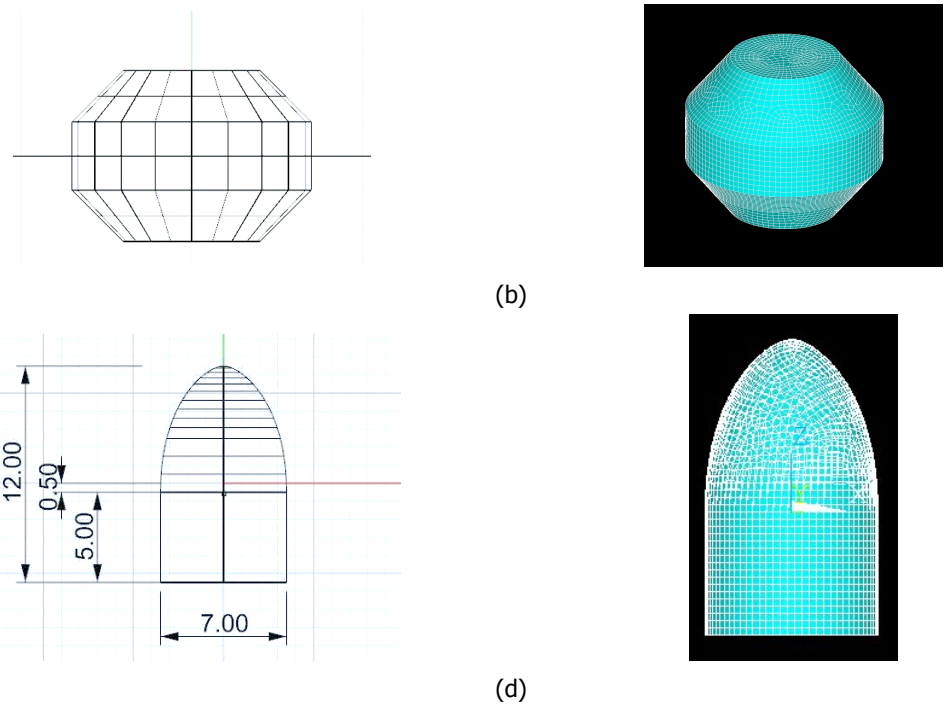

(a) (b)

(c) (d)

Figure 5.3: Design (left) and mesh (right) used for verification of the methods. C1. chamfered cylinder (5.3(a) and 5.3(b)), C2. Bullet shaped cylinder (5.3(a) and 5.3(b))

The mesh created for this model divides the object in 4000 (+) panels.

5.2.2. Selected model (SPD)

The selected model C3 that is created to model the Submerged Pressure Differential device, is the main model for this thesis. The design of the test-concept in Rhino and the mesh in Ansys APDL are created for this model, see Figure 5.4.

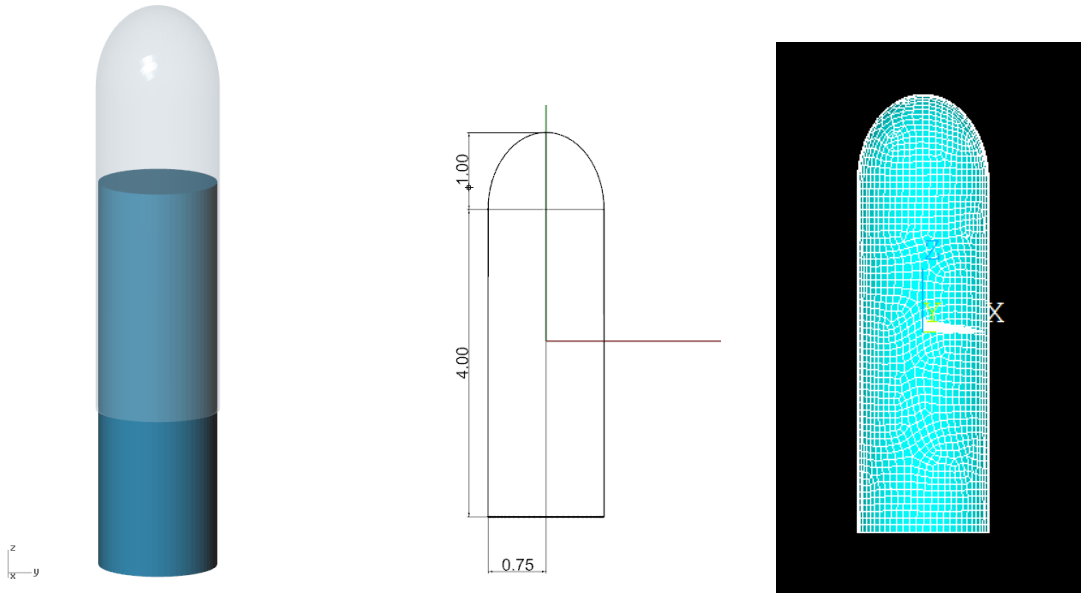

(a) (b) (c)

Figure 5.4: The design of the selected model (C3) for this research, is a small SPD-device based on the symphony WEC-device. The images show the composition of cap and base (left), the dimensions of the cap (center) and the mesh of the cap (right)

Dimensions of the research model

The model that is used for this research is an early generation symphony concept and is relatively small compared to designs for next generation concepts. The company plans on schaling towards larger devices. The dimensions are presented in Section 5.2.2. A demo model with similar dimensions is scheduled to be tested in real sea in Portugal in 2019.

Property	Value	Unit
Diameter of the buoy (top shell)	1.5	m
Height of the buoy (top shell)	5	m
Submersion (top of the buoy)	6	m
Displacement (closed top shell)	8.233	m^3
Mass of the buoy (top shell)	1000	t
Centre of mass (from the top)	2.71	m
Moment of inertia Iy	21.46	t·m^2
Stroke length	5	m
Stiffness upper end stop spring	30000	N/m
Stiffness lower end stop spring	30000	N/m
Water depth	1000	m
Displacement (base component)	1~6	m^3
Turbine efficiency	90 %	

Table 5.1: System parameters

5.3. Determining hydrodynamic coefficients (Step 2)

5.3.1. Method

Hydrodynamic coefficients are calculated from velocity potentials. The velocity potentials are derived from boundary element method software (BEM-software), in this case: Ansys AQWA.

In Offshore and Maritime Engineering, the boundary-element method (BEM) is usually used to accomplish the hydrodynamic analysis of maritime structures. This software calculates the hydrodynamic coefficients in the frequency domain. (More detailed explanation is found in Appendix E).

The boundary element method (BEM) is a numerical method for solving partial differential equations (PDEs).

Alternative options would be the use of Computational Fluid Dynamics (CFD). With CFD the area around the 3D object is discretized (meshed) in order to calculate all forces on all the surrounding mesh elements. Generally CFD results in much higher accuracy and is able to simulate various complex flow interaction. However, for this size of system CFD would be very time consuming with respect to the amount of accuracy it would increase. For smooth bodies and simplified For the BEM method, the software of Ansys AQWA is used. Initially the AQWA software did not allow for calculation of non-rigid bodies. With the panel selection tool (PST) illustrated in Figure 5.17, AQWA is partly used. The BEM software calculates the potentials for every panel. From the potentials per panel the hydrodynamic coefficients of the body are obtained. Figure 5.2 shows a flowchart for the phases of creating performance indicators with the use of panel selection.

AQWA

AQWA solves the potential functions and determines the pressures along the hull of the (semi-)submerged body. From the pressures at the floating body AQWA calculates the forces and moments by which the equation of motion is derived. The the total of forces exciting the (semi-)submerged body consists of a hydrodynamic force and a hydrostatic force. The hydrostatic force is the buoyancy force in still water. The hydrodynamic force is divided into wave forces and radiation forces. This is graphically shown in Figure 5.5. The equation of motion, which is in fact a damped-spring-mass-system is also shown in this figure.

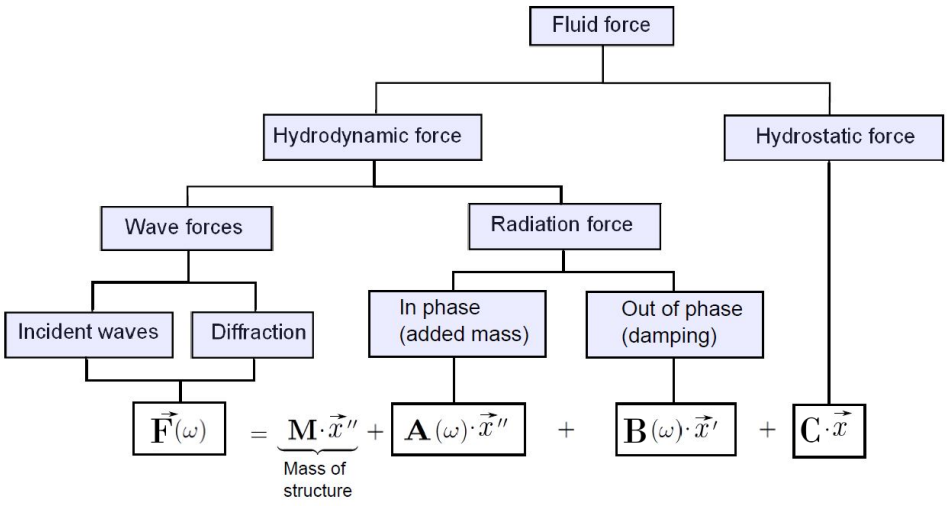

Figure 5.5: Overview of hydrodynamic fluid forces on (semi-) submerged objects

5.3.2. Verification

For the verification study the hydrodynamic coefficients are compared with results from Babarit et al. (2011) [3]. As an example, Figure 5.6 shows the wave force excitation for AQWA calculations using model C1.

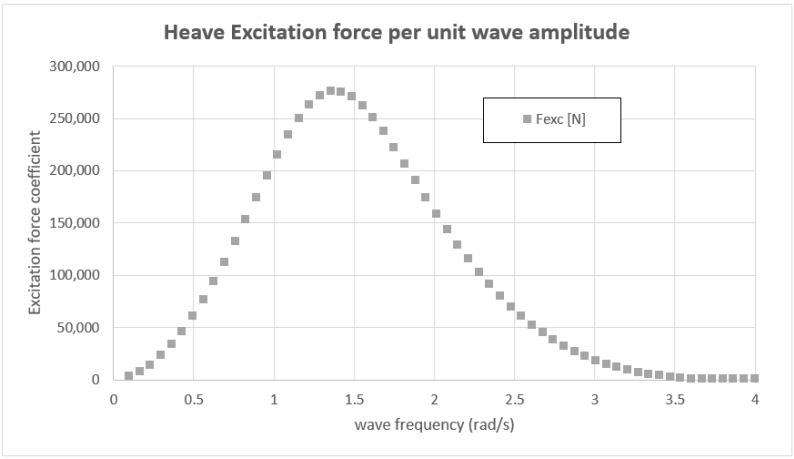

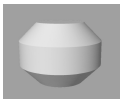

Figure 5.6: The excitation force coefficients for model C1. (Submerged Chamfered Cylinder). Shown is the output from BEMIO. The input (velocity potentials) was obtained from AQWA. Result from BEMIO are automatically normalised, meaning multiplication with $\rho g = 10055$, is required in order to obtain the excitation force coefficients. The results shown have been corrected in that way.

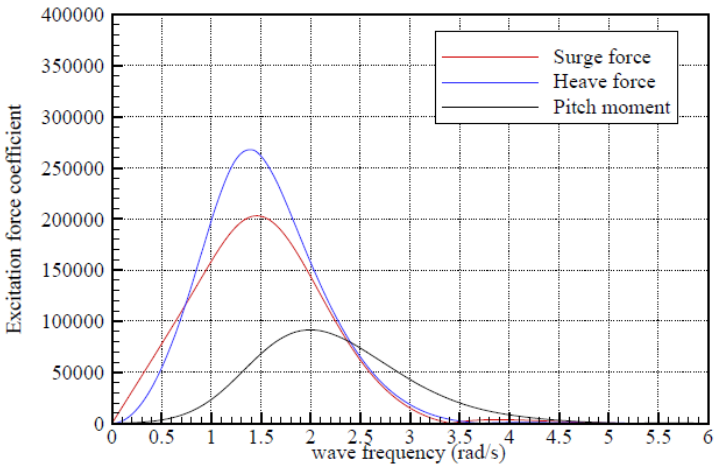

Figure 5.7: Excitation force coefficients from Babarit and Hals (2011) [2]

From all hydrodynamic coefficients that can be obtained from AQWA simulations, the excitation force coefficients are chosen to be presented here as they are most relevant for power absorption. The excitation force is the only force contributing energy to the buoy system. Radiation damping is the extraction of energy from the system to the waves. The relations describing the dynamics of a body in interaction with waves are described in Appendix D and in [47].

5.3.3. Results

Results have been obtained for the added mass and radiation damping for submerged devices using AQWA. These results will be discussed in the next chapter, where theyare used for further assessment of non-rigid bodies (See blue lines in Figure G.2 and Figure 5.12

representing coefficients for rigid body)

In Figure 5.8, the heave excitation force coefficients (or Force RAO) of a floating buoy (blue line) is compared with a submerged buoy (red line). These coefficients are obtained from calculations in AQWA. The reference model C2 is used in floating position with a draft equal to half its height, and in submerged position where the top of the body is 2.5 m below the mean water level. This experiment shows that the same buoy shape in floating position has overall higher excitation force coefficients than the submerged buoy. There are two factors that causes the decrease of the excitation force coefficients. The increase in depth overall reduces the interaction with the wave loads which are strongest at the surface and decrease with depth as their orbital velocity reduces. Secondly, the forces on the submerged body are caused by a summation of the vertical components of pressures on both the upward facing sides as well as on the downward facing side. These top and bottom pressures act in opposite direction, and in general the two resulting forces largely cancel each other out. Only for wave frequencies close to the natural frequency of the submerged body, the bottom force is smaller than the top force such that a resulting force is obtained.

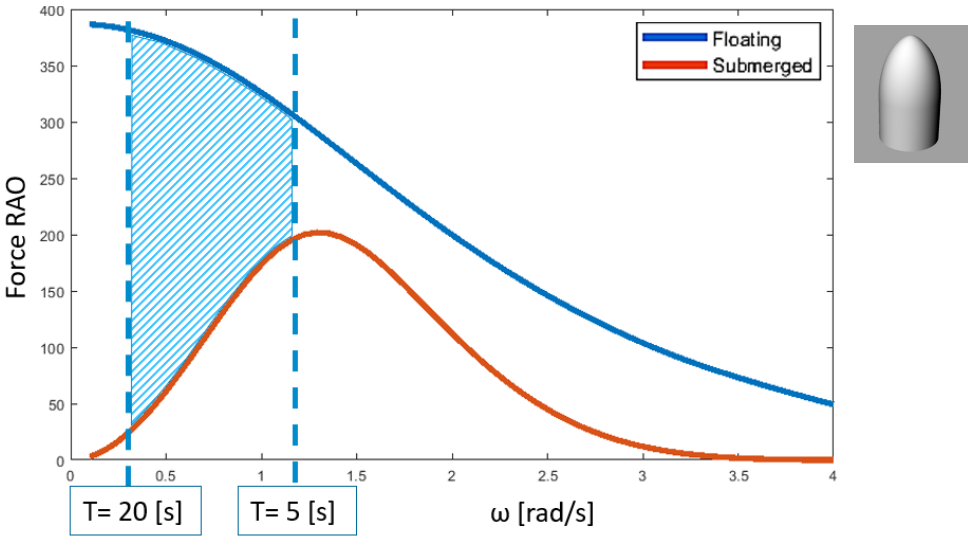

Figure 5.8: Excitation force coefficients for a floating buoy (blue line) compared to a submerged buoy (red line) of equal shape (reference-model (1)). For clarification purpose, the difference is highlighted over a selected range of wave periods. For much offshore locations most of the energy in waves is present in a range of 5 to 20 seconds.

Experimentation with hydrodynamic calculations performed with AQWA, did not result in a solution that allows to calculate the hydrodynamics to represent the selected model (C3). After examining the AQWA manual and related literature, it has been concluded that the functionality of AQWA did not facilitate in solving this problem.

5.4. Panel selection for hydrodynamic coefficients (Step3)

5.4.1. Method

To be able to simulate the forces that act on the top hull of the SPD accurately, the hydrodynamic forces should be excluded from the bottom surface of the hull. Only the PTO forces should be applied to the bottom surface. The bottom edge, would in reality receive wave induced pressures, but these are neglected in this calculation. To allow for this exclusion, the Panel Selection Tool was created.

This tool calculates hydrodynamic coefficients from velocity potentials in the same way as AQWA, but the functionality of selecting parts of the submerged body to include or exclude

in the calculation is added. As described, this allows for more accurate calculation of the coefficients for a non-rigid body.

The Panel Selection Tool (PST) calculates the following coefficients:

- Added mass
- Radiation damping
- Excitation force

For this calculation the PST uses output from AQWA. The output contains velocity potential for every panel on the 3D object. The input consists of 6 potentials (Φ_1 to Φ_6) for all 6 degrees of freedom, and includes the undisturbed (Froude-Krylov) potential (Φ_0) and the diffraction potential (Φ_7). When obtaining these results from AQWA, these potentials are arranged per panel, then for every heading (wave direction) and then per frequency (all frequencies AQWA was instructed to evaluate the velocity potentials for).

Description of the panel selection process.

1. Loading the raw data from AQWA. Every line from the AQWA data files (.AH1 and .LIS) is stored into two arrays.
2. Reading the data. With use of search clues, the data file is scanned and extracted data is stored in the matrices. The following data is scanned from the raw data:
   - Water depth [h]
   - Water density [ρ]
   - Gravity acceleration [g]
   - COG - centre of gravity
   - Restoring stiffness
   - Added mass (data to be overwritten)
   - Radiation damping (data to be overwritten)
   - Excitation force (magnitude and phase)
   - Froude Krylov potentials (undisturbed wave potential)
   - Diffraction potentials
   - Element locations
   - Element areas
   - Element normal vectors
3. Creating a normal vector (n_k) that includes a lever arm vector, see eq. 5.1. This vector consists of three normal components ($n_{1\ldots3} = [\,n_x\ n_y\ n_z\,]$) at position 1 to 3 (for obtaining forces along the translations x, y and z) and contains the cross product of the normal vector (n) with the panel position relative to COG ($x_{panel} = [\,x_{panel}\ y_{panel}\ z_{panel}\,]$) at the 4th to 6th position ($x_{panel} \times n$) for obtaining moments along the rotations: roll, pitch and yaw.

$$n_k = \begin{bmatrix} n_x \\ n_y \\ n_z \\ y_{panel} \cdot n_z - z_{panel} \cdot n_y \\ z_{panel} \cdot n_x - x_{panel} \cdot n_z \\ x_{panel} \cdot n_y - y_{panel} \cdot n_x \end{bmatrix} \tag{5.1}$$

4. Calculation of the added mass (a_{kj}) and radiation damping (b_{kj}) for all frequencies.

$$a_{kj} = -\Re\left[\rho \iint_{S_0} \phi_{j_{amp}} \cdot e^{-i\cdot\phi_{j_{ph}}} \cdot n_k \, dS_0\right] \tag{5.2}$$

$$b_{kj} = -\Im\left[\rho\omega \iint_{S_0} \phi_{j_{amp}} \cdot e^{-i\cdot\phi_{j_{ph}}} \cdot n_k \, dS_0\right] \tag{5.3}$$

Where the integrals are taken over the real part of the velocity potentials ($\phi_{j_{amp}} \cdot e^{-i \cdot \phi_{j_{ph}}}$) multiplied by the normal vector n_k integrated over the wetted surface (S_0). The added mass consists of the real part of the integral multiplied by the water density. While the radiation damping is obtained by taking the imaginary part of the integral multiplied by the density times the frequency [32].

5. Calculation of the force RAO with the undisturbed and diffracted wave potentials. The force RAO is the excitation force coefficient at a unit wave amplitude ($a = 1$). The diffraction potentials are obtained from the velocity potential the AQWA. For calculation of the force RAO also the Froude-Krylov potentials are required. The Froude Krylov potentials are calculated by the PST, using Equation (5.5). First is defined in Equation (5.4) how the time dependent part of the velocity potential can be left out of the equations and results in a space-dependent term ϕ.

$$\Phi(x, y, z, t) = \phi(x, y, z) \cdot e^{-i\omega t} \tag{5.4}$$

$$\phi_0 = \frac{ig}{\omega} e^{kz} e^{ik(x \cdot \cos(\mu) + y \cdot \sin(\mu))} \tag{5.5}$$

In order to add-up the Froude Krylov potential to the diffraction potential, the potential is split into the absolute value and the phase angel.

$$\phi_{0_{amp}} = |\phi_0| = \sqrt{(\Re(\phi_0))^2 + (\Im(\phi_0))^2} \tag{5.6}$$

$$\phi_{0_{ph}} = \angle\phi_0 = \tan^{-1} \frac{\Im(\phi_0)}{\Re(\phi_0)} \tag{5.7}$$

The force RAO is described as:

$$F_{RAO} = i\rho\omega \iint_{S_0} \phi_{0_{amp}} \cdot e^{i\phi_{0_{ph}}} + \Phi_{7_{amp}} \cdot e^{i\phi_{7_{ph}}} \cdot n_k \, dS_0 \tag{5.8}$$

In a similar way as with the Froude Krylov wave potential, the Force RAO is split into a magnitude and a phase angle, see Appendix E. This time is only denoted with the absolute value and the phase angle.

$$F_{RAO\_mag} = |F_{RAO}| \tag{5.9}$$

$$F_{RAO\_ph} = angle[F_{RAO}] \tag{5.10}$$

5.4.2. Verification

The tool that is built to select panels for the hydrodynamic calculations is verified in two stages. The first check is whether all panels are read, saved and addressed appropriately by comparing the results with the expected pressures, visually. Output from the tool was presented in 3D graphs, such as: Panel positions, normal vectors, and pressure vectors. When a mistake is made in the panel data by incorrectly processing the input files, the error is noticed directly by misplaced visualisation of data points. Figure 5.9 shows the distribution of vertical components of the pressure amplitude along the hull of reference model C1 in submerged position. The pressure amplitudes components show to be smaller in waves with larger wave periods. This is the expected result since the object in long waves will only be forced slightly by the waves in order to move with the waves. The mass of the object is such than in this long period wave the free-body motion will repeat the wave motion, meaning it has a wil very small phase difference to the incoming wave. The verification of the panel selection tool is continued by a comparison of the results with similar calculations performed in AQWA, when all panels are selected. Figure 5.10 shows how the panel selection

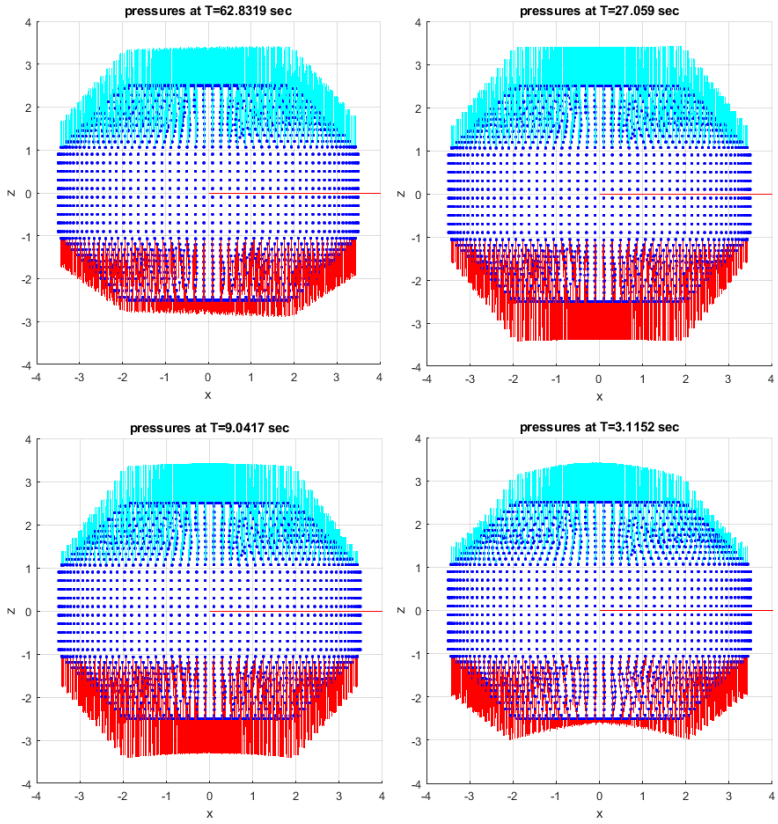

Figure 5.9: verification of processing data from AQWA input files to the panels

tool (circles) presents the same output as the result from AQWA (lines). Figure 5.10 shows the results for the added mass (blue and yellow) and the radiation damping (red and purple). This simulation is performed with reference model C2 in submerged position.

When a hydrodynamic force is split into two sub-forces: forces acting on the top and forces acting on the bottom, then it is logical to assume that the summation of these two forces are equal to the initial hydrodynamic force. This leads to the next verification step, that compared the hydrodynamic coefficients obtained for the total body with summation of hydrodynamic coefficients obtained for the top and bottom. From Figure 5.11(a) it is clearly visible that the total added mass (blue line) is a composition of the added mass coefficients from the top (red line) and the bottom parts (yellow line). The peak at frequency 1 [rad/s] and the low point at 2 [rad/s] is visible in both the blue and the red line. The added mass at the bottom, represented by the yellow line, works counteractive compared to the red line and smooths part of the frequency dependent variation.

What stand out in Figure 5.12(a) is the large difference in added mass for the top part versus the bottom part. The top is submerged an equal distance as the chamfered cylinder (2,5m). However, the top shape is different and a larger part of the contributing panels is submerged deeper below the mean water level. This clarifies the reduction in added mass at the top side. The bottom part is much deeper below the water level compared to the chamfered cylinder. This explains both the increase of added mass at the bottom as well as the shift towards lower frequencies of the maximum and the minimum values.

Both parts show dependency on the frequency, although it is a reduced and mirrored effect for the bottom part. The changes in added mass over the frequency occur in opposite direction.

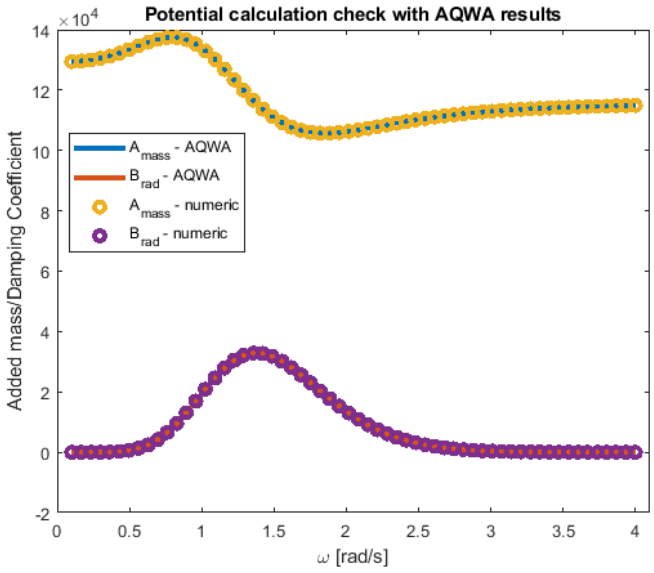

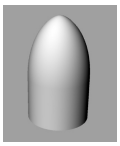

Figure 5.10: verification of the added mass and Radiation damping coefficients compared to AQWA

Now analysing the radiation damping in Figure 5.11(b) and Figure 5.11, it stands out that the bullet shaped topside produces much less radiation damping than the chamfered cylinder. The damping at the top part is higher than the total damping for frequencies between 0.25 - 1.5 [rad/s] because the bottom component contributes negatively to the total damping for specific frequencies. these lie mainly below the natural period.

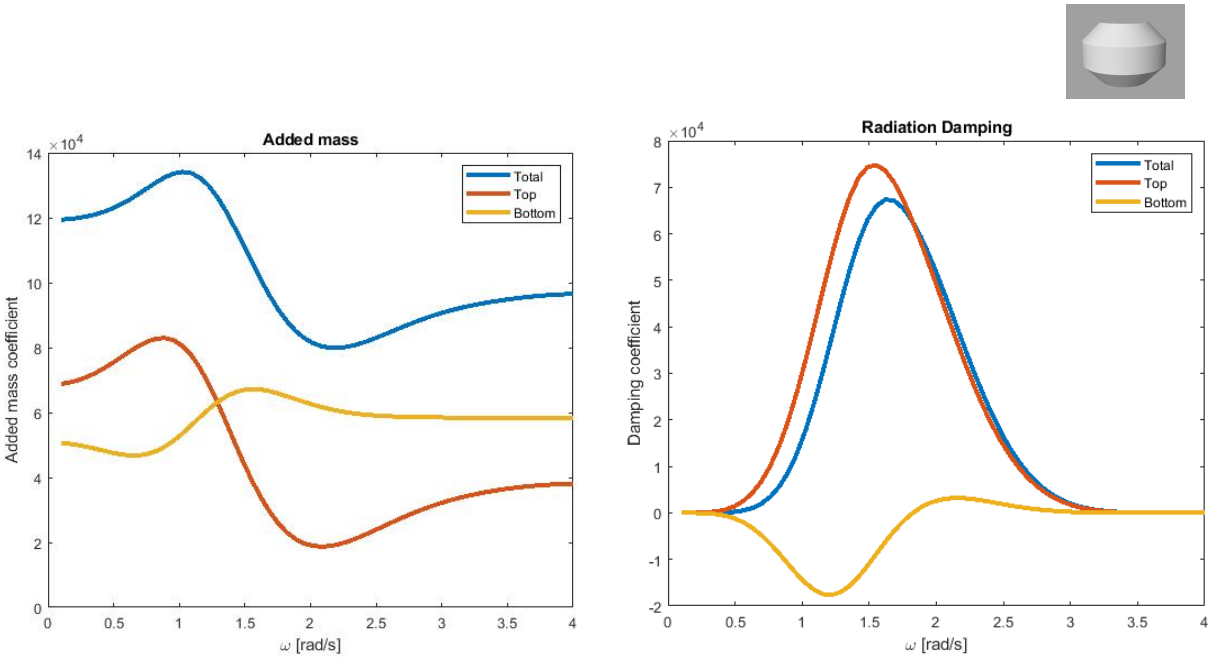

(a) (b)

Figure 5.11: Hydrodynamic coefficients, for the reference model C1, left: the added mass and right the radiation damping coefficients

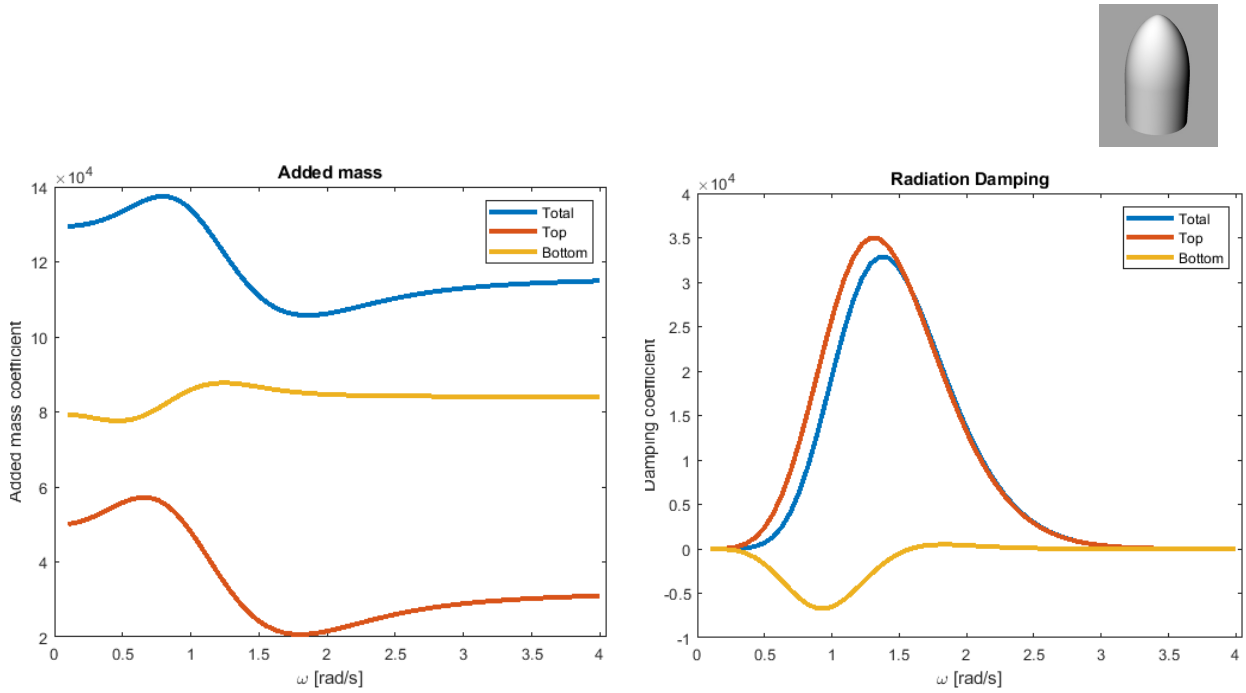

(a) (b)

Figure 5.12: Hydrodynamic coefficients, for the bullet shaped model, left: the added mass and right the radiation damping coefficients

The graph shown in Figure 5.13, describes the experiment with calculations for the heave excitation force coefficients of reference model C2. The purple line in this graph, describes the resulting coefficients of reference model C2 assuming it to be a rigid body in submerged condition, because this is allowed to be calculated in AQWA. The SPD concept is, however, quasi rigid. When the suggested method for selecting panels is applied, it allows calculations of hydrodynamic coefficients assuming it to perform as non-rigid body. The quasi-rigid coefficients are shown by the red line in Figure 5.13, it shows the result when the suggested method for selecting panels is applied to reference model C2, presenting only the excitation forces acting on the top of the body. This is selection is made by selecting all panels excluding the bottom, which are all the panels that are facing downwards. If the selecetion was inverted, and only the bottom panels would be included, the result described by the yellow line in Figure 5.13 is obtained. Where the excitation force acting on all panels (purple line), has a peak close to 1 rad/s, and starts and ends at zero at the extremes, the the excitation force acting on the top of the body (red line) starts similar for large frequencies but starts to deviate at 1.5 rad/s. At 1 rad/s the force coefficient at the top is almost 40% larger than the rigid-body coefficient. The difference further increases towards smaller frequencies, when rigid body coefficients tend to zero and the force coefficient at the top asymptotically heads towards a fixed value, in this case 400 N.

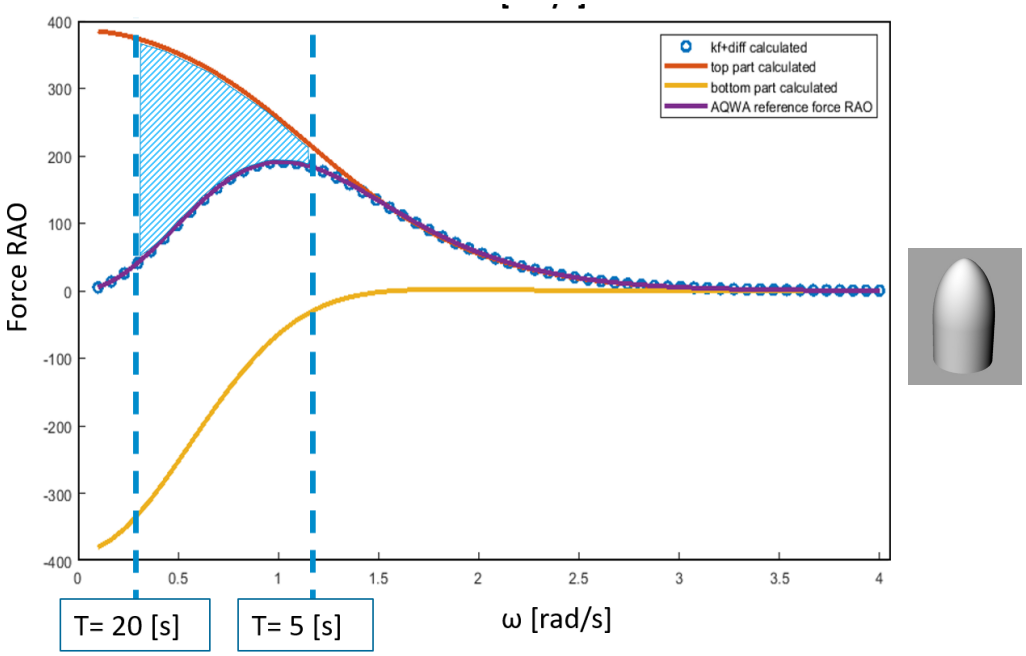

Figure 5.13: Heave excitation force coefficients in [N] for a submerged buoy. Including seperation of heave forces acting on top or bottom of the buoy. For clarification purpose, the difference between top forces and total forces is highlighted over a selected range of wave periods. For much offshore locations most of the energy in waves is present in a range of 5 to 20 seconds.

5.4.3. Results

A full hydrodynamic description of the selected model C3 is obtained. Part of this result is visualised in Figure 5.14 and Figure 5.15, showing the hydro dynamic coefficients in heave. These hydrodynamic coefficients are obtained with the panel selection method. They represent the contributions of forces acting on the top panels for the top part (cap) of the selected model. This allows to simulate the forces for this quasi-rigid body. The quasi-rigid body is submerged at a depth of 6m and 9m (measured from the top). Two results are specified, one at 1000m water depth and on at 30 m water depth. The differences are observed to be small. Figure 5.14(b) shows the change in Radiation damping. Figure 5.14(a) shows the added mass. The hydrodynamic coefficient calculation for the research model is performed

with variable depths. Results are shown for submerged depths of 6 and 9 meters below the waterline, measured from the top of the object.

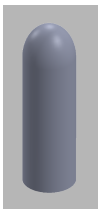

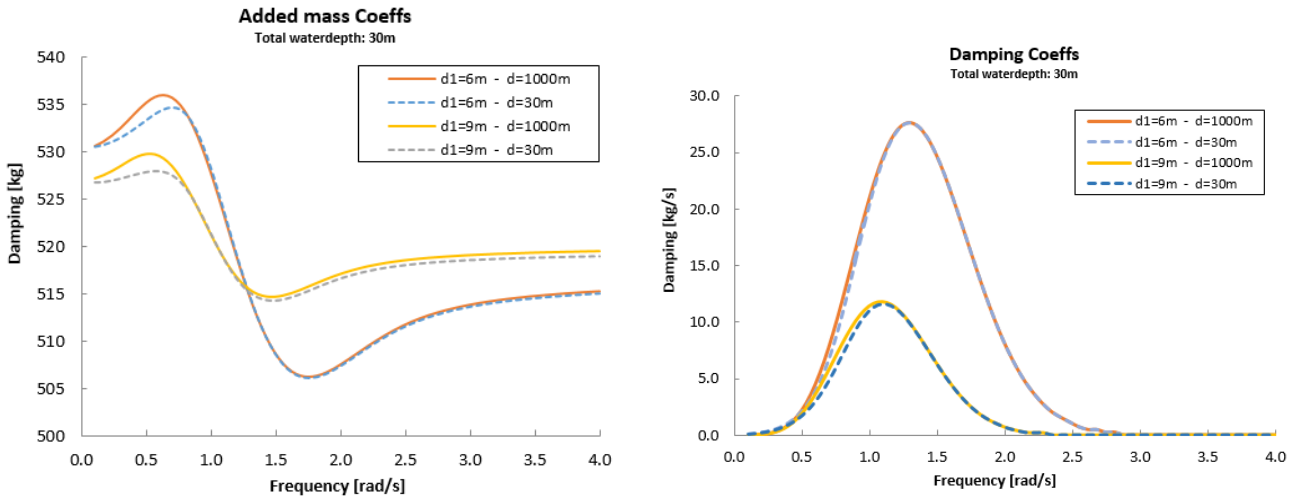

(a) (b)

Figure 5.14: Hydrodynamic coefficients, for the selected SPD model, left: the added mass and right the radiation damping coefficients

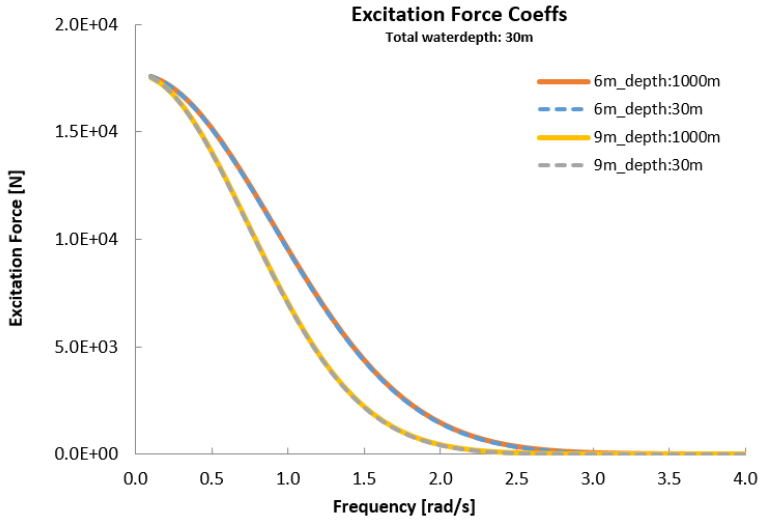

Figure 5.15: Hydrodynamic coefficients, for the selected SPD model: the Wave excitation force coefficient (Force RAO)

5.5. Time-domain modelling (Step 4)

5.5.1. Method

For time-domain modelling the open-source tool WECSim is used in combination with MATLAB. WECSim is a 6 degree of freedom time-domain simulation tool, developed in MATLAB/Simulink.

WECSim is a software tool for performing time domain simulations on objects in interaction with water. It solves hydrodynamic equations (i.e. Cummins equation) to determine body motions and forces for given sea states. Sea states can be inserted as regular, irregular(random), irregular from a spectrum or from a record. Apart from hydrodynamic objects, other dynamic objects such as ropes, power take off devices and ground/earth connections can be included. It also supports body to body interactions, Morison elements and viscous forces.

WECSim uses MATLAB/Simulink to define the connection and interaction of (hydrodynamic) bodies. It allows the user to graphically connect multiple pre-assembled simulation objects and constraints.

Time-domain Simulations with irregular wave conditions are to be performed for a certain duration in order to obtain estimated power production values of acceptable accuracy. This duration is estimated to be 1200 seconds.

The subsystem connected to the PTO block, allows to define specific non-linear conditions. For example the limitations of the stroke of the heaving buoy. When the stroke limit is reached the stiffness is increased rapidly to simulate end-stop forces.

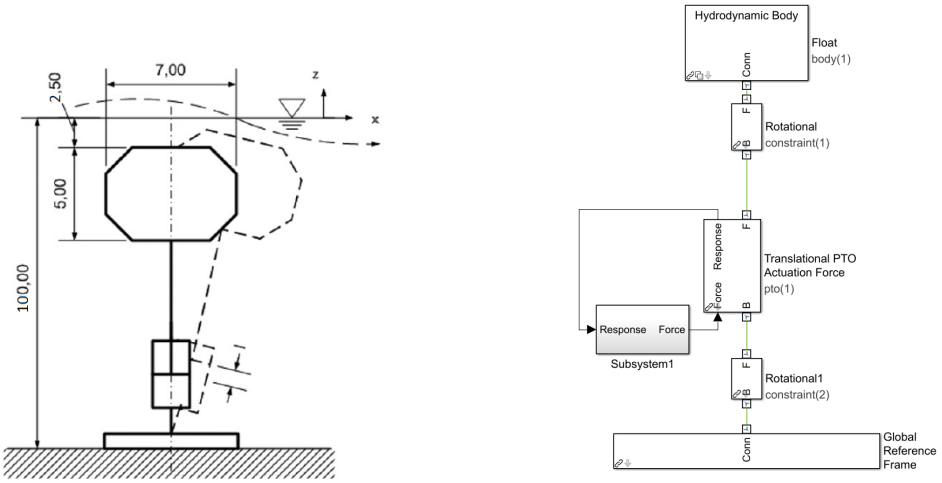

(a) (b)

Figure 5.16: Submerged verification concept 1 (C1), a schematic drawing of the system (a), the model in WECSim (b)

The SPD model is created by connecting two hydrodynamic bodies in WECSim. The first body is the cap, the second body is the base. In order to run a simulation, the hydrodynamic bodies require input of the hydrodynamic data obtained from radiation/diffraction software (AQWA).

The two bodies are connected with a power take-off block that only allows transnational motion (no rotation). The power take-off block used here allows to define additional PTO forces as result of the relative motion response. The power take-off force is modelled by a spring and damper.The spring requires pre-tension since the mass of the displaced water of the submerged body is larger than the mass of the body, resulting in a buoyancy force. Pre-

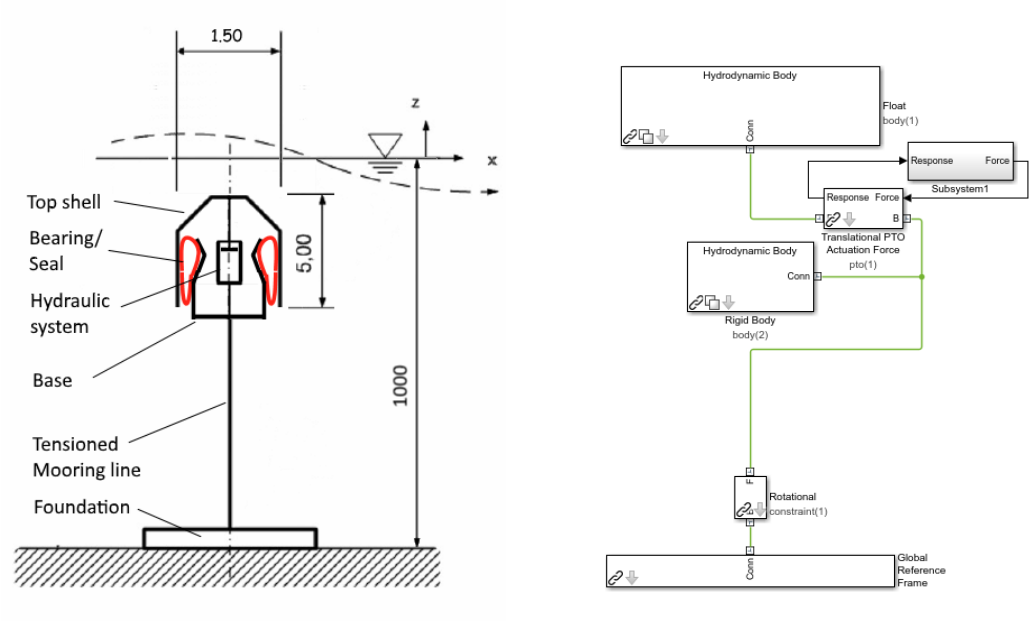

(a) (b)

Figure 5.17: SPD-WEC concept: a schematic drawing of the system (a), the model in WECSim (b)

tensioning is required to bring the top buoy into a balance at the appropriate location. The relation of this spring in the total power take off is presented in 5.11 The stiffness of the SPD can be can be adjusted when simultaneously adjusting the pre-tension length, in order to keep the balance. The spring stiffness that is created with this pre-tension is a linear spring. This seems not a very large simplification as the developers of the symphony WEC concept, Teamwork, have indicated that their concept is able to create a linear stiffness behaviour with their system. An early indication of the spring force curve, presented by teamwork, for the symphony is included in 5.18(a). This images shows the linear behaviour of the spring force, between the two end buffers.

$$F_{PTO} = z_{pre} \cdot c_{pre} + \dot{z} \cdot b_{PTO} \tag{5.11}$$

The end buffers have been implemented in WECSim by including a statement that increases the force between the top and the base, when the end-stop position is surpassed. The reaction to this force is visible in the motion behaviour of the top in time-simulation analysis.

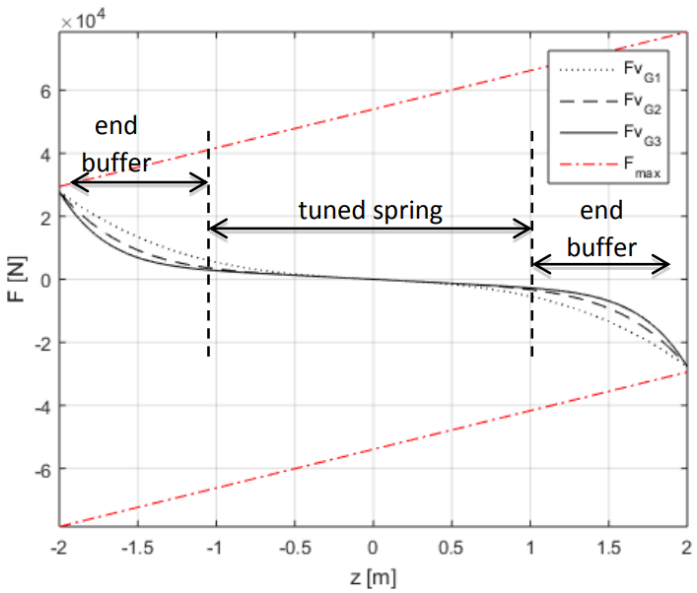

(a)

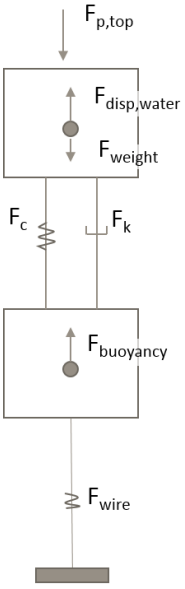

(b)

Figure 5.18

5.5.2. Verification

A verification simulation performed in WECSim, assesses whether the tool is used correctly and performs as expected. The results of this verification-concept have been compared with values obtained from the frequency-domain equations for unconstrained-heave-motion for floating and submerged bodies in regular waves, see figure 5.19(a) and 5.19(b).

The test case consists of a specific simulation in WECSim that with the right constraints could be compared to an analytical solution. First verification is based on a floating body in heave, the second verification is based on a submerged buoy in heave. The comparison was obtained by performing several WECSim time domain simulations. The following steps were used:

- performing simulations in WECSim at regular increasing wave frequencies
- average the amplitude of the buoy motion over long enough duration ($D > 10 * t_p$).
- excluding the start-up phase of the heave motion, the wave amplitudes are measured starting from a steady oscillating part of the simulation.

The motion amplitudes produced by WECSim have been verified with an analytical equation for free floating objects. (Result in Figure 5.19(a) and 5.19(b). This verification is created by comparing the average amplitude responds of the floating body, without constraints with the with a mathematical frequency-domain formulation for free floating objects. Both are calculated using regular waves and are conducted for a range of wave-periods. The mathematical frequency-domain formulation is described by 5.12.

$$\hat{Z}_a = \frac{1}{\omega} \frac{F_0}{b_{hyd}^2 + (\omega(m + a_{mass} - \frac{c}{\omega})^2)^{\frac{1}{2}}} \tag{5.12}$$

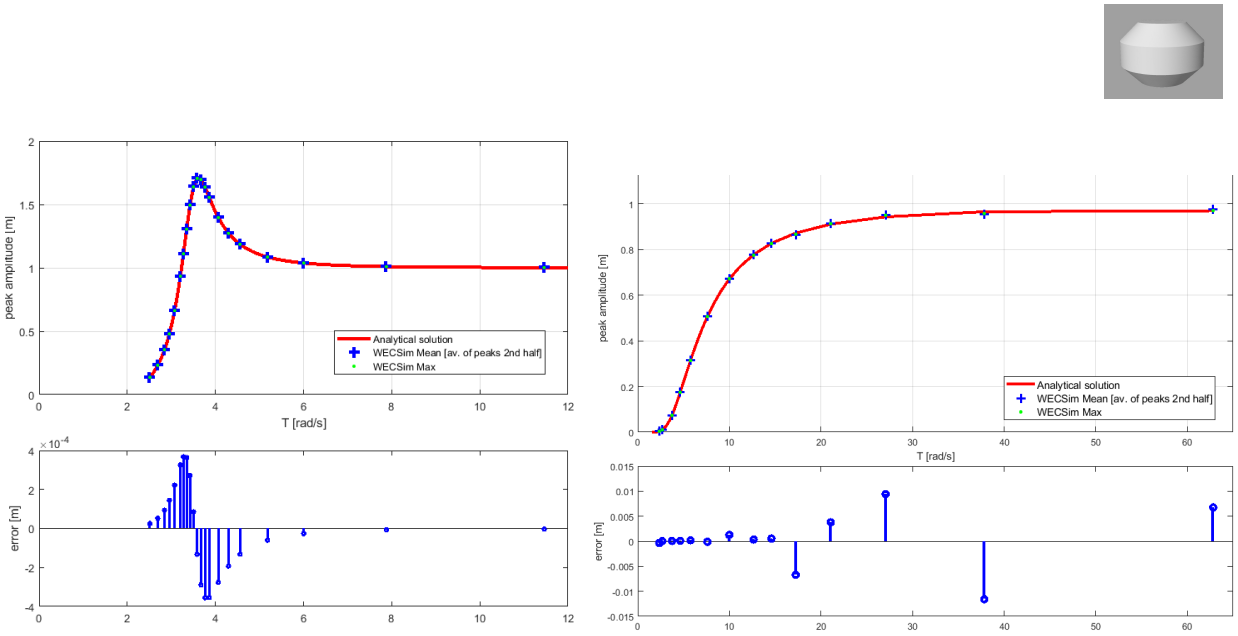

(a) Floating buoy (b) Submerged buoy

Figure 5.19: Free body motion response for wave amplitude $A = 1[m]$. The red line represents the analytical approach and the blue line represents the results obtained in WECSim. (For larger figures, see Appendix G)

5.5.3. Results

The results from the time domain simulations require post processing in order to present relevant information. WECSim automatically calls a file, userdefinedFunctions.m. In this file a default output-settings can be programmed. It could for example be helpful to present the average power after each simulation. For this setting the domain of calculation can be adjusted, such that transient behaviour has time to settle. Other options are to select signals to present in a graph, such as the displacement of all bodies and the surface elevation over time, or the power absorbed by the PTO sytem over time. Two example plots presenting the raw data from the time-simulations are shown in Figure 5.20(a) and Figure 5.20(b).

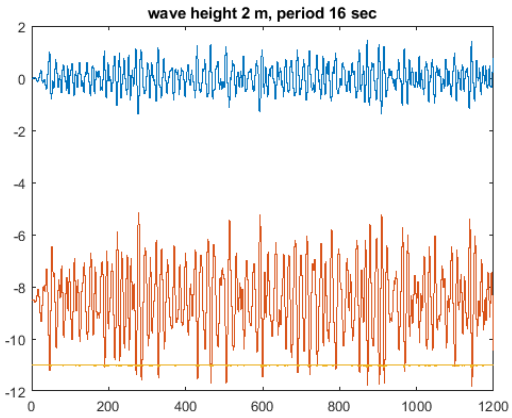

(a) Motions [m]

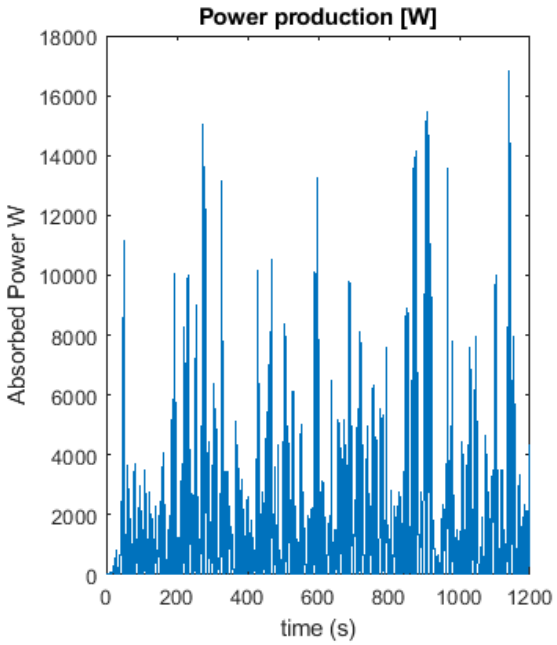

(b) Absorbed power [W]

Figure 5.20: Raw data from time-simulations of SPD modelling, Left: heave motion of the top-cap (red), the bottom buoy (yellow) and the water level (blue). Right: Power production

WECSim includes two options for three-dimensional presentation that allows to visualise all objects and their motions combined. The first method is implemented and consequently gives a fast response. However, it does not show the surface elevation. The second method includes the surface elevation in its visualisation, but the output takes more time as it saves a full description of all 3D objects for every simulated time-step.

A first assessment is made of the motion behaviour of the SPD, based on WECSim simulations with the selected model C3. The results shows that the base of the SPD hinges around the mooring connection at the bottom. There is no occurrence of the mooring line becoming slack, this indicated that the buoyancy that was given to the base was sufficient. The top of the SPD,

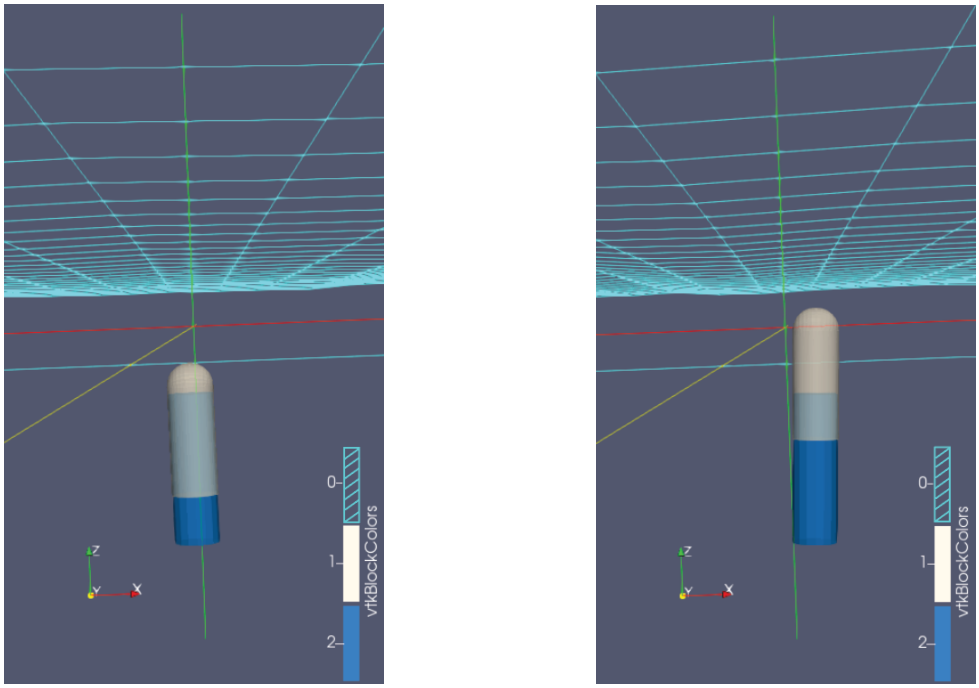

Figure 5.21: Examplary screenshots from the SPD in the 3D time-domain model. Representing the watersurface (0), the top-cap of the SPD (1) and the base-body of the SPD (2).

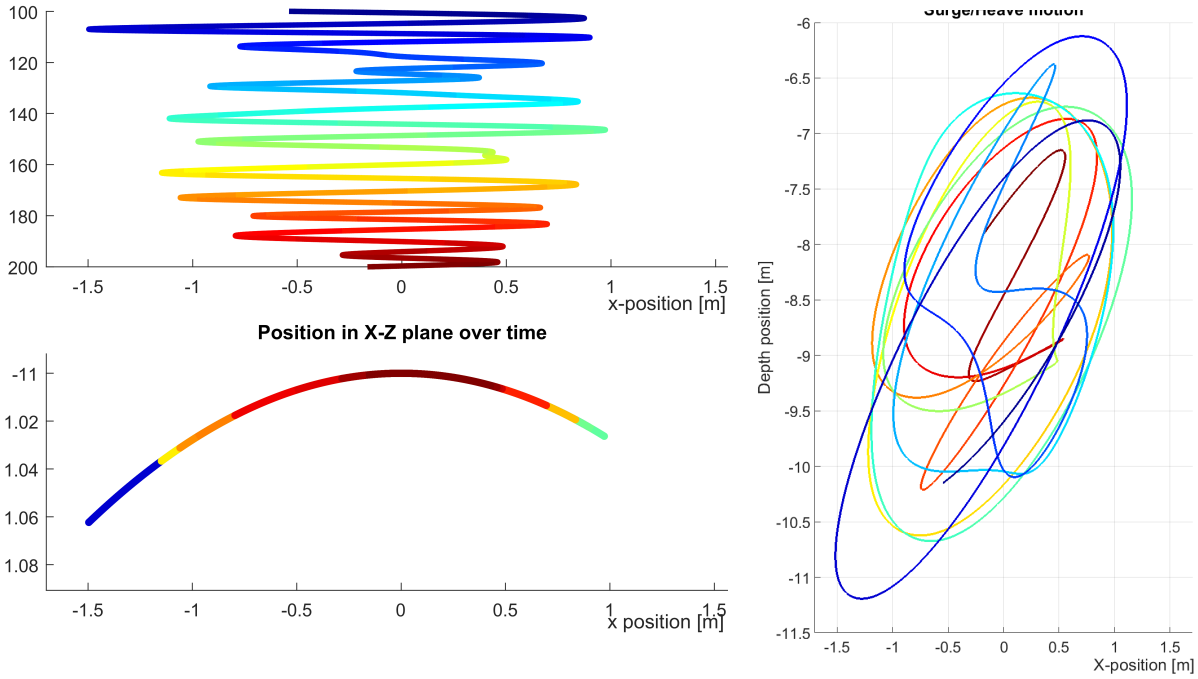

(a) Base-body (b) Top-cap

Figure 5.22: Left, top-cap motions observed from a side view. Right: the motion of the base buoy observed from a side view. Top, surge motion over time and Bottom surge/heave positions coloured over time.

5.6. Power matrix generation (Step 5)

5.6.1. Method

When performing multiple dynamical simulations for a range of sea states (combinations of wave height and wave period), a power matrix is obtained. The power matrix represents the estimated average of produced power depending on the sea state. A power matrix can be created with either regular waves or with irregular waves. Irregular waves are used for this study. For this research 140 sea states have been assessed, where wave peak periods ranged from 3 to 16 seconds with a 1 second interval, and wave heights ranged from 0.5 to 5 meters with 0.5 m interval.

5.6.2. Verification

For the reference model (C1) the power matrix has been created. See the result in Figure 5.3. The result is compared to the data available in the prior study and shows to vary from the data within [10% to -10%]. It is assumed that results are overlapping with high enough accuracy for the intended purpose of this research.

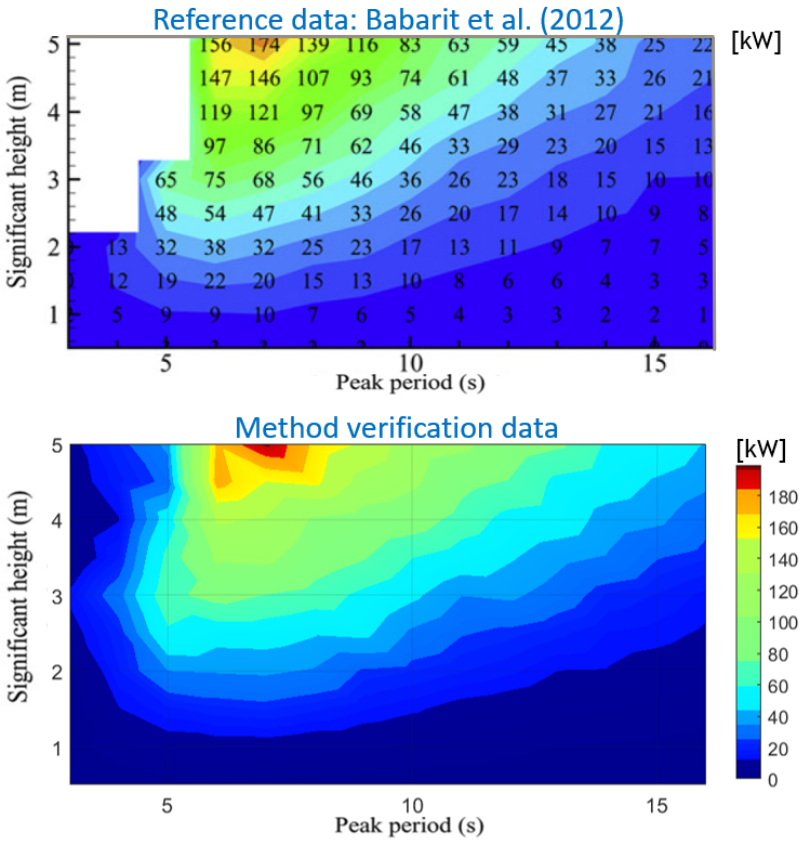

Figure 5.23: Power matrices for reference model (top figure), (the submerged heaving buoy) and the reference model from literature (bottom figure)) [4]

5.6.3. Results

As the method produced comparable results with the reference study that where deemed accurate enough for the intended purpose of this study, the method has also been applied

to the selected model C3. The power matrix for the selected model C3 (SPD) is presented in Figure 5.24: Multiple simulations showed output that was consistent, with variations

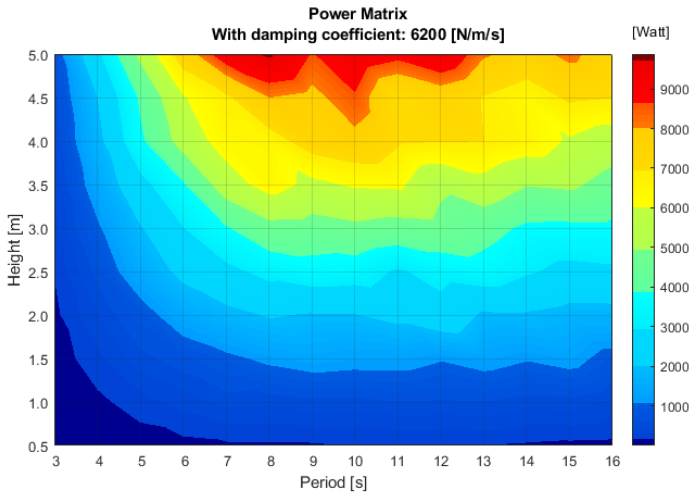

Figure 5.24: The power matrix for the selectet model (SPD) shaped rigid body with radius $a = 0.75[m]$ and submerged depth from top $dh = 6[m]$

whitin 5%, this shows the duration of the simulations was long enough. Inconsistent results would have been obtained when the duration for average power was too short and the power performance of the device was less steady.

The result shows that the performance becomes stable/constant for higher wave periods. This is the expected characteristic of a device that is brought in motion by forces acting in one direction, instead of a summation of positive and negative forces. Since the selected model C3 (SPD) is very small compared to the other devices, the power levels in the power matrix are also much lower. However, compared to the volume differences, the power has not changed equally. The reference model C1 has a displacement of $148m^3$ while the selected model C3 (SPD) has a displacement of $8m^3$, this means the SPD is 18.5 times smaller in volume. When comparing the power levels from their power matrices the reduction lies close to 10.

5.7. Power performance indicators (Step 6)

5.7.1. Method

With the power matrix obtained in Section 5.6, an estimate of the power production can be calculated with the use of statistical data of local sea conditions at a specific location.

Data is required that represent the occurrence of each sea state in hours during a year. This data is generally presented in a wave scatter diagram.

Sea conditions for 5 locations in Europe have been copied from Babarit et al. (2012) [4] and used as input, in order to create comparable results as presented in that study. The 5 locations and scatter data are: see fig. 5.25 The obtained power matrices described in Section 5.6, have both been used to assess performance for these 5 locations. Multiplying the wave occurrences (in hours/year) from the wave scatter-diagram with the average power production from the power matrix, results in the total produced energy over a year. First this assessment is conducted for the verification model, in order to test what level of agreement would be found with respect to the results form Babarit et al. (2012) [4]. Then the same assessment is conducted for selected model C3.

The reference study determined these indicators for five example locations:

- SEM- REV
- EMEC
- Yeu
- Lisboa
- Bel-mullet

Results of the study are the following performance measures:

- The annual mean output power
- The yearly energy output / mass
- The yearly energy output / wetted surface.
- The average power per unit of significant PTO force.
- The average power per unit of excitation force.
- The duration curves

These criteria were estimated for the SPD device using the mathematical model described in this report.

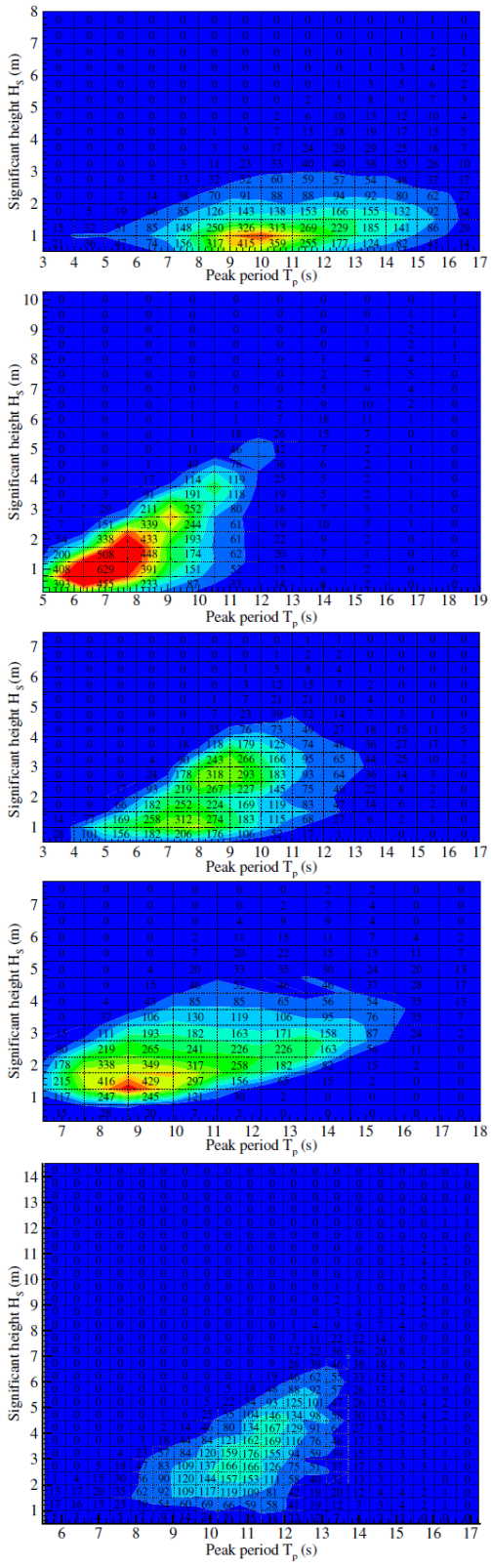

Figure 5.25: Seastate scatter plots (Babarit[4])

5.7.2. Verification

Table of performance indicators

Table 5.2 shows the verification result for the calculated performance indicators. The result can be compared to table 5.3, showing a copy of the results from the reference study.

Table 5.2: Performance indicators obtained in the verification study

Parameter [Symbol]	Unit [-]	Site SEM-REV	EMEC	Yeu	Lisboa	Belmullet
J	[kW/m]	15.0	20.3	23.0	30.2	66.2
Annual Mean absorbed power	[kW]	13.5	26.9	34.7	27.8	34.3
Capture Width	[m]	0.90	1.33	1.51	0.92	0.52
Capture Width Ratio	[%]	12.9	18.9	21.6	13.1	7.4
Ey/mass	[kWh/kg]	0.59	1.18	1.52	1.22	1.50
Ey/Awet	[MWh/m2]	0.54	1.07	1.38	1.11	1.37
Ey/{FPTO}RMS	[kWh/N]	-	-	-	-	-
Ey/{Fwave}RMS	[kWh/N]	-	-	-	-	-

In order to compare this result with the result from Babarit, below the original results are presented:

Table 5.3: Performance indicators obtained by the reference study (Babarit, 2012)

Parameter [Symbol]	Unit [-]	SEM- REV	EMEC	Yeu	Lisboa	Bel-mullet
J	[kW/m]	13.3	19.6	23.5	33.7	72.5
Annual Mean absorbed power	[kW]	8.8	18.5	22.0	19.0	31.3
Capture Width	[m]	0.66	0.94	0.94	0.57	0.43
Capture Width Ratio	[%]	9	13	13	8	6
Ey/mass	[kWh/kg]	0.39	0.81	0.97	0.83	1.37
Ey/Awet	[MWh/m2]	0.35	0.74	0.88	0.76	1.24
Ey/{FPTO}RMS	[kWh/N]	1.53	2.08	2.37	2.29	2.95
Ey/{Fwave}RMS	[kWh/N]	2.57	3.60	4.05	3.84	4.73

This table shows that there are certain differences in the answers. It seemed not possible to exactly reproduce the same results. The mean energy source has an error within bounds of 10%. The error is not consistent for each location, increased values have been found for SEM-Rev and EMEC, while a reduction was obtained for the locations: Yeu, Lisboa and Belmullet. The mean power absorption is higher for all locations in the verification study, generally 30 to 50%, only for Belmullet the value is within 10% error. A readily consistent error seems to occur at the capture width ratio. Newly found values occur to be around 30% to 60% higher than the original study suggests. The differences might have been caused by differences in input values, since the sea states are adopted by visual inspection. Another reason for varying results are differences in the different control, deviate assumptions and input parameters, strategy or due to errors made in the original study. Method optimisation could possibly improve the reliability of the result. Although errors are large, the method is assumed to be accurate enough to work with for the intended use. For further research on estimated power it is recommended to further validate the method and model to increase accuracy.

5.7.3. Results

Power performance indicators are calculated for the selected model C3. A comparison of the actual performance values is a faulty comparison, since the selected device C3 is much smaller that the reference model C1. When comparing the energy over mass ratio with the results from Babarit et al. (2012) [4], results are obtained that are presented in Table 5.4.

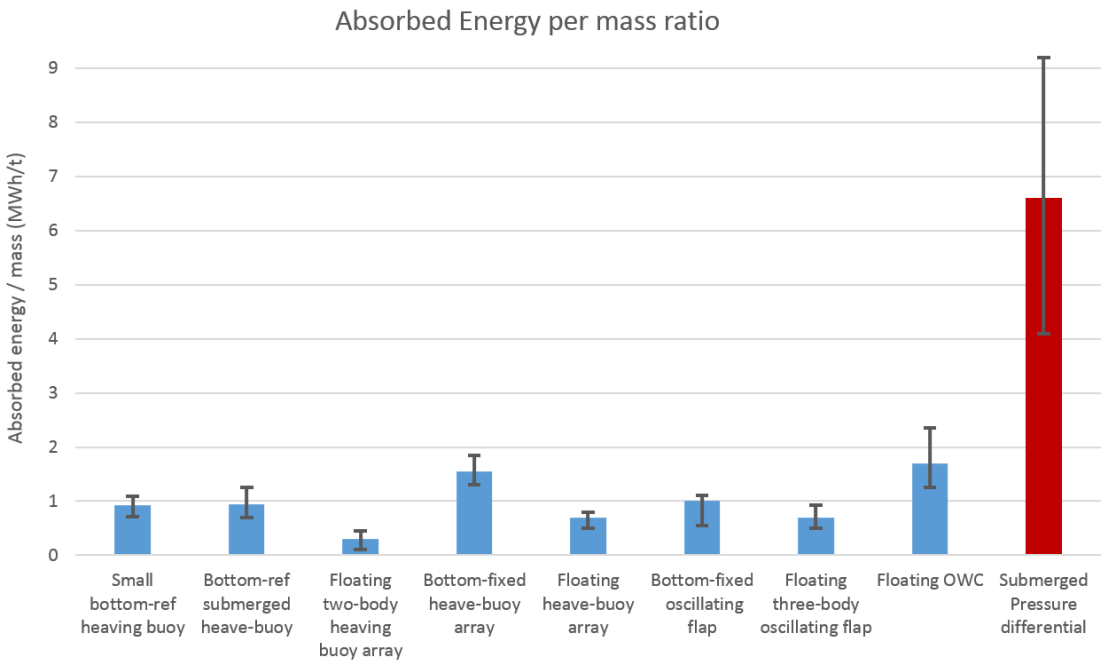

Figure 5.26: Performance indicator: Absorbed energy per characteristic mass for the SPD with a radius of $a = 0.75[m]$ and a mass $m = 3.0\ [t]$

The red bar on the right is the result for the selected model, obtained by the proceedings described in this study. The result look very promising, as the SPD scores more than six times higher than the other point absorbers and 3.5 times higher than the second best result. However the result includes large uncertainty, most importantly because the mass had to be estimated without quantitative support. Another reason for uncertainty can be found in the assumption of a turbine/generator efficiency of 90%.

Table 5.4: The performance indicators via the method of Babarit, for the selected model C3 (SPD) with radius $a = 0.75[m]$, submerged depth from top dh = 6 [m], the characteristic mass is assumed to be $m = 3000[kg]$

Parameter [Symbol]	Unit [-]	SEM- REV	EMEC	Yeu	Lisboa	Bel-mullet
J	[kW/m]	18.6	22.9	26.7	37.9	79.6
Mean power	[kW]	1.4	1.7	2.4	2.6	3.1
Capture width	[m]	0.073	0.076	0.090	0.068	0.039
Capture width ratio	[%]	10	10	12	9	5
Ey/mass	[kWh/kg]	4.0	5.1	7.0	7.6	9.1
Ey/Awet	[MWh/m2]	6.8	8.6	11.8	12.8	15.4
Ey/{FPTO}RMS	[kWh/N]	-	-	-	-	-
Ey/{Fwave}RMS	[kWh/N]	-	-	-	-	-

5.8. Conclusion

This chapter showed an the assessment for estimating power performance by dynamically modelling WEC-systems. Although aspects of the tools could be improved, with further elaboration, the complete method is applied and operational. Among the improvements, it could be made more refined and user friendly.

It can be concluded that use of panel selection allows to address wave effects separately for the top hull and the bottom hull. The hydrodynamic output is verified and show that

the panels selection tool meets expectations. The verification of the AQWA results for the verification model with the results from the literature study, showed negligible differences.

The performance of WECSim has been verified for free-floating buoys and mass-balanced, free-motion submerged buoys. The numerical results performed by WECSim showed a close resemblance with the analytical solution for floating and submerged bodies.

A method has been presented to obtain power matrices by repeated execution of simulations in WECSim. The power matrix verification results show clear resemblance. In the last phase, the performance indicators were calculated. Some differences are observed in the calculations of the Annual Mean absorbed power. This might require further investigation. Differences might be smaller when the original data was acquired.

6. Theoretical maximum power production

This chapter describes the Method 2 for top-down technical assessment. The method is used in Sergiienko et al. (2017) [47] to describe the fundamental differences of floating and submerged point absorbers. This chapter assesses the fundamentals of the quasi-rigid Submerged Pressure Differential device (SPD).

The method is used to estimate boundaries for theoretical maximum absorbed power for the selected model (C3). Estimates for maximum absorbed power can be used to optimise WEC control strategies and to compare the viability independent of technology readiness. The method is referred to in this thesis as the top down method because it only includes the first step in Wave Energy Conversion, the absorption stage and neglects the hydrodynamic losses for this step.

6.1. Method

In Sergiienko et al. (2017) [47], the theoretical maximum absorbed power for floating and submerged buoys for several configurations are evaluated. The limits that are applied, were first described by Budal and are therefore referred to as the Budal limits. For this research, a calculation tool is created in order to implement the method used by [47]. Verification of this implementation is done by reproducing results from [47]. For the verification step the cilinder model is used, see Figure 6.1(b). After verifying the implementation, the method is extended for the selected model C3 (SPD). With this tool, first the Excitation force coefficients are calculated, then two boundaries for maximum power absorption are calculated. The calculation method to obtain theoretical maximum power production limits, is first verified before it is applied to the test-concept. For verification, the method is applied on the a reference-model.

Model configurations

Figure 6.1(b) shows the model used by the reference study [47]. The figure shows dimension for a floating cylinder (a), superficially submerged cylinder (b) and a deeper submerged cylinder (c). The model used for test-concept is shown in Figure 6.2.

The Figure 6.3 show two important power extraction limits:

1. A high frequency limit P_a. The ability of the body to radiate waves also defines the ability to cancel out the incoming waves. This means absorption is limited by the ability of a body to radiate waves.
2. Low frequency limit P_b. The excitation force that applies on the body in the direction of the power extraction, defines the maximum power absorption for lower frequencies (or in case of a small device in long waves, defines the maximum for all relevant (contributing) frequencies).

Theory for limit P_a

In [47] the limits for a floating and a submerged buoy are derived in Equation (6.2). The limit at higher frequencies is defined by the body's ability to radiate waves. (assuming deep water

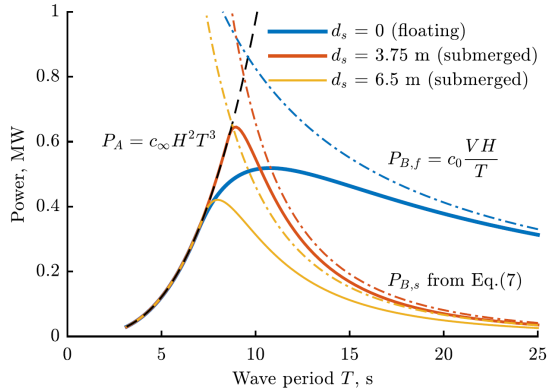

(a) Truncated vertical cylinders

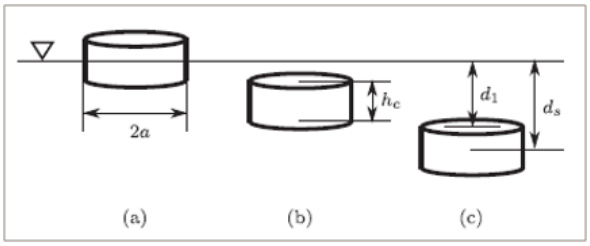

(b) The *Truncated vertical cylinder* in heave, for a floating and submerged situation

Figure 6.1: Left: Power absorbed by the floating and submerged truncated vertical cylinders (b) in regular waves vs. wave period. Wave height is $H = 2m$. The sphere radius is $a = 5m$, heave displacement is constraint to $0.6a$, wave height. Cylinder radius and height are $h_c = a = 5.5m$, heave displacement is constraint to $0.5h_c$. The dashed curve corresponds to the P_a limit from eq. 6.2, and three dash-dotted curves show the P_B bounds. Right: shcematic representation of the floating and submerged truncated vertical cylinders.

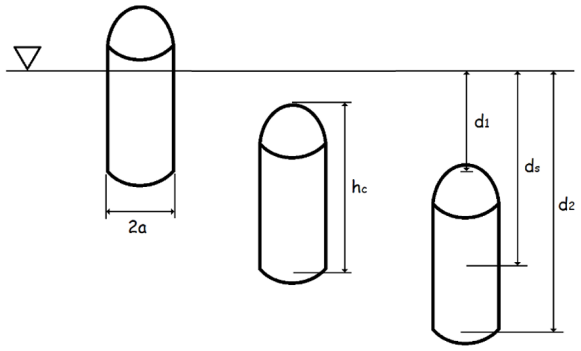

Figure 6.2: Selected model C3, in heave, in floating position (A) with rigid body configuration and in submerged position (b and C) tested in both, rigid body configuration and in SPD configuration

conditions $\omega^2 = kg$:

A well known equation characterising the maximum absorbed power by an axisymetric body in monochromatic waves is [47]:

$$P_a = \frac{J}{k} \tag{6.1}$$

Where $J = \rho g^2 D(kh) A^2/(4\omega)$ is the wave-energy transport per unis frontage of the incident wave, α is a coefficient that depends on the motion oscillation mode ($\alpha = 1$ for heave, $\alpha = 2$ for surge or pitch, and $\alpha = 3$ when the body oscillates in heav, surge and pitch simultaneously)

$$P_a = \frac{J}{k} = \frac{\rho g^2 A^2}{4\omega k} = \frac{\rho g^3 (\frac{H}{2})^2}{4\omega^3} = c_\infty T^3 H^2 \tag{6.2}$$

where $c_\infty = \rho(g/\pi)^3/128$, is the wave velocity at H = 2A is the wave height, $T = 2\pi/\omega$ is the wave period. This shows that the first limit is independent of the objects dimensions.

Theory for limit P_b

The limit at lower frequencies is defined by the maximum swept volume of the body, which applies when the velocity of the converter is smaller than the optimal value due to physical

constraints: Sergiienko uses the theory reviewed by Evans (1981) [19], where the maximum power of a body (excited by the force of the waves) is defined. The body responds to this force by oscillating with a velocity u_j. The paper states that the excitation body in heave could be represented by:

$$P_e = \frac{1}{2}|\hat{F}_{e,j}| \cdot |\hat{u}_j| \cos(\gamma_j) \tag{6.3}$$

In which:

$|\hat{F}_{e,j}|$ - Excitation force amplitude [N]
$|\hat{u}_j|$ - Velocity amplitude [m/s]
$\gamma_j = \phi_u - \phi_F$ - Phase difference [rad]

Where $|\hat{F}_{e,j}|$ is the excitation force amplitude and $|\hat{u}_j|$ is the velocity amplitude and $\gamma_j = \phi_u - \phi_F$) is the phase difference between $\hat{u}_j$ and $\hat{F}_{e,j}$. Then the paper states the optimal velocity is defined as:

$$|\hat{u}_j|_{opt} = (|\hat{F}_{e,j}|/2b_{jj}) \cos(\gamma_j) \tag{6.4}$$

In which:

$|\hat{u}_j|_{opt}$ - Optimal velocity in j direction $[m/s^2]$
b_{jj} - The radiation damping force for direction j in due to direction j [rad]

And that the maximum power is equal to:

$$P = P_{max} = \frac{|\hat{F}_{e,j}|^2}{8b_{jj}} \cos^2(\gamma_j) = (P_r)_{opt} = \frac{1}{2}(P_e P_i)_{opt} \tag{6.5}$$

In which:

P_r - Radiated power $[N\frac{m}{s}]$
P_e - Excitation power $[N\frac{m}{s}]$
P_i - The radiation damping force for direction j in due to direction j [rad]

The excitation force exerted on the body in the j-th direction is obtained by the integration of pressures($\hat{p}$) along the hull (S).

$$\hat{F}_{exc,j} = -\iint_S \hat{p}(x,y,z) n_j \, dS \tag{6.6}$$

In which:

n_j - Normal vector of the panel in the x, y and z direction [-]
$\hat{p}$ - Local pressure at panels along the hull[rad]

$$\hat{F}_{exc,j} = \int_0^a \int_0^{2\pi} (\hat{p}_{top}(r,\theta,-d_1) - \hat{p}_{bot}(r,\theta,-d_2)) r \, dr \, d\theta \tag{6.7}$$

In which:

$\hat{p}_t$ - pressure on the top-side of the hull $[\frac{kg}{m \cdot s^2}]$
$\hat{p}_b$ - pressure on the top-side of the hull $[\frac{kg}{m \cdot s^2}]$
r - Radial distance of position on hull $[m]$
θ - Azimuth angle of position on hull $[rad]$
d_1 - Depth of top part of the hull $[m]$
d_2 - Depth of bottom part on hull $[m]$

The hydrodynamic pressure on the top of the floater is often located close to the surface. Free-surface effects become more significant due to resonance amplification of waves in the water domain above the cylinder and, therefor, the hydrodynamic pressure cannot be simplified using e^{kz} function. There is a first order approximation for this effect described by Jiang et al. (2014) [30]. This approximation makes use of the besel function $J_0(kr)$.

Simple deep water estimation of wave forces would introduce to much inaccuracy.

The hydrodynamic pressure on the cylinder top can be described by

$$\hat{p}(r,\theta,-d_1) = \rho g A e^{i(-krcos\theta - phi_z)} \frac{J_0(kr)}{J_0(kr)cosh(kd_1)} \tag{6.8}$$

When only top pressure is included to model a quasi-rigid SPD, then the excitation force is obtained by:

$$|F_{exc,3}| \leq |\rho g A \pi a^2 (\frac{1}{\cosh kd_1})| \tag{6.9}$$

In order to obtain the power bound P_b, the excitation force would be substituted into:

$$P \leq \frac{1}{2}|\hat{F}_{e,3}| \cdot |\hat{u}_j| \tag{6.10}$$

This method shows that an analytical approximation of the excitation force can be obtained under the simplification that bottom panels can be excluded. In addition, this method shows that the power boundary, P_b, which depends on device dimensions, can be obtained. With this method a fast optimisation method is obtained.

6.2. Verification

The calculation tool that is created to apply the method (described in previous section) is verfied with the results from Sergiienko et al. (2017) [47]. Figure 6.3 shows that similar limits are obtained for the heaving cylinder submerged at a depth of 3.75 m (red line).

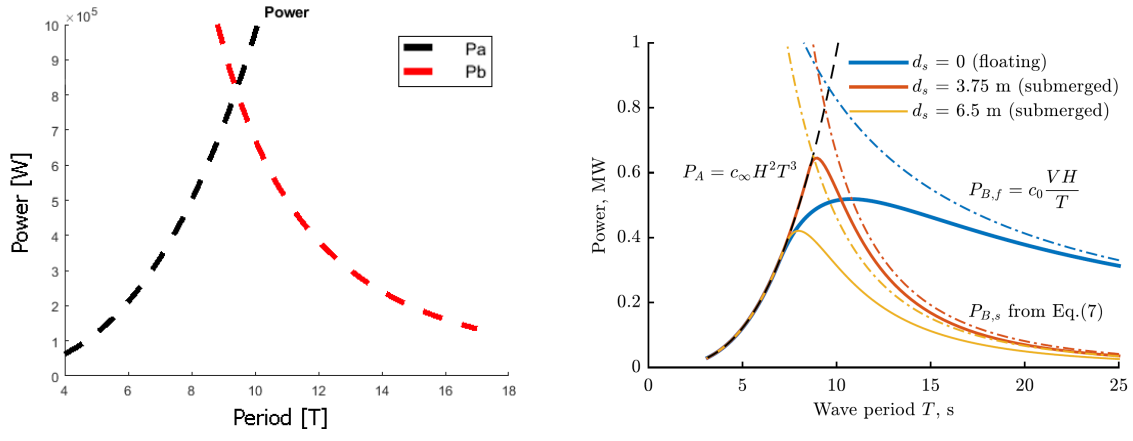

(a) (b)

Figure 6.3: Validation of the power limits for a submerged truncated vertical cylinders (b) in regular waves vs. wave period. Wave height is $H = 2m$. Cylinder radius and height are $h_c = a = 5.5m$, heave displacement is constraint to $0.5h_c$. The dashed curve corresponds to the P_a limit from eq. 6.2, and three dash-dotted curves show the P_B bounds from eqs.

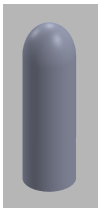

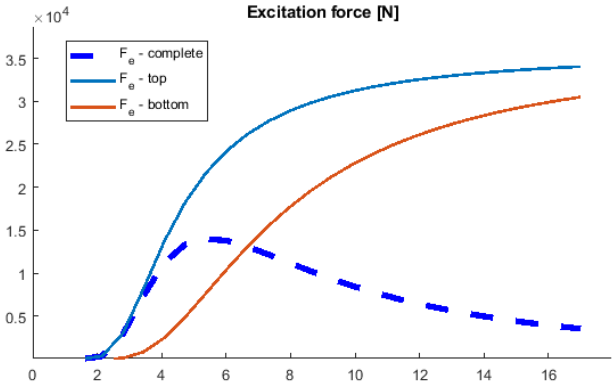

(a) The force excitation at the top panels (blue), and the bottom panels (red) that works in the opposite direction (here for visualisation purpose multiplied by -1) are considered separately or combined(blue dash).

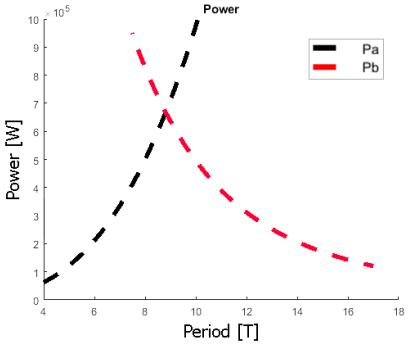

(b) The power limits (dashed lines) represent limits for a submerged rigid body with the shape of C3. Rigid body behaviour is obtained since the red dashed line includes both the top and bottom forces.

6.3. Results

The method to calculate the Budal limits (as used by Sergiienko et al. (2017) [47]) is now extended for quasi-rigid Submerged Pressure Differential devices (SPD), and by example applied to the selected model C3.

A first partial result is found, when observing the calculated force excitation, see Figure 6.4(a). Similar to what was found with method 1 (Estimation of power performance by dynamic simulation, Chapter 5) the force excitation for the SPD differs from the submerged buoy, for larger wave periods (for $T > 4$). As was explained in Chapter 5, the lower excitation force for the submerged buoy is caused by the cancellation of the upward forces and the downward forces. The submerged buoy only utilises the difference between top and bottom forces, while the submerged pressure differential can address the full wave excitation force present that is available at that depth, without the cancellation effect.

It can be concluded that the power limit P_b is found to be significantly higher when the bottom part is not included. Figure 6.5 presents two solid lines: red for the forces acting on the bottom of the buoy and blue for the forces acting on the top panels. The other lines are dashed, the yellow line is the high frequency limit (Pa) and does not change for variations in shape. The blue dashed line would be the limit when the body is rigid. While the solid blue line would be the limit if this body would act as a quasi-rigid body (representing the SPD-WEC).

Simulation results show, fig.6.6 that with optimised PTO-control settings the extracted power exceeds the limit for rigid bodies. The simulated power results seem to match with the curve for the bottom limit. However, it is expected that further improving the PTO-control settings the performance could increase even further, up to the limit of the upper panels.

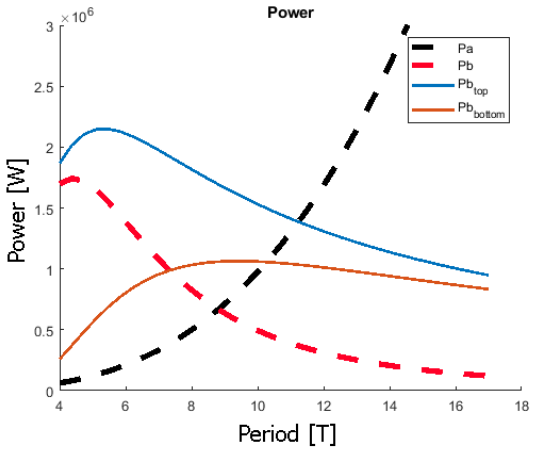

Figure 6.5: The power limits (dashed lines) represent limits for a submerged rigid body with the shape of C3. Bullet shaped rigid body with radius $a = 5.5[m]$ - Dashed lines represent the limiting power when bottom and top form one rigid body, power absorption without volume changing characteristics. The blue line however, would And thus it does not represent a pressure differential device.

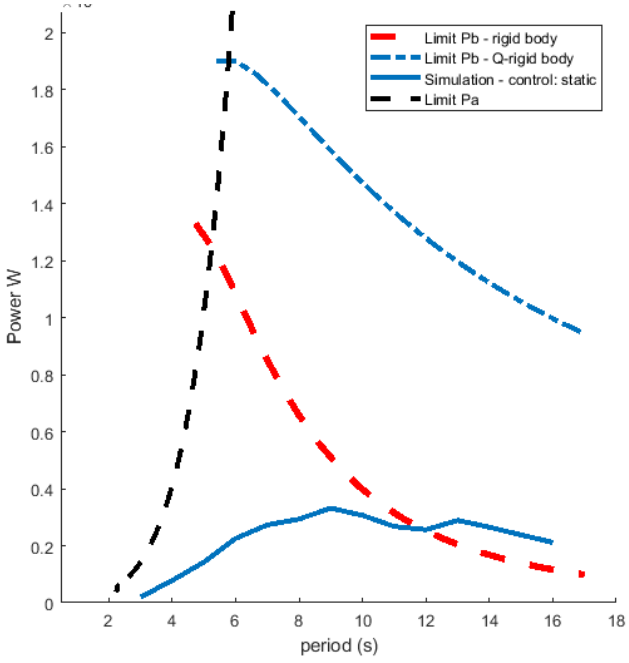

Figure 6.6: The power limits for the SPD with radius $a = 0.75[m]$

7. Conclusion and recommendations

7.1. Conclusions

The need for alternative sources of energy is apparent. And the desire to assess whether wave energy could contribute is recognised. Several earlier WEC-concepts have failed to achieve commercial viability.

Although oceanic waves contain a significant amount of potential energy, initial costs for WEC-realisation are high and the ROI, as with all innovations, is difficult to predict. What makes this prediction difficult is that the amount of energy that can be generated is depending on a vast amount of factors. Offshore device locations are susceptible to extreme wave conditions as they are located in deep water. WEC-systems have to resist even tougher conditions than wind farms, as they will be positioned in areas with higher wave intensity, which are generally in less sheltered locations. The risk of damage to the devices before revenue pays back the initial installation costs (CAPEX) and maintenance costs (OPEX) is significant. More information on these factors can be found in chapter 3.

To encourage investors governmental funding should support the consumption of wave energy to the local grid through feed-in tariffs. To achieve this support, a concept should show a certain level of maturity, but unlike the wind industry, opinions about the best approach to harvesting wave energy are divided. Moreover, the WEC-concepts that are currently being developed are based on a large variety of working principles, which impedes comparison.

Because of this need for convergence towards one WEC-concept and the urge for a method to evaluate concepts that are promising, this research aims to assess existing comparison studies WEC-system viability and to complement these studies by adapting them for application on potential concepts.

This convergence should be based on the level to which a concept combines limited cost for production and operation (1) with high power performance (2) without being damage prone (3). With the method described in this research the performance of several types of point absorber WEC concepts could be compared which illustrated the favour-ability of the Submerged Pressure Differential concept (SPD).

From this research the following conclusions have been obtained in relation to the three aspects of optimal WEC concept determination:

1. Although several types of WEC-concepts exist, point absorbers, of which the SPD is one example, have illustrated valuable advantages in comparison. Their constructions are relatively small, which supports reproduction in manufacturing purposes and decreased cost of transport. Due to their axisymmetry, they do not require a rotation compensation system to benefit from all wave directions. A grid of smaller WEC components is easier to maintain because individual components can be repaired without halting production. The largest contributor, however, is the fact that point absorbers are able to interact as a fictitious larger object, due to resonance by optimal control of the dynamic parameters resulting in a power production increase. (See chapter 4)
2. The advantage of the resonance effect in point absorbers is illustrated in Figure 5.26 by an energy over mass estimation where the SPD performed significantly better than other types of WEC concepts . The note should be made that the defined mass for the SPD in this calculations, although according to the specs defined by company developing the sample SPD, does not include the mass of the foundation to which the device would be

connected. More detailed description of the steps for the time-domain analysis can be found in chapter 5. The analysis of the dynamic principles of the SPD illustrates that the limits of maximum absorbed power for this concept are significantly higher than a rigid-submerged buoy. They are within the range of power that could theoretically be reached with a floating buoy. (See chapter 6)

3. In contrast to a floating point absorber that shows a high power performance due to its surface position, the SPD is better shielded from storm conditions. The working principle of the SPD allows for an increased power performance when compared to other submerged WEC's that also profit form the shelter. Bearing these benefactors in mind it can be concluded that among the point absorber WEC devices, the SPD has the highest rate of potential success.

7.2. Recommendations

It is important to realise that, although the concept of the SPD presented in this study shows promising, it consists of new components and includes an uncommon technology to transform energy. The multi-purpose membrane of the SPD, for example, is a vital part of the concepts structural integrity but due to its location within the device, is also a difficult component to repair.

Apart from the aforementioned aspects, the SPD contains the advantage of increased controllability. This concept supports the adjustment of settings that allow for optimal interaction with different wave conditions as they change during the operation of the device. By adjusting the spring stiffness, the natural frequency of the SPD can match the peak frequency of the wave, resulting in the capture of the highest wave forces. Floating and submerged buoys are restricted in this aspect as altering spring stiffness, directly results in a change of positioning.

The WECSim analysis showed that the SPD concept allowed to make use of latching control at certain moments. This way it can fully address the phase difference in the wave motion to increase power production. One design of a floating point absorber [40] applies the same effect for its benefit, but uses it continuously, making the buoy more susceptible to damages. This concept was not included in the study. A comparison between the selected SPD concept and this specific floating buoy could prove interesting for further research.

For further research on the Symphony, extended work could lead to a cash-flow-model, from which the feedback could lead to further optimisation of this concept.

The methods used to assess the performance of the selected SPD concept and to compare it to the two other types of point absorbers showed comparable results when applied to the point absorber concepts of which performance data was available prior to this study. The comparison (of floating, submerged and SPD) that is presented in this study chose specific characteristic to model these devices. Several different device concepts of floating and submerged buoys exist (Variations in dimension, degree of freedom and absorption in heave, surge or pitch). In this study a single device design was selected for each and one specific set of dimensions was chosen. Both these factors could influence the outcome of power performance. The shape and dimensions have not been optimised in this study, further research could investigate this.

The open source software tool WECSim showed to produce reliable results compared to other tools used in other studies in the method to assess performance of the reference devices. The validity of WECSim simulation results, although verified in this study, could be checked by a more renowned software package, for example Orcaflex.

In the reference studies of Babarit [4] and Sergiienko [47] rigidity of device bodies was a prerequisite. The extended methods described in this study allows for calculation of hydrodynamic coefficients of semi-rigid bodies by selective use of panels and velocity potentials in

the coefficient calculation. This supports expansion of the volume when performing time-domain simulations.

The question rises whether the method described could be applied to estimate the performance of other types of WEC devices, beyond point absorbers. Assuming that each concept can be simplified in order to select panels that should be included in the hydrodynamic coefficient calculation, the method is expected to be applicable. The surface area where water enters and exists the column would not be marked for coefficient calculation. Further research should investigate whether the performance estimation through use of the described methods is as reliable for this WEC concept as it is for point absorbers. Although application might be technically feasible, In the case of the OWC the water pressure of delayed waves creating pressure on the inner wall of the device will highly complicate the determination of hydrodynamic coefficients on the included panels.

The technical and economical methods described have been applied only up to a basic extend. Optimisation of the methods through application on different WEC concepts has the potential to lead to a general method to assess power performance, assisting the need for convergence towards a single concept to eventually support the declaration of wave energy as an viable source of renewable energy.

A. Wave power in the oceans

A.1. Defining ocean energy

That ocean waves can contain vast amount of energy is something people have experienced at regular occasions over time: Ships and dykes are both in their own way in a constant fight against oceanic waves and that a single tsunami wave can destroy complete cities is well known. Another experienced phenomena about ocean waves is that a storm at one side of the ocean basin can be the origin for waves measured at the other side, showing waves travel over great distances with very little energy loss [43, p. 20] The scope is limited by looking at ocean surface waves with periods in the range of 0.5-30 seconds [43, p. 20]. Figure A.1 represents the classification of ocean waves by wave period (derived from Munk, 1951).

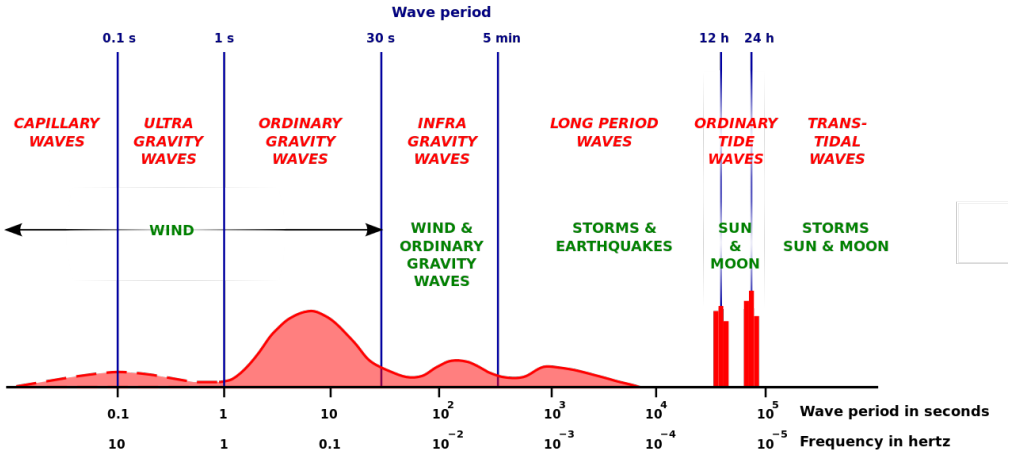

Figure A.1: Classification of ocean waves by wave period (derived from Munk, 1951)

Energy produced from larger periodic waves is defined as tidal energy (long-period waves and tidal waves, 30s to 24h and more), mainly caused by earths position with regard to the sun and the moon, occasionally long-period waves are caused by other phenomena like seiches (only in a bay or gulf, due to motion of the complete enclosed water body as a whole), storm surges (due to wind and atmospheric pressure changes caused by a storm) or tsunamis (shifting landmass). Waves with period smaller than 0.5 seconds are defined as capillary waves, this physics phenomena occurs at the boundary layer of two materials with different density and the surface tension. (ref to book) Assessing wave energy, both wind and swell waves are incorporated. Wind waves are formed by wind blowing over the the already rough ocean surface, creating pressure differences over the wave crests. Above a wave crest the Wind velocity is high and the pressure is low, while above the trough, the wind velocity is low and the pressure high. This pressure distribution induces shear stresses along the sides of the crests, and thereby stimulates the celerity and growth of the waves towards the wind direction. Swell waves are formed by distant storms. The scope is limited by looking at ocean surface waves with periods in the range of 0.5-30 seconds [43, p. 20]. Energy in larger period waves is defined as tidal energy (long-period waves and tidal waves, 30s to 24h and more), mainly caused by earths position with regard to the sun and the moon, occasionally long-period waves are caused by other phenomena like seiches (only in a bay or gulf, due to motion of the complete enclosed water body as a whole), storm surges (due to wind and atmospheric pressure changes caused by a storm) or tsunamis (shifting landmass). Waves with period

smaller than 0.5 seconds are defined as capillary waves, this physics phenomena occurs at the boundary layer of two materials with different density and the surface tension. Without dissipation or insertion of energy the total wave energy is a summation of potential energy and kinetic energy and a constant mutual transfer of energy between the two take place.

In a study commissioned by Carbon trust[1] in the UK, distinguished four definitions for estimated resources: [50]

- Total Resource (TWh/y): The total resource arriving in UK waters. It is the total resource flowing over a single frontage (or group of frontages) that are arranged to give the highest overall energy availability to the UK. These frontages do not take into account potential location constraints such as water depth and distance to shore.
- Theoretical Resource (TWh/y): The maximum energy available from a set of frontages positioned in realistic locations based on areas likely to have the most competitive low cost of energy.
- Technical Resource (TWh/y): The energy available from the theoretical frontages using envisaged technology options.
- Practical Resource (TWh/y): The proportion of the technical resource that can be extracted taking into account locations constraints such as sea uses and environmental impacts.

A.2. Global distribution of wave energy

Several coastal locations on earth are in the vicinity of vast amounts of wave power. Models produced to estimate the global distribution of wave energy show high concentrations north of the *tropic of cancer* and south of the *Tropic of Capricorn*. Furthermore, Coriolis effects causes Western coasts typically to contain higher levels of wave energy than eastern coasts. Models for wave energy estimates are mainly focused on the oceans, as smaller seas generally contain energy levels that currently are not high enough for power extraction. For some countries the estimated yearly averaged power levels even exceeds their national consumption. The consensus tends towards a global theoretical available wave power of around 2 TW ($18 \cdot 10^3$TWh/year).

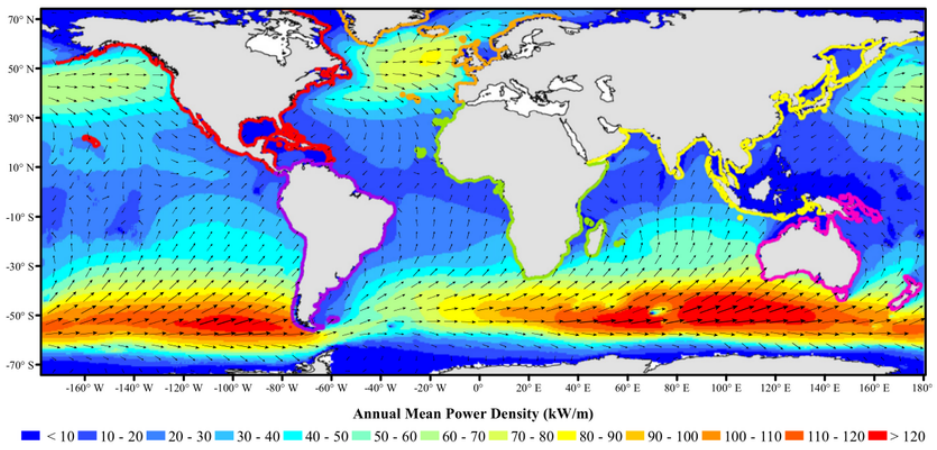

Figure A.2: The global resource of yearly averaged wave power per meter

[1]Carbon trust is a subsidised company stimulating renewable energy production world wide, and has its origin in the UK

B. Physics of waves

This appendix discusses motions of floating bodies excited by incoming waves.

B.1. Linear wave theory

Linear theory is based on two equations: a mass balance equation and a momentum balanced equation. These two equations are describing the kinematics and dynamic aspects of waves. Waves can be described by linear wave theory when the amplitude of the waves is small compared to the water depth and wave length. In this case non-linear effects of waves are negligible. Furthermore, it is assumed that water is an ideal fluid, which implies incompressible, constant density, no viscosity and no rotation of water particles around their own axis. From the mass balance equation the continuity equation can be derived.

$$\frac{\partial u_x}{\partial x} + \frac{\partial u_y}{\partial y} + \frac{\partial u_z}{\partial z} = 0 \tag{B.1}$$

In which:

u velocity
x, y, z indicating direction of a 3-dimensional reference frame

The position of the reference frame is located on the mean water level surface, with the positive x-axis towards the right and the positive z-axis upwards, see also Figure [ref to figure]

To solve this equation use is made of the velocity potential function $\phi = \phi(x, y, z, t)$, shown below as B.2.This function is defined as a function of which the spatial derivatives are equal to the velocities of the water particles [29]. Substituting this in B.1 the Laplace equation is obtained **??**.

$$\begin{aligned} \text{Velocity potential function:} & u_x = \frac{\partial \phi}{\partial x}, \quad u_y = \frac{\partial \phi}{\partial y}, \quad u_z = \frac{\partial \phi}{\partial z} \\ \text{Laplace equation:} & \frac{\partial^2 u_x}{\partial x^2} + \frac{\partial^2 u_y}{\partial y^2} + \frac{\partial^2 u_z}{\partial z^2} = 0 \end{aligned} \tag{B.2}$$

Boundary conditions can be defined at the water surface (η) and at the bottom in terms of the velocity potential function. The kinematic boundary conditions are:

$$\text{Kinematic boundary conditions} \begin{cases} \frac{\partial \phi}{\partial z} = \frac{\partial \eta}{\partial t} & \text{at } z = 0 \\ \frac{\partial \phi}{\partial z} = 0 & \text{at } z = -d \end{cases} \tag{B.3}$$

With the kinematic boundary conditions and the velocity potential function the Laplace equation can be solved. One of the analytical solutions of the Laplace equation with the kinematic boundary conditions is a long-crested harmonic wave, propagating in the positive x-direction. In fact, this wave represents the surface elevation and can be defined as:

$$\eta(x, t) = a \sin(\omega t - kx) \tag{B.4}$$

In which:

a Wave amplitude $[m]$
ω Wave frequency $[rad/s]$
t time $[s]$
k Wave number $[rad/m]$

The velocity potential derived from this equation is:

$$\phi = \hat{\phi}\cos(\omega t - kx) \quad with \quad \hat{\phi} = \frac{\omega a}{k}\frac{\cosh[k(d+z)]}{\sinh(kd)} \tag{B.5}$$

The above solution of the Laplace equation is based on a mass balance (continuity equation) and the kinematic boundary conditions only. This implies that all the kinematic aspects (velocities and accelerations) can be derived from Equation (B.5) and Equation (B.5). Since wave energy implies the movement of water particles, the equations above are essential for describing the distribution of wave energy in the water column.

When waves are propagating they are transporting energy in the direction of propagation. This horizontal transport of energy is due to the work done by the wave induced pressure. This wave induced pressure can be described by the dynamic aspects of waves, which are derived from the momentum balance. Momentum is by definition the mass density of water times the velocity of the water particles. The second law of Newton states that the rate of change of momentum equals force. For momentum in the x-direction the following momentum balance equation is obtained:

$$\frac{\partial(\rho u_x)}{\partial t} + \frac{\partial u_x(\rho u_x)}{\partial x} + \frac{\partial u_y(\rho u_x)}{\partial y} + \frac{\partial u_z(\rho u_x)}{\partial z} = F_x \tag{B.6}$$

$$\text{The dynamic boundary condition is defined as:} p = 0 \text{at} z = 0 \tag{B.7}$$

The pressure (p) at the water surface is assumed as zero and functions as a reference pressure since the interest is in the pressures below the water surface. In Equation (B.6) Fx is the body force in x-direction per unit volume. The second, third and fourth terms are the advective terms and contain non-linear terms. In order to make the theory linear, these terms should be removed from the momentum equation. After applying some mathematics and ignoring the non-linear terms in Equation (B.6) the linearised Bernoulli equation for unsteady flow is obtained, shown as Equation (B.8).

$$\frac{\partial\phi}{\partial t} + \frac{p}{\rho} + gz = 0 \tag{B.8}$$

Just as the kinematic boundary condition, it is possible to express the dynamic boundary condition in terms of the velocity potential. This implies $z = 0$ with $p = 0$ and results in:

$$\frac{\partial\phi}{\partial t} + g\eta = 0 \; z = 0 \tag{B.9}$$

The analytical expression for the wave induced pressure is derived by substituting the solution of the velocity potential function Equation (B.5) into the linearised Bernoulli equation Equation (B.8). After substitution the following result is obtained:

$$P_{wave} = \hat{P}_{wave}\sin(\omega t - kx) \; thith \; \rho g a\frac{\cosh[k(d+z)]}{\cosh(kd)} \tag{B.10}$$

The equations above together with the boundary conditions are summarised in Figure B.1. In this figure the Laplace equation together with the kinematic boundary conditions and the linearised Bernoulli equation with the dynamic boundary conditions are shown.

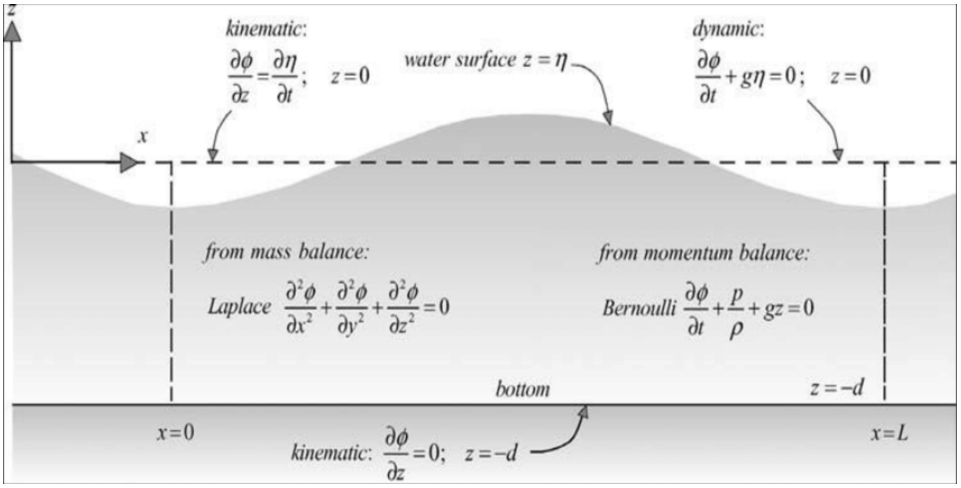

Figure B.1: Linearised basic equations and boundary conditions for the linear wave theory, in terms of velocity potential **??**

B.2. The dispersion relation

The dispersion relation:

$$\omega^2 = gktanh(kh) \tag{B.11}$$

The wave number:

$$k = \frac{2\pi}{\lambda} \tag{B.12}$$

The deep water approximation:

$$\omega^2 = gk \tag{B.13}$$

B.3. Wave length and speed for deep water

Using the deep-water approximation, the wave length is:

$$\lambda = \frac{2\pi}{k} = \frac{2\pi g}{\omega^2} = (\frac{g}{2\pi}T^2) \approx 1.56T^2 \tag{B.14}$$

$$c = \frac{\omega}{k} = \frac{g}{\omega} \tag{B.15}$$

The group speed of the waves is:

$$c_g = \frac{\partial\omega}{\partial k} = \frac{g}{2\omega} = \frac{c}{2} \tag{B.16}$$

B.4. Regular waves

The most interesting result of linear wave theory is a long-crested propagating harmonic wave. This harmonic wave (regular wave) can be defined as a propagating sinusoidal wave with an amplitude (a), radian frequency (ω) and wave number (k). The equation of the sinusoidal harmonic wave is shown below.

$$\eta(x,t) = \frac{H}{2}\sin(\frac{2\pi}{T}t - \frac{2pi}{L}x) = a\sin(\omega t - kx) \tag{B.17}$$

The phase speed is the forward speed (c) by which the wave propagates while the phase (ωtx) remains constant. Mathematically this implies that the time derivative of the phase is zero. From this the phase speed is obtained Equation (B.18). The parameters used in the equations are shown in Figure B.2.

$$c = \frac{\omega}{k} = \frac{L}{T} \tag{B.18}$$

B.5. Irregular waves

If one observes the water surface, it can be seen that it continuously changes without repeating itself. When the water surface elevation is measured, the resulting signal will be like an irregular wave signal, which can be modelled by the sum of a large number of harmonic wave components:

$$\underline{\eta}(t) = \sum_{i=1}^{N} \underline{a_i} \cos\left(2\pi f_i t + \underline{\alpha_i}\right) \tag{B.19}$$

In which:

N	Number of frequencies $[-]$
$\underline{\alpha_i}$	Phase as a random variable $[rad]$
$\underline{a_i}$	Amplitude as a random variable $[m]$
f_i	Wave frequency $[Hz]$

Each wave component is a propagating regular wave which has a sinusoidal shape. From this it follows that the irregular wave signal, which describes the surface elevation, can be decomposed by a Fourier series into a number of harmonic waves, see Figure B.2. The result is a set of values for the amplitude (a_i) and phase (α_i), where the underscores indicate that the variables are random. Each set of values of a_i and α_i belongs to the frequency f_i. This approach is called the random phase amplitude model. The benefit of this model is that it is possible to describe the waves as a spectrum.

The random variables are characterised by their probability density functions. The phase (a_i) at each frequency (f_i) is uniformly distributed between 0 and 2π. The amplitude (a_i) has at each frequency (f_i) a Rayleigh distribution [Holthuijsen (2010) [29]].

If the expected value of the amplitude ($E\underline{a_i}$) is considered, it is possible to generate an amplitude spectrum. However, it makes more sense to consider the variance of the amplitude ($E\frac{1}{2}\underline{a_i}^2$), because the wave energy spectrum can easily be obtained by multiplying the variance spectrum with the density of the water (ρ) and the gravitational acceleration (g). The variance spectrum is discrete, i.e., only the frequencies f_i are present. At sea all frequencies are present. In order to obtain a continues distribution of the variance over the frequency, this approach is modified by dividing the variance of the amplitude by the frequency interval Δf_i. When the width of the frequency interval (Δf_i) approaches zero, a continuous distribution of the variance over the frequency interval is obtained. This distribution is known as the (one-dimensional) variance density spectrum:

$$E(f) = \lim_{\Delta f \to 0} \frac{1}{\Delta f} E\tfrac{1}{2}\underline{a}^2 \tag{B.20}$$

The variance density spectrum gives a complete description of the surface elevation of waves in a statistical sense, under the assumption that the surface elevation can be seen as a stationary Gaussian process [Holthuijsen (2010) [29]].

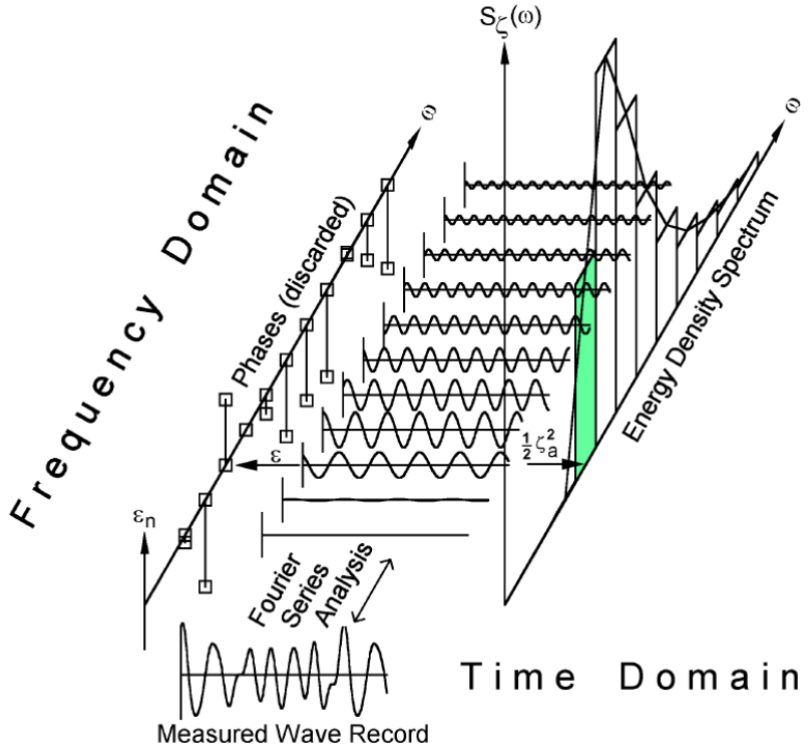

Figure B.2: Wave record analyses, η_a represents wave amplitude, [31]

The variance density spectrum is expressed in terms of frequency (f). Since it is common to use angular arguments for sine and cosine waves, it is useful to express the variance density spectrum in terms of angular frequency (ω). This can be achieved by multiplying Equation (B.21) by $\frac{1}{2\pi}$. For details on this transformation reference is made to [Holthuijsen (2010) [29]].
Waves are propagating in a certain direction, which is not taken into account in the one-dimensional variance density spectrum discussed above. The direction can be taken into account by considering the propagation of the harmonic wave in the x; y-plane. If θ is the angle relative to the positive x-axis and using the principles for the one-dimensional variance density spectrum, the two-dimensional variance density spectrum is obtained:

$$E(f) = \lim_{\Delta f \to 0} lim_{\Delta\theta \to 0} \frac{1}{\Delta f \Delta\theta} E\frac{1}{2}\underline{a}^2 \tag{B.21}$$

E(f, θ) variance density as function of frequency (f) and direction (θ) [$m^2/Hz/rad$]
$\underline{a}$ Amplitude as a random variable [m]

From the variance density spectrum it is relatively easy to obtain the wave energy density spectrum. This can be obtained by multiplying the variance density spectrum with the density of the water and with the gravitational acceleration.

B.6. Energy in a wave field

The distance and duration of the wind flow influences the height and length of the waves. Figure B.4 shows the influence of different wind blowing distances (fetch, distance from shore) over sea surface on the energy transported by the waves.

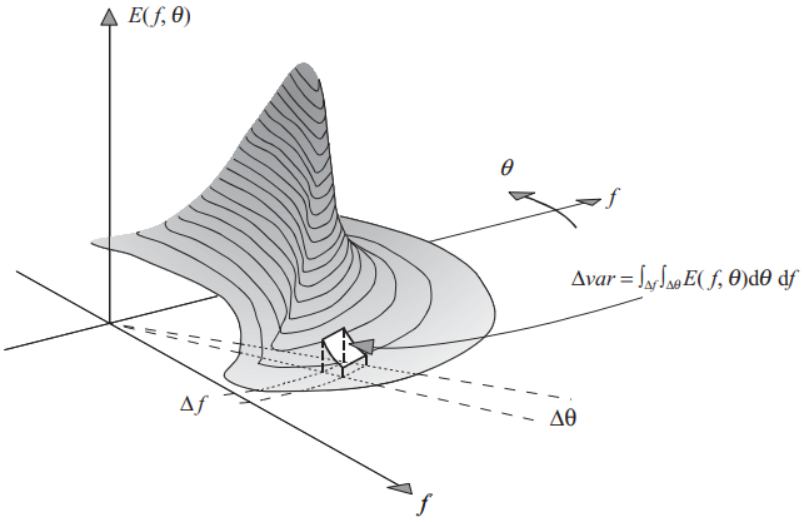

Figure B.3: Two-dimensional variance density spectrum as the distribution of the total variance of the sea-surface elevation over frequency and direction (polar coordinates), [Holthuijsen (2010) [29]].

Waves in water transfer energy in horizontal direction by vibration/oscillation of the water particles. When assuming a small-amplitude wave (linear wave theory) and we choose to write the wave elevation as:

$$\eta(x,t) = a\cos(kx - \omega * t) \tag{B.22}$$

The energy in waves can be described as an alternating balance between potential and kinetic energy. The water particles that are elevated a certain height from their original position contain potential energy. Water particles with a certain velocity contain the kinetic energy. With the use of potential flow theory, the motion (and pressure) of water waves can be calculated. For regular waves the potential flow function is described by:

$$\Phi_0 = \frac{\zeta_a \cdot g}{\omega} \frac{\cosh(k(h+z))}{\cosh kh} \sin(kx - \omega \cdot t) \tag{B.23}$$

Φ_0 - Undisturbed wave potential $[m^2/s]$
ζ_a - Wave amplitude $[m]$
ω - Wave frequency $[rad/s]$
g - Gravitational constant $[m/s^s]$
k - Wave number $[m^{-1}]$
h - Water depth $[m]$
z - Observation depth $[m]$

For deep water the equation can be simplified:

$$\Phi_0 = \frac{\zeta_a \cdot g}{\omega} e^{kz} \sin(kx - \omega \cdot t) \tag{B.24}$$

With the formulation of the potential flow the motion of the water can be calculated.

$$v_x = \frac{\partial \Phi}{\delta x}, v_y = \frac{\partial \Phi}{\delta y}, v_z = \frac{\partial \Phi}{\delta z} \tag{B.25}$$

The kinetic energy of a water mass with a certain velocity is described by:

$$E_k = \frac{1}{2}mv^2 = \frac{1}{2}\frac{\rho}{\lambda}\int_0^{\lambda}\int_{-h}^{\zeta(t)} (v_x^2 + v_z^2) \cdot dz \cdot dx = \frac{1}{4}\rho g \zeta_a^2 \tag{B.26}$$

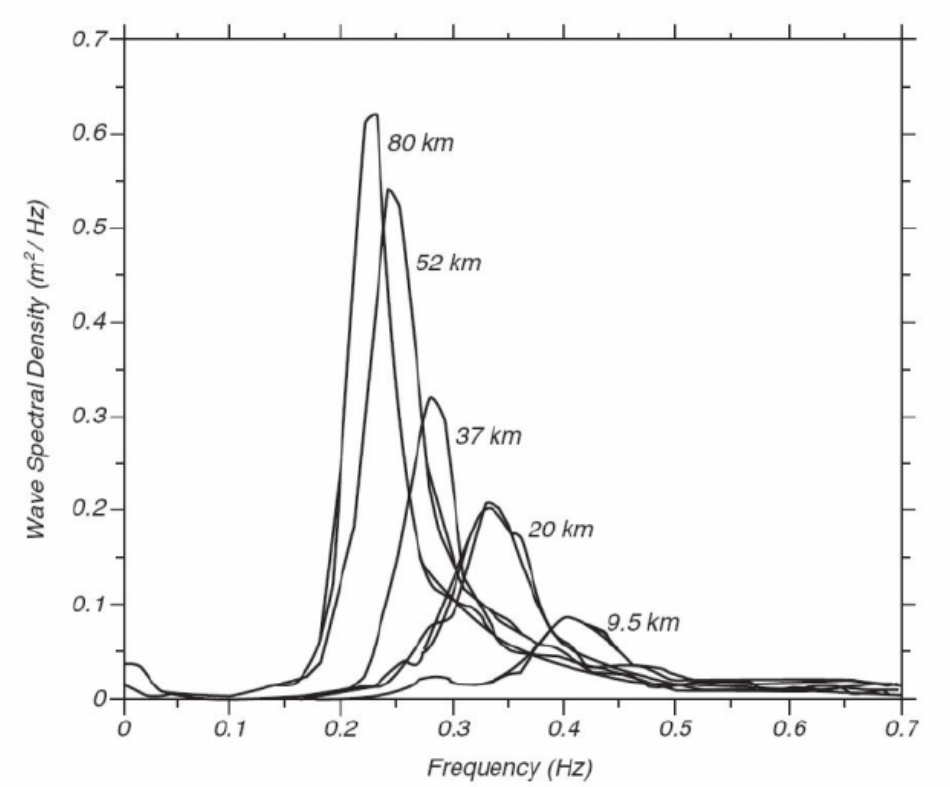

Figure B.4: Observed wave spectra for developing sea during the Jonswap project

At the peak of a wave, water particles have travelled a certain distance upwards from their original position. The change of position against gravitation required work, defined as potential energy. To calculate the potential energy for a unit of horizontal sea surface area ($\Delta x \cdot \Delta y$), from the bottom to the crest, the equation becomes:

$$E_p = mgz = \rho \cdot ((\Delta x \cdot \Delta y) \cdot \Delta z) \cdot gz = \frac{1}{\lambda} \int_0^{\lambda} \rho g \frac{1}{2} \zeta^2 \cdot dx$$
$$= \frac{1}{2} \frac{\rho g \zeta_a}{\lambda} \int_0^{\lambda} \cos^2 (kx - \omega t) \cdot dx = \frac{1}{4} \rho g \zeta_a^2 \tag{B.27}$$

Resulting in a combined energy relation:

$$E_{tot} = E_p + E_k$$
$$E_{tot} = \frac{1}{2} \rho g \zeta_a^2 = \frac{1}{8} \rho g H^2 \tag{B.28}$$

C. Wave power in the oceans

C.1. Wave power theory for regular waves

This section describes the basic equations for calculation of power in waves, used in this thesis. For more detailed description and derivations, see appendix C.

The development of waves by wind, create variations in pressure in the column of water below the water surface. The total energy transport P_{energy} per unit crest length and time-averaged, in x-direction is:

$$P_{energy} = \underbrace{\overline{\int_{-d}^{\eta}(\rho g z)u_x dz}}_{\text{potential energy transport}} + \underbrace{\overline{\int_{-d}^{\eta}(\frac{1}{2}\rho u^2)u_x dz}}_{\text{kinetic energy transport}} + \underbrace{\overline{\int_{-d}^{\eta}(\rho g z + p_{wave\,pressure})u_x dz}}_{\text{work done by pressure}} \tag{C.1}$$

The first term on the right hand side will be cancelled by the $-\rho g z$ part in the third term on the right hand side. The second term is of the third order in amplitude and may be ignored in a second-order approximation. The third expression on the right-hand side is second-order in amplitude and is thus the only integral to be evaluated. For details of the evaluation of C.1 and integration to a certain order accuracy reference is made to Holthuijsen (2010) [29].

If the phase speed is represented by c then the solution of C.1 is:

$$P_{energy} = Enc \qquad with \qquad E = \frac{1}{2}\rho g a^2 \qquad and \qquad n = \frac{1}{2}(1 + \frac{2kd}{sinh(2kd)}) \tag{C.2}$$

The wave induced potential energy, per unit horizontal area, can be obtained by considering potential energy as a function of the water depth (z) and integrating this function from the mean water level surface to the maximum water level [29]. The overbar represents time-averaging and a is the amplitude of the harmonic wave.

$$E_{potential} = \overline{\int_{0}^{\eta} \rho g z\, dz} = \overline{\frac{1}{2}\rho g \eta^2}\frac{1}{4}\rho g a^2 \tag{C.3}$$

The kinetic energy is equal to mass times $\frac{1}{2}$ velocity squared. When time averaged, the kinetic energy for the entire column per unit surface area is then:

$$E_{kinetic} = \overline{\int_{-d}^{\eta} \frac{1}{2}\rho g u^2\, dz} = \frac{1}{4}\rho g a^2 \tag{C.4}$$

where $u = \sqrt{u_x^2 + u_z^2}$.
When assuming $a = \frac{1}{2}H$ The total wave induced energy density is then obtained as function of amplitude (a) or as function of wave height (H).

$$E = E_{potential} + E_{kinetic} = \frac{1}{2}\rho g a^2 = \frac{1}{8}\rho g H^2 \tag{C.5}$$

For a linear wave the energy is defined as C.6,

$$E = \frac{1}{8}\rho g H^2 \tag{C.6}$$

and when assuming linear deep water waves, the group velocity c_g is described by,

$$c_g = \frac{1}{2} \cdot \frac{g}{2\pi} T_e \tag{C.7}$$

the time-averaged power in linear waves can be calculated using equation (C.8):

$$P_w = \frac{\rho g^2}{32\pi} T H^2 \tag{C.8}$$

P_w - Power per meter wave crest [kW/m]
T - Wave period [s]
H - Wave height [m]

Note, that the use of this linear wave equation for power estimations in realistic wave situations is almost always resulting in an overestimation of the power-resource.

The following equations present the amount of power in waves for certain wave conditions (wave height: H and period:T). It must be noted that these equations do not present how much of this power can be converted into usable power. The following theoretical available power relations are used in order to define ratio's for efficiency.

Further elaboration on these relations and knowledge about the extraction method is required to derive the amount of useful power. The theoretic derivation of these equations can be found in [43].

C.2. Power relations, irregular waves

The time-averaged power in irregular waves can be calculated using equation (C.9):

$$P_w = \frac{\rho g^2}{64\pi} T_e H_s^2 \tag{C.9}$$

P_w - Power per meter wave crest [kW/m]
T_e - Wave energy period [s]
H_s - significant wave height [m]

Note that the wave energy period is not exactly the same value as other period definitions, such as: zero crossing period or peak period. Factors are mentioned in [43, p. 59] that can be used to transpose between these definitions.

When including the water depth into the equation C.9, the time-averaged power in linear waves can be obtained by:

$$P_w = \frac{\rho g^2}{64\pi} T_e H_s^2 * \frac{1}{2}\left(1 + \frac{2kd}{\sinh(2kd)}\right) \tag{C.10}$$

P_w - Power per meter wave crest [kW/m]
T_e - Wave energy period [s]
H_s - significant wave height [m]

The power equation C.10, is derived from the wave group-velocity multiplied by the energy. The energy can be obtained in different ways depending on the use.

C.11 describes the group velocity for deep water waves [45]:

$$c_g = \frac{1}{2} \frac{g}{2\pi} T_e \tag{C.11}$$

c_g - Group velocity $[m/s]$
g - Gravitational constant $[m/s^2]$
T_e - Energy period $[s]$

The energy period is calculated using the

$$T_e = T_{m-1,0} = \frac{m_{-1}}{m_0}, m_n = \int_0^\infty f^n E(f) df \tag{C.12}$$

$$1.12T_e = 1.29T_{0,2} = T_p \tag{C.13}$$

$T_{0,2}$ - Mean zero crossing period $[s]$
T_p - Peak period $[s]$

The wave elevation from a record made at sea is not represented by one simple sinusoid as was the case for regular waves. Instead a summation of many sinusoids could be used to construct an almost similar record (method called Fourier transformation). This results in a large number of amplitudes and phases for each sinusoid in the summation. For a duration in which the sea state conditions are constant, often 10 to 30 minutes, a wave variance density spectrum represents all the amplitudes of the sinusoidal components needed to represent this sea state. A continuous variance density spectrum is obtained by the formulation:

$$E(f) = lim_{\Delta f \to 0} \frac{1}{\Delta f} E\frac{1}{2}a^2 \tag{C.14}$$

Where a are all the amplitudes present in the wave field.

The spectrum of energy is usually plotted as energy density with the unit of energy over the frequency interval $[E/hz]$

A wave spectrum can be created from the wave amplitudes measured during an observation. Wave spectral density, represented by the value on the y-axis, is equal to halve the wave amplitude squared.(due to limits on the duration and data points in a measurement extra modifications are applied to represent . Multiplying the spectral density with the density of water and the gravitational constant it results in the energy, the area under the graph then equals the energy the waves contained during the measurement.

When the wave is not regular but defined by a spectrum, which is used commonly when working with measured wave records, the wave energy can be derived from the spectrum using the variance.

$$E = \rho g \cdot m_0 = \rho g \cdot \frac{1}{16} H_{mo}^2 \tag{C.15}$$

The energy over time for waves defined by a spectrum can be calculated using equation (C.16):

$$P_w = \frac{\rho g^2}{64\pi} T_e H_s^2 \tag{C.16}$$

P_w - Power per meter wave crest [kW/m]
T_e - Wave energy period [s]
H_s - significant wave height [m]

The calculation of the available power per meter wave crest is described in [42, p. 59]

$$J = \frac{\rho g^2}{64 \cdot \pi} H_{m0}^2 T_e \tag{C.17}$$

$$P_w = \frac{\rho g^2}{64\pi} T_e H_s^2 \tag{C.18}$$

P_w - Power per meter wave crest [kW/m]
T_e - Wave energy period [s]
H_s - significant wave height [m]

C.3. Spectral, irregular waves

For calculations using a wave spectrum the wave energy is defined as C.20, and finally the power equation becomes C.20.

$$E = \frac{1}{16}\rho g H_s^2 \tag{C.19}$$

In this case the wave height is defined by the variance (m_0) of the spectrum with the following relation: $H_s = 4\sqrt{m_0}$

$$P_w = E \cdot c_g = \frac{\rho g^2}{64\pi} T_e H_s^2 \tag{C.20}$$

P_w - Energy flux per meter wave crest [kW/m]
T_e - Wave energy period [s]
H_s - significant wave height [m]

D. Oscillatory motion of a body in waves

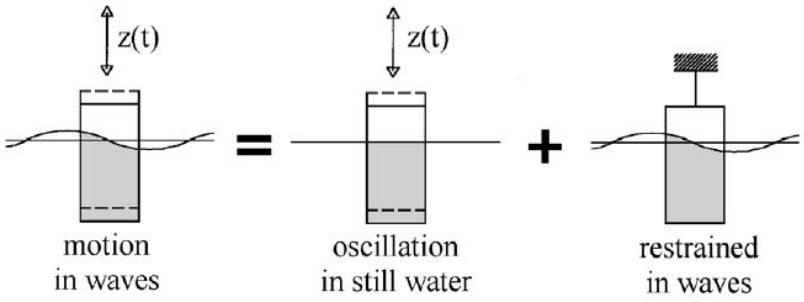

Figure D.1: General assumption in Hydrodynamic modelling of floating bodies

$$(m + a_{mass})\ddot{z} + (b_{rad} + b_{PTO})\dot{x} + kx = F_{wave} \tag{D.1}$$

When defining the wave force to be, $F_{wave} = F_0 cos(\omega t)$, the motion in z direction is defined:

$$z_0^2\omega^2 = w_0^2 = \frac{F_0^2}{(b_{rad} + b_{PTO})^2 + (\omega(m + a_{mass}) - \frac{k}{\omega})^2} \tag{D.2}$$

Time averaged power is defined as:

$$\overline{P}_{PTO} = \overline{b_{PTO}\dot{z}^2} = \frac{1}{T}\int_{t+T}^{T} b_{PTO}\dot{z}_0^2\omega^2 \cos(\omega t - \phi)^2\, dt = \frac{1}{2}b_{PTO}z_0^2\omega^2 \tag{D.3}$$

where the overbar indicates time averaging.

Substituting the motion equation D.2 in the equation for useful power D.3:

$$\bar{P}_{PTO} = \frac{\frac{1}{2}b_{pto}F_0^2}{(b_{rad} + b_{pto})^2 + (\omega(m + m_0) - \frac{k}{\omega})^2} \tag{D.4}$$

Maximum power is obtained when: $\omega(m + a_{mass} - \frac{k}{\omega} = 0)$, meaning the system operates in resonance. Maximum power at resonance:

$$\bar{P}_{PTO} = \frac{\frac{1}{2}b_{pto}F_0^2}{(b_{rad} + b_{pto})^2 + (\omega(m + a_{mass}) - \frac{k}{\omega})^2} \tag{D.5}$$

E. Potential theory

Software tools like AQWA use potential theory to perform Theory described by Newman

Boundary conditions:

$$\frac{\partial \phi}{\partial z} - K\phi = 0 \quad \text{on} \quad z = 0 \tag{E.1}$$

$$\frac{\partial \phi}{\partial z} = 0 \quad \text{on} \quad z = -h \tag{E.2}$$

Here, $K = \omega^2/g$, with g for the acceleration of gravity. The velocity potential of the incident wave is defined by

$$\phi_i = \frac{igA}{\omega} \frac{\cosh[k(z+h)]}{\cosh kh} \exp -ik(x\cos\beta + y\sin\beta) \tag{E.3}$$

With the dispersion relation

$$\frac{\omega^2}{g} = k\tanh kh \tag{E.4}$$

The total velocity potential can be expressed as

$$\phi = \phi_R + \phi_D \tag{E.5}$$

where

$$\phi_D = \phi_i + \phi_s \tag{E.6}$$

is the diffraction potential. Here, ϕ_s is the scattering component representing the disturbance of the incident wave by the fixed body.

E.1. Solving potentials

$$\phi_j(x,y,z) = \frac{1}{4\pi} \iint_{S0} \sigma_j(\hat{x},\hat{y},\hat{z}) \cdot G(x,y,z,\hat{x},\hat{y},\hat{z})\, dS_0 \tag{E.7}$$

$\Phi_j(x,y,z)$ - Potential function $[m^2/s]$
$\sigma_j(\hat{x},\hat{y},\hat{z})$ - Souce strength $[m]$
$G(x,y,z,\hat{x},\hat{y},\hat{z})$ - Greens function of the pulsating source σ_j at location $(\hat{x},\hat{y},\hat{z})$ on the potential ϕ_j on locati

This greens function satisfies the laplace equation, the linearized boundary condition on the sea bed and on the free surface and the radiation condition at infinity.

To calculate pressure from potentials, **??** is used

$$p = \rho \frac{\partial \phi}{\partial t} \cdot n_3\, dS \tag{E.8}$$

As forces are obtained from the integration of the pressures on a surface:

$$\overline{F} = \iint_S -\overline{p} \cdot \overline{n}\, dS \tag{E.9}$$

Substitution of the relation between potentials and pressure gives:

$$F_3 = \iint_S -(\rho \frac{\partial \phi}{\partial t} \cdot n_3)\, dS \tag{E.10}$$

F. WEC devices information

This appendix includes a selection of examples of various developed concepts and a list of companies and countries.

1. Devices that got much attention before funding ended, figures F.1
2. Devices that have been deployed and are still in development, figures F.2
3. Devices in early stage of development aiming to realise, prove and improve the underlying theoretic principles, figures F.3

(a) Pelamis

(b) Oyster 800

(c) WaveDragon

(d) Oceanlinx

(e) Wavebob

(f) Robusto - Langlee

Figure F.1: Illustrations of various devices that are not being developed anymore.

(a) Seabased

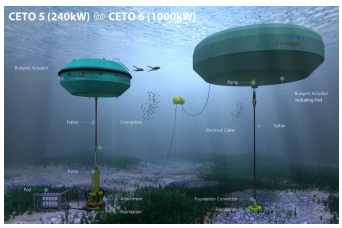

(b) Ceto 6 - Carnegie

(c) Poseidon - FPP

(d) OEbuoy - Ocean Energy

(e) Penguin - Wello OY

(f) WaveEl Buoy - Waves4Power

Figure F.2: Illustrations of various devices that are currently continuing development after demonstration testing

(a) Teamwork

(b) KNSwing - Kim Nielsen

(c) CorPower buoy

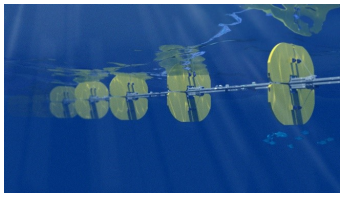

(d) OEbuoy - Ocean Energy

(e) PolyGen

(f) Weptos

Figure F.3: Illustrations of various devices that are in an early stage of development and pre-demonstration stage

Table F.1: Submerged pressure differential device developers.

Company	Technology	Country
Bombora Wave Power	mWave	Australia
M3 Wave, LLC	DMP Device	USA
Teamwork	Symphony	NL
CalWave	WaveCarpet	USA

Table F.2: Oscillating Water Column technology developers.

Company	Technology	Country
KNSwing	KNSwing	Denmark
OceanEnergy	The OEbuoy	Ireland
Havkraft	Havkraft	Norway
ORECON	MRC	UK
Mighty Waves Energy Team	Mighty whale	USA
IOWEC	IOWEC	USA

Table F.3: Oscillating Wave Surge Converters technology developers.

Company	Technology	Country
AW energy	Waveroller	Finland
Aquamarine Power	Oyster	UK
PolyGen Ltd	Volta	UK
RME	RME wave2O^{tm}	UK

Table F.4: Point Absorbers technology developers.

Company	Technology	Country
Carnegie Wave Energy Ltd	CETO 6	Australia
Aquagen Technologies	Rig Drive	Australia
FlanSea	Wave Pioneer	Belgium
Seawood Designs Inc	SurfPower	Canada
Guangzhou Institute (GIEC)	Neza II	China
RESEN ENERGY	Resen Waves LOPF buoys	Denmark
Wave Star Energy ApS	Wave Star	Denmark
Hydrocap Energy SAS	Seacap	France
Nemos GmbH	NEMOS	Germany
Sinn Power	Sinn Power	Germany
Slow Mill	Slow Mill	Holland
Joules Energy Efficiency Services Ltd	Wave Train	Ireland
Northwest Energy Innovations	Azura	New-Zealand
NTNU (Norwegian tech. University)	CONWEC	Norway
Fred Olsen Ltd	Lifesaver	Norway
Pontoon Power	Pontoon Power Converter	Norway
Pelagic Power AS	W2Power	Norway
Ocean Wave and Wind Energy (OWWE)	Wave Pump	Norway
Applied Technologies Company (ATC)	FWEPS	Russia

Table F.5: Continuation; Point Absorber technology developers.

Company	Technology	Country
Sigma Energy	MD Wave Power Converter	Slovenia
Ingine Inc	INWave	South Korea
PIPO Systems	APC-PISYS	Spain
Oceanic Power	SeaHeart	Spain
CorPower ocean	CorPower WEC	Sweden
Seabased AB	S	Sweden
Ocean Harvesting Technologies	InfinityDrive	Sweden
Waves4Power AB	WaveEL-buoy	Sweden
Sea Potential	DUO	UK
SEEWEC Consortium	FO3	UK
The Bobber Company Ltd	Manchester Bobber	UK
Seatricity	Oceanus 2	UK
Ecotricity	Searaser	UK
Snapper Consortium	Snapper	UK
Neptune Renewable Energy Ltd	Triton	UK
MakerStrong	eBuoy	USA
Aqua-Magnetics Inc	Electric Buoy	USA
ELGEN Wave	Horizon Platform	USA
Tremont Electric	nPower WEC	USA
Green Ocean Wave Energy	Ocean Wave Air Piston	USA
Ocean Power Technologies (OPT)	Power Buoy	USA
Independent Natural Resources	SEADOG	USA
Oscilla Power, Inc	TritonWEC	USA
Marine Energy Corporation	Wave Catcher	USA
Ocean Electric Inc	Wave platform	USA
Atmocean	Wave Rider	USA
Ocean Energy Industries Inc	WaveSurfer	USA
AquaHarmonics	AquaHarmonics	USA
Neptune Wave Power	Triton	USA

Table F.6: Pitching Buoy Converters technology developers.

Company	Technology	Country
Weptos	Wetos	Denmark
Wello OY	penguin	Finland
Centrale Nantes	SEAREV	France
Waves For Energy	ISWEC	Italy

Table F.7: Overtopping device developers.

Company	Technology	Country
Wave Dragon	Wave Dragon	Denmark
WavePlane production	WavePlane	Denmark

G. Results enlarged

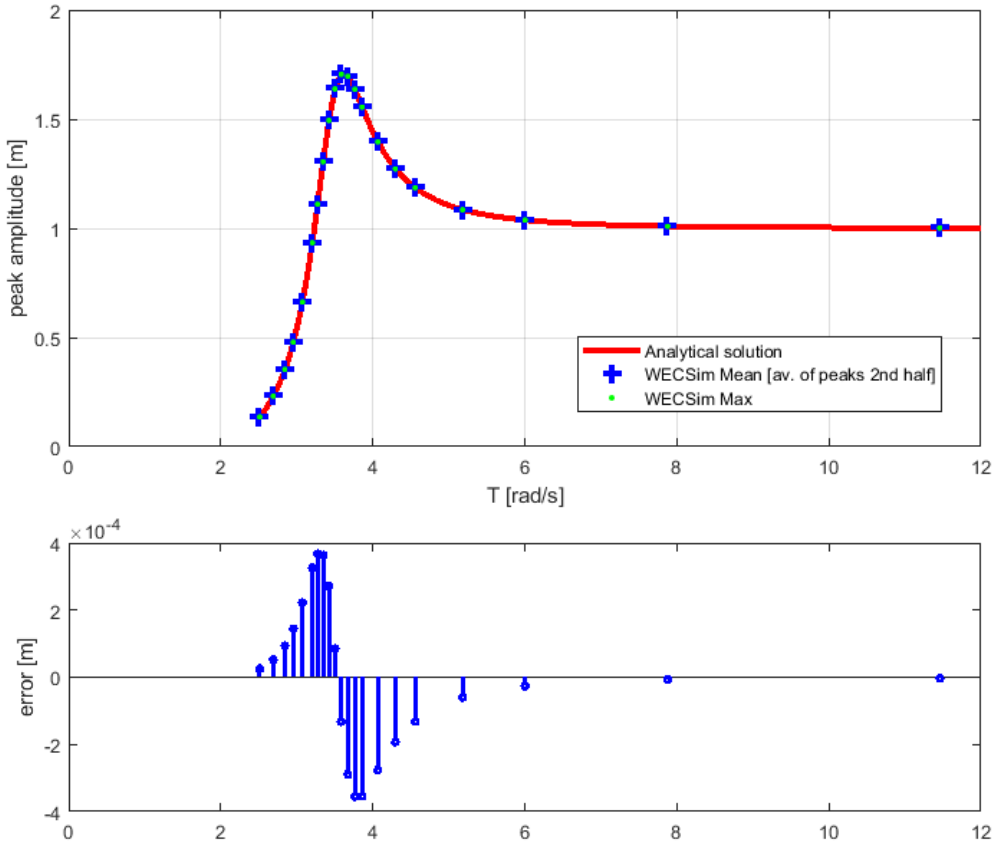

(a) Free body motion - Floating buoy

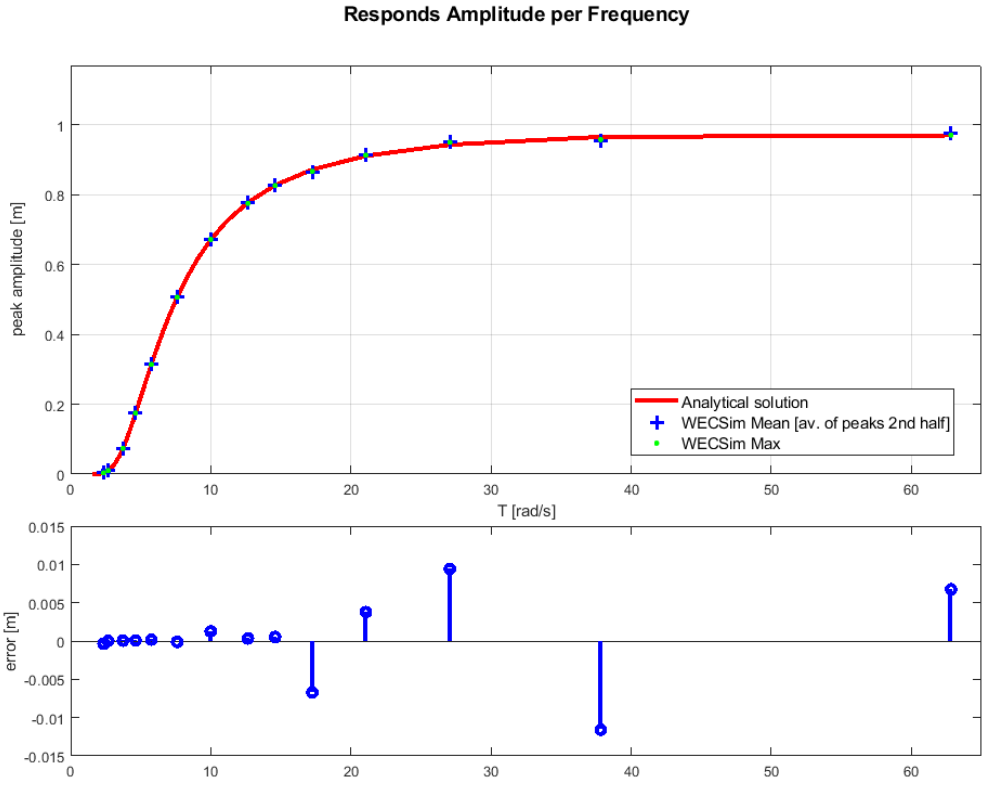

(b) Free body motion - Submerged buoy

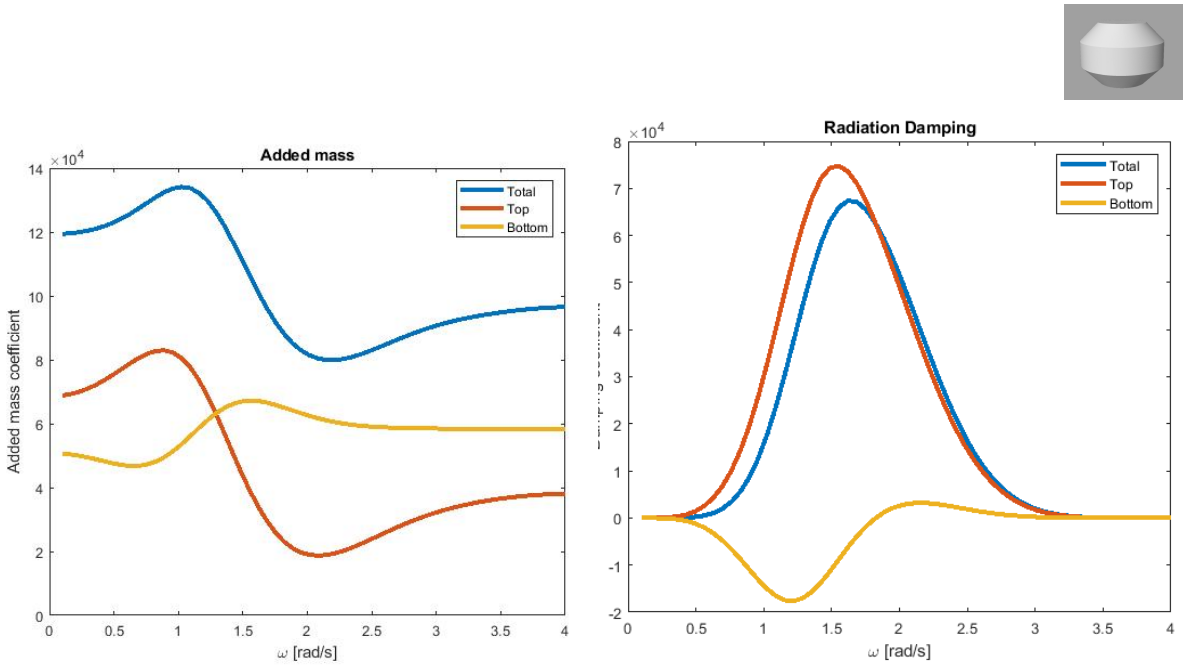

(a) (b)

Figure G.2: Hydrodynamic coefficients, for the chamfered cylinder model, left: the added mass and right the radiation damping coefficients

Bibliography

[1] A Babarit. A database of capture width ratio of wave energy converters. *Renewable Energy*, 80:610–628, 2015.

[2] A. Babarit and J. Hals. On the maximum and actual capture width ratio of wave energy converters. *Proceedings of the 9th European Wave and Tidal Energy Conference*, (September):1–7, 2011.

[3] A. Babarit, J. Hals, A. Kurniawan, M. Muliawan, T. Moan, and J. Krokstad. Numerical estimation of energy delivery from a selection of wave energy converters. (December): 1–317, 2011.

[4] A. Babarit, J. Hals, M. J. Muliawan, A. Kurniawan, T. Moan, and J. Krokstad. Numerical benchmarking study of a selection of wave energy converters. *Renewable Energy*, 41: 44–63, 2012. ISSN 09601481. doi: 10.1016/j.renene.2011.10.002. URL http://dx.doi.org/10.1016/j.renene.2011.10.002.

[5] K. Budal. Correction, 1975.

[6] K. Budal and J. Falnes. Proposals for conversion of the energy in ocean waves. 1974.

[7] K. Budal and J. Falnes. Power generation from ocean waves using a resonant oscillating system. *Marine Science Communication*, 1:269–288, 1975.

[8] K. Budal and J. Falnes. Interacting point absorbers with controlled motion. *Power from sea waves*, pages 381–399, 1980.

[9] M. Chatzigiannakou, I. Dolguntseva, and M. Leijon. Offshore Deployments of Wave Energy Converters by Seabased Industry AB. *Journal of Marine Science and Engineering*, 5(2): 15, 2017. ISSN 2077-1312. doi: 10.3390/jmse5020015. URL http://www.mdpi.com/2077-1312/5/2/15.

[10] J. F Chozas. cost of energy for ocean energy technologies. pages 5–48, May 2015.

[11] J. Sa da Costa, P Pinto, A Sarmento, and F Gardner. Modeling of an ocean waves power device aws. In *Control Applications, 2003. CCA 2003. Proceedings of 2003 IEEE Conference on*, volume 1, pages 618–623. IEEE, 2003.

[12] J Cruz. *Ocean wave energy: current status and future prespectives*. Springer Science & Business Media, 2007.

[13] A. De Andrés, A. Macgillivray, R. Guanche, and H. Jeffrey. Factors affecting LCOE of Ocean energy technologies: a study of technology and deployment attractiveness. *5th International Conference on Ocean Energy*, pages 1–11, 2014.

[14] A. De Andres, E. Medina-Lopez, D. Crooks, O. Roberts, and H. Jeffrey. On the reversed LCOE calculation: Design constraints for wave energy commercialization. *International Journal of Marine Energy*, 18(2017):88–108, 2017. ISSN 22141669. doi: 10.1016/j.ijome.2017.03.008. URL http://dx.doi.org/10.1016/j.ijome.2017.03.008.

[15] Wave Dragon. Wave dragon technology, 2018. URL http://www.wavedragon.co.uk/technology-2/.

[16] B. Drew, A. Plummer, and M. Sahinkaya. A review of wave energy converter technology, 2009.

[17] Entec UK Ltd. Cost estimation methodology. *Carbon Trust*, (May), 2006.

[18] D. Evans. A theory for wave-power absorption by oscillating bodies. *Journal of Fluid Mechanics*, 77(1):1–25, 1976.

[19] D. Evans. Maximum wave-power absorbtion under motion constraints. *Applied Ocean Research*, 3(4):200–203, 1981.

[20] D. Evans. Maximum wave-power absorption under motion constraints. *Applied Ocean Research*, 3(4):200–203, 1981.

[21] A.F.O. Falcão. Wave energy utilization: A review of the technologies. *Renewable and Sustainable Energy Reviews*, 14(3):899–918, 2010. ISSN 13640321. doi: 10.1016/j.rser.2009.11.003.

[22] J. Falnes. *Ocean waves and oscillating systems: linear interactions including wave-energy extraction*. Cambridge university press, 2002.

[23] J. Falnes. A review of wave-energy extraction. *Marine structures*, 20(4):185–201, 2007.

[24] J. Falnes and J. Hals. Heaving buoys, point absorbers and arrays. *Phil. Trans. R. Soc. A*, 370(1959):246–277, 2012.

[25] M. Folley. *Phase-Averaging Wave Propagation Array Models*. Elsevier Inc., 2016. ISBN 9780128032107. doi: 10.1016/B978-0-12-803210-7.00011-6. URL http://linkinghub.elsevier.com/retrieve/pii/B9780128032107000116.

[26] M. Folley, T. Whittaker, and J. Van't Hoff. The design of small seabed-mounted bottom-hinged wave energy converters. In *Proceedings of the 7th European wave and tidal energy conference*, volume 455. Citeseer, 2007.

[27] D. Harleman and W. Shapiro. The dynamics of a submerged moored sphere in oscillatory waves. *Coastal Engineering Proceedings*, 1(7):41, 1960.

[28] J.C.C. Henriques, L.M.C. Gato, A.F.O. Falcão, E. Robles, and F.-X. Faÿ. Latching control of a floating oscillating-water-column wave energy converter. *Renewable Energy*, 90:229 – 241, 2016. ISSN 0960-1481. doi: https://doi.org/10.1016/j.renene.2015.12.065. URL http://www.sciencedirect.com/science/article/pii/S0960148115305693.

[29] L.H. Holthuijsen. *Waves in oceanic and coastal waters*. Cambridge university press, 2010.

[30] S. Jiang, Y. Gou, B. Teng, and D. Ning. An analytical solution of wave diffraction problem on a submerged cylinder. *Journal of Engineering Mechanics*, 140:225–232, 01 2014. doi: 10.1061/(ASCE)EM.1943-7889.0000637.

[31] J.M.J. Journée, W.W. Massie, and R.H.M. Huijsmans. *Offshore Hydromechanics: Course OE4630*. TU Delft, 2000.

[32] Johan M.J. Journée and W.W. Massie. Offshore hydrodynamics. *Delft University of Technology*, 4:38, 2001.

[33] J.P. Kofoed and M. Folley. *Determining Mean Annual Energy Production*. Elsevier Inc., 2016. ISBN 9780128032107. doi: 10.1016/B978-0-12-803210-7.00013-X. URL http://linkinghub.elsevier.com/retrieve/pii/B978012803210700013X.

[34] M. Lawson, Y. Yu, K. Ruehl, C. Michelen, et al. Development and demonstration of the wec-sim wave energy converter simulation tool. 2014.

[35] Giulio Lorenzini, Maria Fernanda Espinel Lara, Luiz Alberto Oliveira Rocha, Mateus das Neves Gomes, Elizaldo Domingues dos Santos, and Liércio André Isoldi. Constructal design applied to the study of the geometry and submergence of an oscillating water column. *International Journal of Heat and Technology*, 33(2):31–38, 2015.

[36] D. Magagna, R. Monfardini, and A. Uihlein. Jrc ocean energy status report 2016 edition. *Technology, market and economic aspects of ocean energy in Europe*, 2016.

[37] S.A. Mavrakos and G.M. Katsaounis. Effects of floaters' hydrodynamics on the performance of tightly moored wave energy converters. *IET renewable power generation*, 4(6): 531–544, 2010.

[38] G. Mork, S. Barstow, A. Kabuth, and M. Pontes. Assessing the global wave energy potential. In *ASME 2010 29th International conference on ocean, offshore and arctic engineering*, pages 447–454. American Society of Mechanical Engineers, 2010.

[39] J. N. Newman and D. Taylor. *The exciting forces on fixed bodies in waves /*. Washington, D.C. :Dept. of the Navy, David Taylor Model Basin„ 1963. URL https://www.biodiversitylibrary.org/item/102114. https://www.biodiversitylibrary.org/bibliography/47501 — "May 1963.".

[40] Corpower Ocean. Corpower ocean webpage. URL http://www.corpowerocean.com/.

[41] OES. an Overview of Ocean Energy Activities in 2017 Annual. 2017.

[42] A. Pecher and J.P. Kofoed. *Handbook of Ocean Wave Energy*, volume 7 of *Ocean Engineering & Oceanography*. Springer International Publishing, 2017. ISBN 9783319398884. doi: 10.1007/978-3-319-39889-1. URL http://link.springer.com/10.1007/978-3-319-39889-1.

[43] A. Pecher and J.P. Kofoed. *Handbook of Ocean Wave Energy*. Springer, 2017.

[44] A. Pecher and J.P. Kofoed. Introduction. In *Handbook of Ocean Wave Energy*, pages 1–15. Springer, 2017.

[45] E. Rusu and F. Onea. Estimation of the wave energy conversion efficiency in the atlantic ocean close to the european islands. *Renewable Energy*, 85:687–703, 2016.

[46] E. Rusu and F. Onea. A review of the technologies for wave energy extraction. *Clean Energy*, 2018.

[47] N.Y. Sergiienko, B.S. Cazzolato, B. Ding, P. Hardy, and M. Arjomandi. Performance comparison of the floating and fully submerged quasi-point absorber wave energy converters. *Renewable Energy*, 108:425–437, 2017.

[48] SI Ocean. Ocean Energy: Cost of Energy and Cost Reduction Opportunities. (May):29, 2013. URL http://si-ocean.eu/en/upload/docs/WP3/CoEreport3{_}2final.pdf.

[49] J. Tedd and J.P. Kofoed. Measurements of overtopping flow time series on the wave dragon, wave energy converter. *Renewable Energy*, 34(3):711 – 717, 2009. ISSN 0960-1481. doi: https://doi.org/10.1016/j.renene.2008.04.036. URL http://www.sciencedirect.com/science/article/pii/S096014810800195X.

[50] Carbon Trust. Uk wave resource. Technical report, AMEC, 2012.

[51] D.A.N. Van der Pluijm and A.W. Voors. Power from ocean waves: A study to power conversion with the archimedes wave swing. 2001.

[52] G.A.M. Van Kuik. The lanchester–betz–joukowsky limit. *Wind Energy: An International Journal for Progress and Applications in Wind Power Conversion Technology*, 10(3):289–291, 2007.

[53] D. Wikkerink, R. Schuitema, and F. Garnder. Global analysis of the selected pto for the symphony. *WETFEET – Wave Energy Transition to Future by Evolution of Engineering and Technology*, 4.4, 2018.